NASA CR-66893

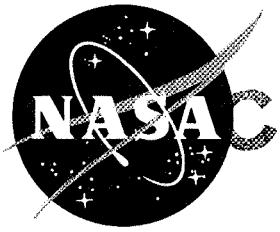

THEORETICAL AND EXPERIMENTAL STUDY OF SUPERSONIC MIXING OF TURBULENT DISSIMILAR STREAMS

by

James P. Woolley

prepared for

NATIONAL AERONAUTICS AND SPACE ADMINISTRATION

CONTRACT NAS 1-6076

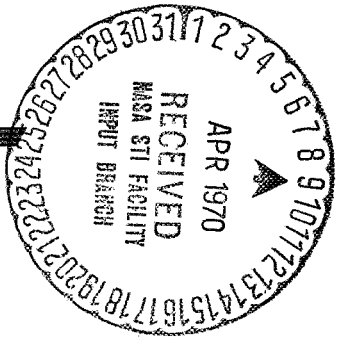

CONSOLIDATED ENGINEERING TECHNOLOGY CORPORATION

THEORETICAL AND EXPERIMENTAL STUDY OF SUPERSONIC MIXING OF TURBULENT DISSIMILAR STREAMS

By James P. Woolley

Prepared under Contract No. NAS 1-6076
CETEC Corporation
Mountain View, California

for

NATIONAL AERONAUTICS AND SPACE ADMINISTRATION
Langley Research Center
Hampton, Virginia 23365

TABLE OF CONTENTS

TABLE OF CONTENTS (continued)

LIST OF ILLUSTRATIONS

LIST OF ILLUSTRATIONS (continued)

ABSTRACT

A theoretical and experimental program was conducted to investigate the effects of molecular weight and other gas properties on the rate of mixing of dissimilar supersonic gas streams. An analysis of the supersonic mixing process was made by extending the original analysis of Channapragada and Woolley. A reference density criteria was developed which permits prediction of isobaric turbulent mixing rates in the near field for compressible flow of similar gases. This unique reference density approach has been confirmed experimentally for isoenergetic streams. The prediction method was also extended analytically to compressible flows with streamwise pressure gradients.

The effects of molecular weight on the mixing process were also described analytically.

Experimental mixing data with air streams are reported for several velocity ratios and for conditions of an adverse pressure gradient.

1.0 SUMMARY

A theoretical and experimental program was conducted under Contract No. NAS 1-6076 to investigate the effects of molecular weight and other gas properties on the rate of mixing of dissimilar supersonic gas streams. An analysis of the supersonic mixing process was made and the original analysis of Channapragada and Woolley was expanded. A reference density criteria was developed which permits prediction of isobaric turbulent mixing rates in the near field for compressible flow of similar gases. This unique reference density approach has been confirmed experimentally for isoenergetic streams. The prediction method was also extended analytically to compressible flows with streamwise pressure gradients. The reference density for this condition appears to be the same as for the isobaric flow evaluated with conditions existing at the onset of mixing.

The relation between the enthalpy and velocity distribution in turbulent shear flows is shown to be different analytically from the relation for laminar flows. Preliminary experimental confirmation of this analytical observation is reported.

The effects of molecular weight on the mixing process were described analytically. However, tests were not performed to test the validity of the analytical model.

An experimental mixing system was developed and tested under several conditions of Mach No. Experimental mixing data with air streams are reported for several velocity ratios and for conditions of an adverse pressure gradient.

2.0 INTRODUCTION

In recent years many investigations of gas fueled scramjet systems have been conducted with particular emphasis on their operating regimes, critical performance design criteria, and inlet and combustor design for operation over a wide Mach corridor. From the standpoint of hardware and effective utilization of fuel, the combustor design plays a vital role in the scramjet vehicle design. The function of an efficient combustor is to mix rapidly the reactant streams and obtain the maximum energy release with a minimum loss in mechanical energy. This is very seldom possible.

Rapid mixing, for example, of the reactant streams can be enhanced by injection of the fuel normal to the airstream flow. By doing so, however, the preservation of total pressure is lost in resultant shocks generated by the impinging stream. An alternate approach of tangential injection for practical systems has hitherto been restricted due to the long mixing lengths and combustion chambers that were considered to be necessary. However, tangential injection of fuel can be accomplished with only minor shock losses and, thus, can ultimately produce the highest thermodynamic cycle efficiency if these mixing lengths can be tolerated. Hence, our attention in this program was directed at understanding the mixing rate mechanism for tangential injectants in an effort to improve practical systems.

Large shock losses are again encountered when one considers the detonation wave as the combustion mode for the high speed ram jet. The most promising combustion mode for this application appears to be the supersonic diffusion flame which is possible with tangential injection. In this mode a fuel and an oxidizer are brought together in parallel streams at constant pressure. Ideally, then, shock free mixing and chemical energy release can take place between the streams.

In order to attain this idealized situation in practical hardware as well as to obtain means to further optimize the system, the ability to describe analytically the gas dynamics and chemical kinetics of the processes involved must be developed. Furthermore, in order to increase the confidence in any such analysis, the analysis must be accompanied by accurate experimental data.

Under the present contract an analytical and experimental program was conducted to develop and evaluate analytical techniques

which would appropriately describe such processes in supersonic combustors. In particular the objectives were to: (1) extend and combine existing analytical tools to obtain a coherent analysis of the non-reactive turbulent mixing of compressible, parallel streams with arbitrary molecular weight and streamwise pressure gradient; (2) search the literature for existing data to permit experimental verification of the analyses; (3) design and fabricate sub-scale test configurations for optimized supersonic combustors using non-reactive systems; (4) conduct tests with these sub-scale configurations and (5) compare the analytical studies with correlated experimental data.

The program completed under contract, NAS 1-6076, was designed to develop the required analytical methods and to provide a broad experimental background for evaluation of the supersonic turbulent mixing processes. The plane mixing of non-reactive streams are treated for the near field mixing regime.

The original program contemplated analyses and experimental verification tests over a broad range of parameters and a comprehensive coverage of parameter combinations of interest. The stagnation temperature ratio was to range between 0.5 and 6.0 and the velocity ratio to range from 0 to 1.0. Experimentally, the velocity ratio was to be determined from 0 to 0.95. Molecular weight ratios were to be investigated in the range of 0.07 to 1.5 corresponding to hydrogen, air and carbon dioxide streams. In addition, pressure gradients in the streamwise direction were to be investigated for both positive and negative values with a Mach number at the final station to be a maximum of 5. The supersonic Mach number range to be covered was from 1.75 to 4.0 at the mixing juncture.

This final report contains the details of the analytical studies, the experimental verification tests, comparison of data and theory and recommendations for future work.

3.0 TECHNICAL ACTIVITIES

3.1 Analytical and Theoretical Studies

3.1.1 General Background - The Governing Equations

An analytical extension of the turbulent mixing analysis of Channapragada and Woolley[1] * to include dissimilar molecular weight effects for isobaric mixing was developed. In the development, a modification to the energy equation employed in the original development was necessary. This new formulation[2] of the energy equation does not invalidate the approach originally used but merely results in different algebraic expressions. Both alternative formulations are presented and discussed.

The extension of the supersonic mixing analysis to include gases of dissimilar molecular weight also requires an extension of the reference state definition. In particular, the additional degree of freedom for the thermal states, the composition, had to be incorporated into the evaluation of the reference state.

Expressions defining the reference thermodynamic state for multicomponent mixtures were set down in forms compatible with each of the two energy equations. Again, two alternatives are developed. Briefly, they are to express the reference state in terms of a reference composition and either a related reference enthalpy or a reference temperature. The propriety of these two must await evaluation from the results of a complete experimental program.

Formulation of the basic computer program for the mixing study begins with construction of the routines for evaluating the integral functions derived in the the sections that follow. In the final analytical section, the analysis is extended to provide an analytical approach to turbulent mixing with a streamwise pressure gradient. The extension is approached along the lines of the transformation given by Low[3] for laminar boundary layers with streamwise pressure gradients. This work is a direct extension of the Howarth[4] transformation to streamwise pressure gradient flows. The translation of the approach to the turbulent regime is straightforward using normal techniques.

---

* Superscripted numbers denote references.

We are concerned in this analysis with the mixing of dissimilar streams of compressible fluids. By dissimilar, it is meant that the chemical species (and, therefore, probably the molecular weight and thermal properties) contained in each stream are not identical. To represent the physical problem the present analysis is applied to the turbulent mixing of two homogeneous streams. Thus, the assumptions of unit Prandtl and Lewis number are retained.

The near field or two-dimensional problem is treated here, making the analysis an extension of reference 1. The governing equations stated in reference 1 are restated here as a point of reference.

Mass

$$\frac{\partial(\bar{\rho}\,\bar{u})}{\partial x} + \frac{\partial(\overline{\rho v})}{\partial y} = 0 \tag{1}$$

Streamwise Momentum

$$\bar{\rho}\,\bar{u}\,\frac{\partial \bar{u}}{\partial x} + (\overline{\rho v})\,\frac{\partial \bar{u}}{\partial y} = \frac{\partial \tau_T}{\partial y} \tag{2}$$

Energy

$$\bar{\rho}\,\bar{u}\,\frac{\partial \bar{h}}{\partial x} + (\overline{\rho v})\,\frac{\partial \bar{h}}{\partial y} = \frac{\partial \bar{q}}{\partial y} + \tau_T\,\frac{\partial \bar{u}}{\partial y} \tag{3}$$

where it is assumed that:

$$\tau_T = -\overline{[(\rho v)''\,u']} = \bar{\rho}\,\epsilon_m\,\frac{\partial \bar{u}}{\partial y} \tag{4}$$

and

$$q_T = -\overline{[(\rho v)''\,h']} = \frac{\epsilon_h}{C_p}\,\frac{\partial \bar{h}}{\partial y} \tag{5}$$

where

$$(\rho v)'' = (\rho v)' + \rho' v'$$

where τ_T and q_T are the so-called, "apparent shear stress" and "apparent heat flux" for the turbulent motion and $\bar{h}$ is the static enthalpy of the fluid. These terms may be interpreted as convective transports of momentum and energy, respectively.

The relations above are the boundary layer equations for a single chemically homogeneous gas, where, the convective transports functions have been set in an analogous form, and have been assumed to be much greater than the molecular transport functions. With the further assumption of unit turbulent Prandtl number,

$$Pr_T \equiv \frac{\bar{\rho}\,\overline{C_p}\,\epsilon_m}{\epsilon_h} = 1 \tag{6}$$

The Crocco expression becomes

$$\bar{h} = A + B\bar{u} - \frac{\bar{u}^2}{2} \tag{7}$$

and satisfies equation (3). The constants A and B are expressible in terms of the thermodynamic parameters and velocities of the unmixed streams. Letting the subscripts 1 and 2 signify the high and low speed streams, respectively, we have:

$$\bar{h} = \frac{h_1}{(1-\lambda)(1-C_1^2)}\left[\beta - \lambda + (1-\beta)\frac{\bar{u}}{u_1} - C_1^2(1-\lambda)\left(\frac{\bar{u}}{u_1}\right)^2\right] \tag{7a}$$

where:

$$\beta = \frac{h_2 + \frac{u_2^2}{2}}{h_1 + \frac{u_1^2}{2}}$$

$$\lambda = \frac{u_2}{u_1} \leq 1$$

$$C^2 = \frac{\frac{u^2}{2}}{h + \frac{u^2}{2}}$$

In subsequent investigations, the equations of motion for time-mean turbulent flow have been derived from the level of the Navier-Stokes equations. The resultant equations and their derivation appear in reference 2. An apparent discrepancy between the energy equation derived in reference 2 and equation (3) is noted.

Due to the importance of the energy equation in the present study, and due to the uniqueness of the result, an abbreviated derivation is presented here.

3.1.2 Derivation of the Alternate Energy Equation

For the present derivation it is sufficient to begin with the Prandtl boundary layer form of the conservation equations. The conservation equations are:

Mass

$$\frac{\partial \rho u}{\partial x} + \frac{\partial \rho v}{\partial y} = 0 \tag{8}$$

Momentum

$$\frac{\partial \rho u^2}{\partial x} + \frac{\partial \rho v u}{\partial y} = \frac{\partial \left(\mu \frac{\partial u}{\partial y}\right)}{\partial y} \tag{9}$$

Energy

$$\frac{\partial \rho u h}{\partial x} + \frac{\partial \rho v h}{\partial y} = \frac{\partial}{\partial y}\left(\frac{k}{C_p}\frac{\partial h}{\partial y}\right) + \mu\left(\frac{\partial u}{\partial y}\right)^2 \tag{10}$$

The field properties are then assumed to be composed of a time-mean and a fluctuating component such that:

$$(\quad) = \overline{(\quad)} + (\quad)'$$

where

$$\overline{(\quad)} = \frac{1}{\Delta t}\int_{-\frac{1}{2}\Delta t}^{+\frac{1}{2}\Delta t} (\quad)\, dt$$

therefore,

$$\int_{-\frac{1}{2}\Delta t}^{+\frac{1}{2}\Delta t} (\quad)'\, dt = 0 .$$

but in general

$$\int_{-\frac{1}{2}\Delta t}^{+\frac{1}{2}\Delta t} (a)'\,(b)'\,dt \neq 0$$

Where, a' and b' are the fluctuating components of any field properties, a and b. Hence,

$$\overline{(ab)} = \bar{a}\,\bar{b} + \overline{(a'\,b')}$$

and

$$(ab)' = \bar{a}\,b' + a'\,\bar{b}$$

Substituting the expanded form of the field properties into equations 8, 9 and 10 yields for the quantities of mass, momentum and energy:

Mass

$$\frac{\partial}{\partial x}\left[(\bar{\rho} + \rho')(\bar{u} + u')\right] + \frac{\partial}{\partial y}\left[(\bar{\rho} + \rho')(v + v')\right] = 0 \qquad (8a)$$

Momentum

$$\frac{\partial\left[(\bar{\rho} + \rho')(\bar{u} + u')^2\right]}{\partial x} + \frac{\partial\left[(\bar{\rho} + \rho')(\bar{v} + v')(\bar{u} + u')\right]}{\partial y} = \frac{\partial\left[\mu\,\frac{(\bar{u} + u')}{\partial y}\right]}{\partial y} \qquad (9a)$$

Energy

$$\frac{\partial\left[(\bar{\rho} + \rho')(\bar{u} + u')(\bar{h} + h')\right]}{\partial x} + \frac{\partial\left[(\bar{\rho} + \rho')(\bar{v} + v')(\bar{h} + h')\right]}{\partial y} = \frac{\partial}{\partial y}\left[\frac{k}{C_p}\,\frac{\partial(\bar{h} + h')}{\partial y}\right] + \mu\left[\frac{\partial(\bar{u} + u')}{\partial y}\right]^2 \qquad (10a)$$

Note, the fluctuations of the transport properties μ and $\frac{k}{C_p}$ have been ignored. These terms may then be multiplied out and the equations time-averaged.

Mass

$$\frac{\partial\,\overline{(\rho u)}}{\partial x} + \frac{\partial\,\overline{(\rho v)}}{\partial y} = 0 \qquad (8b)$$

Momentum

$$\frac{\partial}{\partial x}\left[(\overline{\rho u})\,\bar{u} + \overline{(\rho u)''\,u'}\right] + \frac{\partial}{\partial y}\left[\overline{(\rho v)}\,\bar{u} + \overline{(\rho v)''\,u'}\right] = \frac{\partial}{\partial y}\left(\mu\frac{\partial \bar{u}}{\partial y}\right) \quad (9b)$$

Energy

$$\frac{\partial}{\partial x}\left[\overline{(\rho u)}\,\bar{h} + \overline{(\rho u)''\,h'}\right] + \frac{\partial}{\partial y}\left[\overline{(\rho v)}\,\bar{h} + \overline{(\rho v)''\,h'}\right] = \frac{\partial}{\partial y}\left[\frac{k}{C_p}\frac{\partial \bar{h}}{\partial y}\right] + \mu\left[\left(\frac{\partial \bar{u}}{\partial y}\right)^2 + \overline{\left(\frac{\partial u'}{\partial y}\right)^2}\right] \quad (10b)$$

where:

$$(ab)'' = (ab)' + a'b'$$

Next, it is assumed that longitudinal fluctuations are small, and in particular, their longitudinal gradients are small, i.e.,

$$\frac{\partial}{\partial y}\left[\overline{(\rho v)''\,u'}\right] >> \frac{\partial}{\partial x}\left[\overline{(\rho u)''\,u'}\right]$$

$$\frac{\partial}{\partial y}\left[\overline{(\rho v)''\,h'}\right] >> \frac{\partial}{\partial x}\left[\overline{(\rho u)''\,h'}\right]$$

and also,

$$\bar{\rho}\,\bar{u} >> \overline{(\rho' u')}$$

we next set

$$-\overline{(\rho v)''\,u'} = \tau_T = \bar{\rho}\,\epsilon_m\,\frac{\partial \bar{u}}{\partial y}$$

and

$$-\overline{(\rho v)''\,h'} = q_T = \frac{\epsilon_h}{C_p}\,\frac{\partial \bar{h}}{\partial y}$$

Employing these assumptions and by use equation 8b, the governing equations are reduced to:

Mass

$$\frac{\partial \bar{\rho}\,\bar{u}}{\partial x} + \frac{\partial \overline{(\rho v)}}{\partial y} = 0 \quad (8c)$$

Momentum

$$\bar{\rho}\,\bar{u}\,\frac{\partial \bar{u}}{\partial x} + \overline{(\rho v)}\,\frac{\partial \bar{u}}{\partial y} = \frac{\partial}{\partial y}\left[(\bar{\rho}\,\epsilon_m + \mu)\,\frac{\partial \bar{u}}{\partial y}\right] \qquad (9c)$$

Energy

$$\bar{\rho}\,\bar{u}\,\frac{\partial \bar{h}}{\partial x} + \overline{(\rho v)}\,\frac{\partial \bar{h}}{\partial y} = \frac{\partial}{\partial y}\left[\left(\frac{\epsilon_h}{C_p} + \frac{k}{C_p}\right)\frac{\partial \bar{h}}{\partial y}\right] + \mu\left[\left(\frac{\partial \bar{u}}{\partial y}\right)^2 + \overline{\left(\frac{\partial u'}{\partial y}\right)^2}\right] \qquad (10c)$$

If one prescribes a consistant order of magnitude to terms in general, the equations may be reduced further by the following techniques:

Let: (1) Time average terms, i.e., $\overline{(\ )}$, be of order unity, except

(2) $\overline{(\rho v)}$ be of order δ

(3) $\frac{\partial}{\partial x}$ be of order unity

(4) $\frac{\partial}{\partial y}$ be of order $\frac{1}{\delta}$

Where δ is a small number (e.g., the mixing layer thickness)

It is observed that the left hand sides of the governing equations are now all of the order unity. In order to have a consistent set of equations, the right hand members must also be of order unity.

We may now determine the order of magnitude for the transport coefficients under the assumptions stated. It is easily recognized that the momentum transport coefficients

$$(\bar{\rho}\,\epsilon_m + \mu) = 0\,(\delta^2)$$

Likewise, the energy transport coefficients may be assumed to be of this order:

$$\left(\frac{\epsilon_h + k}{C_p}\right) = 0\,(\delta^2)$$

in order to satisfy the consistency conditions as well as the assumption that the Prandtl number is of order unity.

Returning to the assumption that the convective transport coefficients are much greater than the molecular transport coefficients, it is implied that

$$\mu \leq 0\,(\delta^3)$$

Then, the last term in equation 10c may be ordered:

$$\mu\left[\left(\frac{\partial \bar{u}}{\partial y}\right)^2 + \overline{\left(\frac{\partial u'}{\partial y}\right)^2}\right] \leq 0\,(\delta^3)\,\left[0\left(\frac{1}{\delta}\right)^2\right]$$

$$\leq 0\,(\delta)$$

Therefore, the molecular transports completely dissappear from the first order governing equations.

The resulting form of the conservation equations parallels equations (1), (2) and (3)

Mass

$$\frac{\partial(\bar{\rho}\bar{u})}{\partial x} + \frac{\partial(\overline{\rho v})}{\partial y} = 0 \tag{8d}$$

Momentum

$$\bar{\rho}\bar{u}\,\frac{\partial \bar{u}}{\partial x} + \overline{(\rho v)}\,\frac{\partial \bar{u}}{\partial y} = \frac{\partial}{\partial y}\left[\bar{\rho}\epsilon_m \frac{\partial \bar{u}}{\partial y}\right] = \frac{\partial \tau_T}{\partial y} \tag{9d}$$

Energy

$$\bar{\rho}\bar{u}\,\frac{\partial \bar{h}}{\partial x} + \overline{(\rho v)}\,\frac{\partial \bar{h}}{\partial y} = \frac{\partial}{\partial y}\left[\frac{\epsilon_h}{C_p}\frac{\partial \bar{h}}{\partial y}\right] = \frac{\partial q_T}{\partial y} \tag{10d}$$

Equations (8d) and (9d) are, respectively, identical to equations (1) and (2). However, in the derivation of present energy equation (equation 10d) no term containing the "apparent shear stress", τ_T, arises, indicating an important discrepancy between equations (3) and (10d).

It is re-emphasized that the essential features of the more detailed development of referenced 2 have been retained in the abbreviated development presented here. Particular attention was paid to the absence from equation (10d) of the $\tau_T \frac{\partial \bar{u}}{\partial y}$ term as shown in the more complete development.

The difference in the form of the energy equation (Eq. 10d) voids the Crocco expression (Eq. 7) as a solution. However, under identical assumptions a new solution may be derived, which is very similar to the Crocco relation. The details of the derivation are contained in reference 2, but the essence of the development originates from the similarity in form of the momentum and energy equations.

For unity turbulent Prandtl number

$$Pr_T \equiv \frac{\epsilon_m C_p}{\epsilon_h} = 1.0$$

Equation 10d may be written as:

$$\bar{\rho}\,\bar{u}\,\frac{\partial \bar{h}}{\partial x} + \overline{(\rho v)}\,\frac{\partial \bar{h}}{\partial y} = \frac{\partial}{\partial y}\left(\bar{\rho}\,\epsilon_m\,\frac{\partial \bar{h}}{\partial y}\right)$$

The similarity in form suggests

$$\bar{h} = \bar{h}(\bar{u})$$

With some manipulation of these relations, one concludes:

$$\bar{h} = A + B\,\bar{u}$$

For the present case, the evaluation of A and B yields:

$$\bar{h} = h_1 \left\{ 1 - \frac{[1 - \beta - C_1^2 (1 - \lambda^2)]\left(1 - \frac{\bar{u}}{u_1}\right)}{(1 - C_1^2)(1 - \lambda)} \right\} \qquad (11)$$

where:

$$\beta = \frac{h_2 + \frac{u_2^2}{2}}{h_1 + \frac{u_1^2}{2}}$$

$$\lambda = \frac{u_2}{u_1} \leq 1.0$$

as in equation 7.

Notice that the Crocco relation indicates a linear relation between the stagnation enthalpy and the streamwise velocity for laminar flow, while equation (11) states that a linear relation exists between the time-mean values of the static enthalpy and the streamwise velocity for turbulent flow.

Although its derivation appears to be straightforward, the revised energy equation has not, as yet, been exposed to the criticism of the open literature, nor is there sufficient data immediately available to verify it completely.* Since there is only a slight algebraic difference in the form of the equations which is finally used, the Crocco

* A recent summary of data was published in AIAA Journal[18] showing the Crocco relation to be inappropriate for hypersonic turbulent boundary layers. Computation by the revised relation shows excellent agreement.

relation (equation 7) and the static enthalpy relation of equation 11, the analysis will be carried out for both equations.

3.1.3 Dissimilar Streams Analysis

In order to extend the equations of motion from the previous section to include more than one chemically homogeneous system, it is necessary to obtain an additional equation and to introduce some elaborations of these already developed.

First, the additional equation is obtained by consideration of the conservation of species. After time averaging and invoking assumptions parallel to those for the other conservation equations, the species equation is:

$$\bar{\rho}\bar{u}\ \frac{\partial \bar{c}_i}{\partial x} + \overline{(\rho v)}\ \frac{\partial \bar{c}_i}{\partial y} = \frac{\partial}{\partial y}\left[\bar{\rho}\epsilon_i\ \frac{\partial \bar{c}_i}{\partial y}\right] + \dot{w}_i \qquad (12)$$

where:

$\bar{c}_i$ = Mass Concentration of i^{th} species

$$\bar{\rho}\epsilon_i\ \frac{\partial \bar{c}_i}{\partial y} \equiv -\overline{(\rho v)''\ c_i'} \qquad (13)$$

and

$\dot{w}$ = Mass rate of production (or destruction) of i^{th} species.

For the non-reacting system:

$$\dot{w}_i = 0$$

When concentration fluctuations are introduced into the equations of motion additional correlations survive the time averaging process. A redefinition of the convective transport is in order due to these additional terms. In particular

$$q_T = \frac{\epsilon_h}{C_p} \sum_i \overline{\left(c_i\ \frac{\partial h_i}{\partial y}\right)} + \bar{\rho}\epsilon_c \sum_i \overline{\left(h_i\ \frac{\partial c_i}{\partial y}\right)}$$

$$= -\overline{(\rho v)''\ \sum_i (c_i h_i)'} - \overline{(\rho v)'\ \sum_i c_i'\ h_i'} \qquad (14)$$

Noting that

$$\sum_i \overline{\left(c_i \frac{\partial h_i}{\partial y}\right)} + \sum_i \overline{\left(h_i \frac{\partial c_i}{\partial y}\right)} = \frac{\partial \bar{h}}{\partial y} \tag{15}$$

We define two turbulent Lewis numbers

$$LE_{T_i} = \frac{\bar{\rho}\, \epsilon_i\, \bar{c}_p}{\epsilon_h} \tag{16}$$

$$LE_T = \frac{\bar{\rho}\, \epsilon_c\, \bar{c}_p}{\epsilon_h} \tag{17}$$

However, it will be assumed that

$$\epsilon_i = \epsilon_c \tag{18}$$

and thus,

$$LE_{T_i} = LE_T \tag{19}$$

since turbulent convection of a species should be essentially independent of its molecular properties.

Examination of equations (13) and (14) reveals that ϵ_i is dependent only on the concentration fluctuations, whereas ϵ_c is also dependent on the enthalpy fluctuation. The additional parameter involved in ϵ_c could differentiate it from ϵ_{c_i} thus suggesting a relation between these parameters similar to that between the molecular and molecular plus thermal diffusion coefficients of laminar flows. The difference between these coefficients in laminar flows is usually negligible, therefore, this assumption is arbitrarily extended to turbulent flows as indicated by equations (18) and (19).

Next, we impose the assumption that both the turbulent Lewis and Prandtl numbers are unity. These assumptions allow the retention of the previous relations equations (3) and (7) or equations (10c) and (11), for the energy equation. Equation (12) may be treated similarly. In the absence of chemical reaction, $\dot{w}_i$ vanishes, and with the unity Prandtl and Lewis number assumptions, equation (12) may be written in a form similar to the momentum equation.

$$\bar{\rho}\,\bar{u}\,\frac{\partial \bar{c}_i}{\partial x} + \overline{(\rho v)}\,\frac{\partial \bar{c}_i}{\partial y} = \frac{\partial\left(\bar{\rho}\,\epsilon_m \frac{\partial \bar{c}_i}{\partial y}\right)}{\partial y} \tag{12a}$$

This form suggest the relation:

$$\bar{c}_i = \bar{c}_i\ (\bar{u}) \tag{20}$$

Imposing equation (20) on equation (12a) and employing the momentum equation, equation (2) and the definition of equation (4), yields:

$$0 = \bar{\rho}\epsilon_m \left(\frac{\partial \bar{u}}{\partial y}\right)^2 \frac{\left(\frac{d^2 \bar{c}_i}{d\bar{u}^2}\right)}{\left(\frac{d\bar{c}_i}{d\bar{u}}\right)}$$

Which has a solution:

$$\bar{c}_i = A_i + B_i \bar{u} \tag{21a}$$

analogous to the enthalpy relations of equation (11) or equation (7). Just as in those equations, the constant A and B are expressible in terms of the parameter values in the unmixed streams.

$$\bar{c}_i = \frac{{}^1c_i}{1-\lambda} \left[\xi - \lambda + (1-\xi)\frac{\bar{u}}{u_1}\right] \tag{21b}$$

where $\xi = \dfrac{{}^2c_i}{{}^1c_i}$ = Concentration ratio of the i^{th} species in streams 1 and 2.

${}^jc_i$ = Concentration of i^{th} species in j^{th} stream

Before proceeding into the formulation of the mixing analysis, one more consequence of the assumptions already imposed will be discussed. The relation indicated by equation (18) also implies that all the mass transfer coefficients, ϵ_i, of the various species are equal.

Consider two streams, each composed of multiple chemical species in homogeneous mixtures. Upon exposing the two streams to each other, all gradients of concentration differences for species between the streams are identical. If their mass transport coefficients are also equal, they will diffuse through the mixing zone at the same rate. The relative concentrations of the species from a given stream will, then, remain unchanged at any position in the mixing zone. However, this is equivalent to each stream behaving as a single species.

Thus, under the present assumptions, each homogeneous stream, no matter what its detailed composition, may be treated as a single species in the mixing study. Therefore, it is only necessary to treat the mixing of two dissimilar gases, each having the average chemical and thermodynamic properties of their respective mixtures.

The constants in equation 21a may now be evaluated for the present mixing study problem as were the constants in the previous enthalpy relations (equations 7 and 11). The concentration field of the primary (higher speed stream) stream species in the mixing zone may be expressed as:

$$\bar{c}_1 = \left(\frac{\bar{u}}{u_1} - \lambda\right) \frac{1}{1-\lambda} \tag{22}$$

The concentration of the secondary stream species is

$$\bar{c}_2 = \left(1 - \frac{\bar{u}}{u_1}\right) \frac{1}{1-\lambda} \tag{23}$$

Knowing the concentration field, other useful parameters may also be determined. For example, the average molecular weight field may be determined for a mixture of perfect gases.

Since

$$\hat{W} = \frac{W_1 \; W_2}{\bar{c}_1 W_2 + \bar{c}_2 W_1} = \frac{\rho R_o T}{p} \tag{24}$$

$$\hat{W} = \frac{W_1 \, \omega \, (1-\lambda)}{1 - \omega\lambda - (1-\omega)\,\frac{\bar{u}}{u_1}}$$

Also, the average specific heat field

$$\hat{C}_p = \bar{c}_1 \, C_{p_1} + \bar{c}_2 \, C_{p_2}$$

$$\hat{C}_p = \frac{\left[\alpha - \lambda + (1-\alpha)\,\frac{\bar{u}}{u_1}\right] \; C_{p_1}}{1-\lambda} \tag{25}$$

where:

$$\omega = \frac{W_2}{W_1}$$

$$\alpha = Cp_2 / Cp_1$$

This equation along with equation 7 or 11 will be necessary to evaluate the compressibility transformation in the next section.

3.1.4 The Compressibility Transformation

The transformation of the mass and momentum conservation equations to the form for an incompressible flow is shown in reference 1. As a point of reference, the transformation is briefly repeated here.

Beginning with equations 1 and 2 (which are equivalent to equations 8d and 9d, respectively):

Mass

$$\frac{\partial \bar{\rho}\,\bar{u}}{\partial x} + \frac{\partial \overline{(\rho v)}}{\partial y} = 0 \tag{1}$$

Momentum

$$\bar{\rho}\,\bar{u}\ \frac{\partial \bar{u}}{\partial x} + \overline{(\rho v)}\ \frac{\partial \bar{u}}{\partial y} = \frac{\partial\, {}^{\tau}T}{\partial y} \tag{2}$$

We apply the Howarth Transformation defined by:

$$x^* = x, \quad y^* = \int_o^y \frac{\rho}{\rho_r}\, dy \tag{26}$$

where ρ_r is the density at some reference state, i.e., ρ_r = constant. We further define a set of stream functions:

$$\psi = \int_o^y \bar{\rho}\,\bar{u}\, dy = -\int_o^x \overline{(\rho v)}\, dx \tag{27}$$

$$\psi^* = \int_o^{y^*} \rho_r u^*\, dy^* = -\int_o^{x^*} \rho_r v^*\, dx^* \tag{28}$$

If we set

$$\psi^* = \psi \tag{29}$$

and, thus, $\bar{u} = u^*$, it is found that equation 2 is transformed to

$$\rho_r u^* \frac{\partial u^*}{\partial x^*} + \rho_r v^* \frac{\partial u^*}{\partial y^*} = \frac{\partial\, (\tau_T)}{\partial y^*} \tag{30}$$

It is recalled now that the momentum equation for an incompressible boundary layer of density ρ_r is:

$$\rho_r u^* \frac{\partial u^*}{\partial x^*} + \rho_r v^* \frac{\partial u^*}{\partial y^*} = \frac{\partial(\tau_T^*)}{\partial y^*} \tag{31}$$

Thus, if one can find a constant density flow field in which the local shear stress τ_T^* is equal to the local shear stress for the compressible flow field, τ_T, the Howarth transformation is the mapping function between the two flow fields. That is, the constant density flow field in the $x^* - y^*$ plane has a one to one correspondence to the compressible flow field in the x-y plane. The Howarth transformation, then, prescribes this correspondence in terms of the ratio of the local density to the density of the incompressible flow, ρ/ρ_r.

3.1.5 Solutions in the Incompressible Domain

Before entering into the approach to determining a density which satisfies these conditions, it is worthwhile to note the conditions for which constant density flow solutions have been found.[5] It is sufficient for the study of mixing flows to apply the approach to self-similar flow fields. That is, flow fields which may be described by a single independent variable, called a similarity variable.

For turbulent boundary layer flows, it is found that there exists a variable, η, which transforms the equations of motion from partial differential equations to ordinary differential equations.

where η is defined as

$$\eta = \frac{\sigma^* y^*}{x^*} = \frac{\sigma y}{x} \tag{32}$$

in terms of the incompressible and compressible plane coordinates, respectively.

where: σ = the jet spread parameter for mixing in the physical plane

σ^* = the jet spread parameter for mixing in the incompressible plane.

In reference 1 it was shown that the two approximations for eddy viscosity, i.e., Prandtl's mixing length concept:

$$\epsilon_m = \ell^2 \frac{\partial \bar{u}}{\partial y} \tag{33}$$

where:

$$\ell = kx \tag{34}$$

and the constant transport coefficient model:

$$\epsilon_m = k (u_1 - u_2) x \tag{35}$$

will yield the solutions to equation (31) corresponding, respectively to the Tollmein[6] solution, later extended by Keuthe[7]; and to the Gortler[8] solution, improved by Crane[9].

At present, there is considerable difference of opinion as to which of the two eddy viscosity formulations is the more representative of free jet mixing flows. In reference 1, it appeared that the Tollmein velocity profile was slightly superior to the Gortler. However, the Gortler error function profile is far more widely used today. It is difficult to assess whether or not the ease of application plays the determining role in the usage frequency of the two formulations.

3.1.6 The Reference State

The transformation of the compressible flow equations to an equivalent incompressible flow was completed only when it was assumed that a constant density flow could be found in which the local shear stress gradient, $\frac{\partial \tau_{T^*}}{\partial y}$, was equal to that for the compressible flow, $\frac{\partial \tau_T}{\partial y}$. This constant density is defined to be the reference state which we will describe in terms of boundary conditions of the flow field.

(A) Fundamental Concepts

In reference 1 it was noted that the reference enthalpy suggested by Eckert[10] for high speed boundary layers was determined such that the local skin friction on a flat plate could be calculated by a constant property solution evaluated at the reference state. Thus, the results presented herein and Eckert's results bears a similarity. The form of Eckert's reference enthalpy was therefore, adopted to evaluate the reference state for free jets. It was recognized that there would be some modification to the empirical constants necessitated by the absence of a solid boundary.

The analysis of reference 1 chose the reference temperature form of the reference state equation. This is equivalent to the reference enthalpy for gases with constant specific heats. Thus, for small temperature differences between streams, i.e, differences small enough that the specific heat of the gas may be assumed independent of temperature the following reference state equation was used:

$$\frac{T_r}{T_1} = 1 + A\left(\frac{T_2}{T_1} - 1\right) + B\frac{(u_1 - u_2)^2}{2\,C_p\,T_1} \qquad (36a)$$

where $(u_1 - u_2)$ is the relative velocity of the free streams. For larger temperature differences a reference enthalpy was employed.

$$\frac{h_r}{h_1} = 1 + A\left(\frac{h_2}{h_1} - 1\right) + B\frac{(u_1 - u_2)^2}{2h_1} \qquad (36b)$$

Eckert found that the same coefficients, A and B applied for both equations when considering flow over flat plate. Sufficient data for large temperature differences was not available to make such a comparison for free jets.

Before considering the complication of changes of specific heat due to composition gradients, the motivation for the third term appearing on the right hand side of each of these equations should be discussed.

For flow past solid boundaries one customarily fixes the reference frame on a solid boundary. Once the reference frame is fixed, the flow velocity is expressed in terms of the relative velocity of the flow with respect to the boundary. It should be noted that until this reference is established, the stagnation or total enthalpy of the flowing medium is not fixed. That is, the stagnation conditions are variant under a Galilean transformation.

The only solid boundary for the free jet mixing flow is the separating plate before the beginning of the mixing zone. Although this has been chosen as the boundary at which the reference frame is to be fixed, one would expect that any analogy between the boundary layer on a plate and the mixing of parallel flowing streams would be in relative terms.

Above, we have merely inserted the relative velocity of the streams in analogy to the relative velocity of flow past a solid object. There has been no overt physical justification for this approach. Let us now propose to establish the operative flow properties for determining the reference state.

Certainly, we would expect the relative momenta of the streams to be important since one of the purposes of the reference condition is the transformation of the shear stress. This leads us to the use of the relative velocity of the streams and the expressions (36a) and 36b).

But, is the relative kinetic energy of the streams not also important? One would expect it to be since it is necessary to establish the thermodynamic states of the streams.

The relative kinetic energy of the streams is not obtained by squaring the relative velocity. It is necessary to augment equations 36 by a term containing the difference of the squares of the absolute stream velocities.

Next, the possibility of the interaction of these terms must not be overlooked. A term added to account for this interaction would take the form:

$$\frac{(u_1 - u_2)\,(u_1^2 - u_2^2)}{2C_p T_1}^{\frac{1}{2}}$$

However, before proceeding further, let us re-examine our intent. First we are seeking a semi-empirical formula for obtaining the reference condition. Each of the velocity terms discussed will be weighted by a constant which is to be determined from experimental data. And last, the interaction term is at most of second order.

Thus, it would appear to be appropriate to relax the structure of our "formula" to represent the essence of the physical considerations discussed, and to allow for greater ease in evaluation of the data. We will therefore, regroup the velocity terms into a general quadratic form in u_1 and u_2, yielding

$$\frac{T_r}{T_1} = 1 + A\left(\frac{T_2}{T_1} - 1\right) + \frac{Bu_1^2 + Du_1u_2 + Eu_2^2}{2C_pT_1} \qquad (37a)$$

or

$$\frac{h_r}{h_1} = 1 + A\left(\frac{h_2}{h_1} - 1\right) + \frac{Bu_1^2 + Du_1u_2 + Eu_2^2}{2h_1} \qquad (37b)$$

The constants A, B, D, and E to be evaluated empirically.

It is noted in passing that the analysis of reference 1 was dealing almost totally with data for which $u_2 = 0$. For this condition, equations 36 and 37 have identical forms.

(B) Effect of Composition Gradients

In the previous section, when considering the stagnation potential for the free jets, effects due to changes in composition did not enter. However, when the mixing of dissimilar gases is considered, the temperature or enthalpy alone is not sufficient to establish directly the thermodynamic state of the reference condition. The composition must also be specified before the state properties, such as the density, can be determined.

Several representations for reference compositions have been suggested for boundary layers with mass addition.[11, 12, 13] Pai[14] also considers an effective density for jet flows. However, these all exhibit considerable arbitrariness as to the physical processes which are assumed to be controlling. Further, the processes chosen as being dominant for the boundary layer with mass addition, as in some of the referenced papers, are not clearly pertinent to free jet flows. Therefore, we will retain the previous form of the reference equations 37. These will now be restated in terms of non-dimensional parameters C_1^2, β, and λ. Thus, the reference temperature relation becomes

$$\frac{T_r}{T_1} = \frac{1 - A(1-\beta) + C_1^2 \left[A + B - 1 + D\lambda - (A-E)\lambda^2\right]}{1 - C_1^2} \qquad (38a)$$

The corresponding reference enthalpy expression is of identical form except the coefficients A, B, D, and E may be a function of primary and secondary stream composition.

$$\frac{h_r}{h_1} = \frac{1 - A(1-\beta) + C_1^2 \left[A + B - 1 + D\lambda - (A-E)\lambda^2\right]}{1 - C_1^2} \qquad (38b)$$

It is seen that in this simple extension, the expressions are equivalent when the gases are identical. However, when the specific heats of the different gases are merely independent of temperature, the reference enthalpy and reference temperature expressions are not identical. The specific heat ratio of the primary and secondary streams remains in equation (38b).

In order to complete the evaluation of the reference state, it is still necessary to establish the composition of the reference state. Recalling the relation between the velocity, enthalpy and concentration derived in an earlier section for unity Prandtl and Lewis number, it is noted that for unity Lewis number, the enthalpy and concentration distributions within the mixing zone may be related.

For two homogeneous but dissimilar streams, the relation is:

$$\bar{H}\ (\eta) = H_2 + (H_1 - H_2)\ \bar{c}_1\ (\eta) \qquad (39a)$$

for the Crocco form of the energy equation and

$$\bar{h}\ (\eta) = h_2 + (h_1 - h_2)\ \bar{c}_1\ (\eta) \qquad (39b)$$

for the revised enthalpy form of the energy equation

The specific heat at any point in the mixing zone will then be determined by

$$C_p\ (\eta) = C_{p_2} + (C_{p_1} - C_{p_2})\ \bar{c}_1\ (\eta) \qquad (40)$$

where $\bar{c}_1$ is input from either equation (39a) or (39b).

Eckert[10] and later Burgraf[15] established that the flat plate reference enthalpy for unity Prandtl number was the stagnation enthalpy of some point within the boundary layer. By extending this concept to the jet mixing region and by employing equations (40) and (39a) or (39b) the reference condition for dissimilar streams may be completely determined by solving either equation (38a) or (38b). The reference density is then determined from the equation of state (e.g. perfect gas).

The constants A, B, D, and E in equation (38a) and (38b) are to be determined experimentally. The probable value of the constant "A", however, is 1/2, since this value is necessary to make the reference state independent of the selection of the primary stream.

3.1.7 Evaluation of the Transformation

The next task was to relate the transformed and physical coordinates of the flow field. The compressibility transformation provides the necessary functional relation in integral form. In order to evaluate the integral it is necessary to express the density field in terms of known quantities. In this case, the known quantities are assumed to be the boundary conditions on the mixing zone. The results of the previous section provide these required expressions.

The compressibility transformation for self-similar flows may be stated in the form.

$$\frac{\sigma^* y}{x} = \frac{\rho_r}{\rho_1} \int_0^{\eta} \frac{\rho_1}{\bar{\rho}} \, d\xi \qquad (41)$$

where $\eta = \dfrac{\sigma^* y^*}{x^*} = \dfrac{\sigma y}{x}$

$\dfrac{\rho_1}{\bar{\rho}}$ In order to evaluate the integral of equation (41), the integrand , must be stated in terms of η . We note that for the present case, where the pressure is everywhere constant:

$$h = h(\rho_i, c_i)$$

For conciseness we will assume that we are dealing with perfect gases with constant specific heats. For such gases,

$$\frac{\bar{\rho}_1}{\bar{\rho}} = \frac{\bar{T}}{\bar{T}_1} \frac{\bar{W}_1}{\hat{W}} = \frac{\bar{h}}{h_1} \frac{C_{p_1} W_1}{\hat{C}_p \hat{W}} \qquad (42)$$

By introducing equations (22), (23), (24) and (25), the density ratio will be expressed in terms of the enthalpy and the velocity profiles

$$\frac{\bar{\rho}_1}{\bar{\rho}} = \frac{1 - \omega\lambda - (1 - \omega) \dfrac{\bar{u}}{\bar{u}_1}}{\omega \left[\alpha - \lambda + (1 - \alpha) \dfrac{\bar{u}}{\bar{u}_1} \right]} \frac{\bar{h}}{h_1} \qquad (43)$$

To complete the expression, one of the two relations between the enthalpy and velocity fields may be substituted for the indicated term above.

(A) Formulation with the Crocco Relation

First, we will evaluate the transformation using the Crocco enthalpy formulation. This will represent a straightforward extension of the analysis in reference (1) to incorporate the results obtained for dissimilar streams.

A simple substitution of equation (7a) into equation (43) yields:

$$\frac{\bar{\rho}_1}{\bar{\rho}} = \frac{1 - \omega\lambda - (1-\omega)\frac{\bar{u}}{\bar{u}_1}}{\omega\left[\alpha - \lambda + (1-\alpha)\frac{\bar{u}}{\bar{u}_1}\right]} \quad \frac{\beta - \lambda + (1-\beta)\frac{u}{u_1} - C_1^2(1-\lambda)\left(\frac{u}{u_1}\right)^2}{(1-\lambda)(1-C_1^2)} \tag{44a}$$

Which may be put in form for numerical evaluation of the integral of equation (41).

$$\frac{\bar{\rho}_1}{\bar{\rho}} = a \cdot b \, \frac{d - \phi'}{f + \phi'} \left[k + \ell\,\phi' - \phi'^2\right] \tag{44b}$$

where:

$$a = \frac{1-\omega}{\omega(1-\alpha)}$$

$$b = \frac{C_1^2}{(1 - C_1^2)}$$

$$f = \frac{\alpha - \lambda}{1 - \alpha}$$

$$d = \frac{1 - \omega\lambda}{1 - \omega}$$

$$k = \frac{\beta - \lambda}{(1-\lambda)C_1^2}$$

$$\ell = \frac{1 - \beta}{(1-\lambda)C_1^2}$$

$$\phi' = \frac{d\phi}{d\eta} = \frac{\bar{u}}{u_1}$$ the normalized velocity profile

(B) Formulation with the Revised Enthalpy Relation

The density ratio, $\frac{\rho_1}{\bar{\rho}}$, of the integral transformation, equation (41), may be alternatively evaluated by means of the revised enthalpy - velocity relation whose derivation was shown earlier. Again, the density profile may be expressed in terms of that velocity profile. Substitution of equation (11) into equation (43) yields the desired expression.

$$\frac{\bar{\rho}_1}{\bar{\rho}} = \frac{1 - \omega\lambda - (1-\omega)\frac{\bar{u}}{\bar{u}_1}}{\omega\left[\alpha - \lambda + (1-\alpha)\frac{\bar{u}}{\bar{u}_1}\right]} \left[\frac{1 - \beta - C_1^2(1-\lambda^2)}{(1 - C_1^2)(1-\lambda)}\left(\frac{\bar{u}}{\bar{u}_1} - 1\right) + 1\right] \tag{45a}$$

The simplified form of equation (45a) for numerical evaluation is:

$$\frac{\bar{\rho}_1}{\bar{\rho}} = a \cdot g \frac{d - \phi'}{f - \phi'} \quad (m + \phi') \tag{45b}$$

where:

a, d, f as for the Crocco formulation

$$g = \frac{(1 - \beta) - C_1^2 (1 - \lambda^2)}{(1 - C_1^2)(1 - \lambda)}$$

$$m = \frac{1}{g} - 1$$

The Runge-Kutta numerical integration routine was used to evaluate the integral of equation (41).

3.1.8 Streamwise Pressure Gradient Analysis

The problem of mixing parallel compressible streams in a streamwise pressure gradient field is analyzed using the "building blocks" obtained in the zero pressure gradient analysis. However, we move to a more general transformation family, of which the Howarth[4] transformation is the member corresponding to zero pressure gradient.

(A) Theoretical Development

The generalized transformation begins in the identical manner as the Coles[16]-Crocco[17] transformation.

Let

$$\frac{\psi_*}{\psi} = a(x) \tag{46}$$

$$\frac{dx_*}{dx} = b(x) \tag{47}$$

$$\frac{\partial y_*}{\partial y} = g(x) \frac{\rho}{\rho_*} \tag{48}$$

where ρ_* is the reference density, a constant.

The velocities are obtained from the stream function in the usual manner.*

$$\psi_{*_{y_*}} = \rho_* u, \quad \psi_{*_{x_*}} = -\rho_* v_* \tag{49}$$

$$\psi_y = \bar{\rho}\,\bar{u}, \quad \psi_x = -\overline{(\rho v)} \tag{50}$$

Equations (46), (48), (49) and (50) yield

$$\frac{u}{u_*} = \frac{g}{a} \tag{51}$$

Applying these relations, the x-momentum equation may be transformed to

$$\rho_* u_* u_{*_{x_*}} + \rho_* v_* u_{*_{y_*}} = \frac{1}{b}\left(\frac{a}{g}\right)^2 \frac{\rho_*}{\bar{\rho}} \left[-\frac{dp}{dx} - \bar{u}^2 \frac{d \ln g/a}{dx}\right.$$

$$\left. - \psi \frac{d \ln a}{dx} \bar{u}_y + \frac{\partial \tau_T}{\partial y}\right] \tag{52}$$

Here we specialize the Coles transformation by setting specific functions in place of a, b, and g.

$$a = g = \left(\frac{p}{p(0)}\right)^{-\frac{1}{2}}, \quad b = 1 \tag{53}$$

where $p(0) = p\ (x = 0)$

This transformation is a form similar to that of Low.[3] Equation (52) then becomes

$$\rho_* u_* u_{*_{x_*}} + \rho_* v_* u_{*_{y_*}} = -\rho_* p_x \left(\frac{1}{\rho} - \frac{1}{2}\frac{1}{p}\frac{\psi_*}{\bar{\rho}_*} u_{*_{y_*}}\right)$$

$$+ \left(\frac{p}{p(0)}\right)^{-\frac{1}{2}} \tau_{T_{y_*}} \tag{54}$$

The energy equation for turbulent boundary layers derived in an earlier section** is transformed from

---

* The shorthand notation $\frac{\partial(\ )}{\partial x} = (\ )_x$ will henceforth be employed.

** The development using the Laminar form of the energy equation is shown by Low[3] in all its essential features. The treatment of the secondary stream is easily included as outlined in the present analysis.

$$\bar{\rho}\bar{u}\,\bar{h}_x + \overline{(\rho v)}\,\bar{h}_y = \bar{u}\,p_x + q_{T_y} \tag{55}$$

to

$$\rho_* u_* h_{x_*} + \rho_* v_* h_{y_*} = \rho_* p_x \left[\frac{u_*}{\rho} + \frac{1}{2}\left(\frac{1}{p}\right) \frac{\psi_*}{\rho_*} h_{y_*}\right] + \left(\frac{p}{p(0)}\right)^{-\frac{1}{2}} \left(\frac{\tau_T}{Pr_T} \frac{h_y}{u_y}\right)_{y_*} \tag{56}$$

Next, we examine the flow in the free streams. In these regions, it is assumed that the transverse gradients vanish, therefore,

$$\rho_\infty u_\infty u_{\infty x} = -\frac{dp}{dx} = \rho_{-\infty} u_{-\infty} u_{-\infty x} \tag{57}$$

For adiabatic flow:

$$H_1 = h_\infty + \frac{u_\infty^2}{2} = h_{o_1} + \frac{u_{o_1}^2}{2}$$
$$H_2 = h_{-\infty} + \frac{u_{-\infty}^2}{2} = h_o + \frac{u_{o_2}^2}{2} \tag{58}$$

and for isentropic flow

$$\frac{p_1}{\rho_1^\gamma} = \frac{p_{t_1}}{\rho_{t_1}^\gamma}, \quad \frac{p_2}{\rho_2^\gamma} = \frac{p_{t_2}}{\rho_{t_2}^\gamma} \tag{59}$$

We note from Eq. (59) that for $p_1 = p_2$

$$\frac{\rho_2}{\rho_1} = \frac{\left(\frac{p_2}{p_{t_2}}\right)^{\frac{1}{\gamma}}}{\left(\frac{p_1}{p_{t_1}}\right)^{\frac{1}{\gamma}}} \qquad \frac{\rho_{t_2}}{\rho_{t_1}} = \frac{\rho_{t_2}}{\rho_{t_1}} \left(\frac{p_{t_1}}{p_{t_2}}\right)^{\frac{1}{\gamma}} = \text{constant} \tag{60}$$

We note that the relation (60) holds as long as γ for both streams is the same.

We introduce the following usual constructions for τ_T and q_T.

$$\tau_T = \bar{\rho}\,\epsilon\,\bar{u}_y$$

$$q_T = \frac{\epsilon_h}{C_p}\,\bar{h}_y$$

Then

$$Pr_T \equiv \frac{\bar{\rho} C_p}{\epsilon_h} = \frac{\tau_T}{q_T}\,\frac{\bar{h}_y}{u_y}$$

Imposing the transformation on these terms yields

$$\tau_T = \left(\frac{p}{p(0)}\right)^{-\frac{1}{2}} \frac{\bar{\rho}^2}{\rho_*}\,\epsilon\,\bar{u}_{y_*}$$

$$q_T = \left(\frac{p}{p(0)}\right)^{-\frac{1}{2}} \frac{\bar{\rho}^2}{\rho_*}\,\frac{\epsilon}{Pr_T}\,h_{y_*}$$

If we set

$$\epsilon_* = \left(\frac{p}{p(0)}\right)^{-1} \left(\frac{\bar{\rho}}{\rho_*}\right)^2 \epsilon \tag{61}$$

We find that

$$\tau_T = \left(\frac{p}{p(0)}\right)^{\frac{1}{2}} \rho_*\,\epsilon_*\,u_{y_*} \tag{62}$$

$$q_T = \left(\frac{p}{p(0)}\right)^{-\frac{1}{2}} \frac{\rho_*\,\epsilon_*}{Pr_T}\,h_{y_*} \tag{63}$$

Substitution of (62), (63) and (57) into (54) and (56) results in

$$u_* u_{*_{x_*}} + v_* u_{*_{y_*}} = \frac{u_\infty u_\infty x}{h_\infty}\left[\bar{h} - \frac{1}{2}\,\frac{\gamma}{\gamma - 1}\,\frac{\psi_*}{\rho_*}\,u_{*_{y_*}}\right] + (\epsilon_* u_{*_{y_*}})_{y_*} \tag{64}$$

$$u_* \bar{h}_{x_*} + v_* \bar{h}_{y_*} = -u_\infty u_\infty x\left[\bar{h} u_* + \frac{1}{2}\,\frac{\gamma}{\gamma - 1}\,\frac{\psi_*}{\rho_*}\,\bar{h}_{y_*}\right] + \left(\frac{\epsilon_*}{Pr_T}\,\bar{h}_{y_*}\right)_{y_*} \tag{65}$$

where the perfect gas relation has been introduced along with the uniform cross sectional pressure to obtain

$$\frac{\rho_\infty}{\rho} = \frac{h}{h_\infty} \tag{66}$$

and

$$\frac{\rho_\infty}{p} = \frac{\gamma}{\gamma - 1} \frac{1}{h_\infty} \tag{67}$$

We may now proceed to solve the problem in the transformed plane.

(B) Perturbation Expansion for Small Pressure Gradients

We wish to obtain solutions valid for isentropic flows with uniform cross sectional properties in the free stream. Of necessity, this restricts us to small streamwise pressure gradients, particularly in the case of supersonic streams. In the latter instance, the restriction enters on two counts: The uniformity of the free streams and the maintenance of isentropic flow in the instance of positive pressure gradients. Accordingly, we introduce a velocity gradient of the following form in the free stream:

$$\begin{aligned} u_\infty &= u_{o_1} + \alpha u_{11}(x) + 0(\alpha^2) \\ u_{-\infty} &= u_{o_2} + \alpha u_{12}(x) + 0(\alpha^2) \end{aligned} \tag{68}$$

where: α is a small number

These conditions are now generalized to the field properties themselves.

$$u_*(x, y_*) = u_o(x, y_*) + \alpha u_1(x, y_*) + 0(\alpha^2) \tag{69a}$$

$$v_*(x, y_*) = v_o(x, y_*) + \alpha v_1(x, y_*) + 0(\alpha^2) \tag{69b}$$

$$\psi_*(x, y_*) = \psi_o(x, y_*) + \alpha \psi_1(x, y_*) + 0(\alpha^2) \tag{69c}$$

$$h(x, y_*) = h_o(x, y_*) + \alpha h_1(x, y_*) + 0(\alpha^2) \tag{69d}$$

$$\epsilon_*(x) = \epsilon_*(x) + \alpha \epsilon_1(x) + 0(\alpha^2) \tag{69e}$$

We further take the following form for the transformed stream function

$$\psi_* = \rho_* \phi(x, y_*) \tag{70}$$

Thus

$$u = u_* = \phi_{y_*} \tag{71}$$

Introducing these expansions into the free stream energy equation results in simplification of the boundary conditions:

$$h_\infty + \frac{u_\infty^2}{2} = H_1 \qquad = \text{constant for adiabatic flow}$$

$$h_{-\infty} + \frac{u_{-\infty}^2}{2} = H_2 \qquad = \text{constant for adiabatic flow}$$

Introducing the expansions and solving for h_∞ and $h_{-\infty}$

$$h_{o_1} + \alpha h_{11} + 0(\alpha^2) = H_1 - \frac{1}{2} \left[u_{o_1}^2 + 2\alpha u_{o_1} u_{11} + 0(\alpha^2) \right]$$

Similarly

$$h_{o_2} + \alpha h_{12} + 0(\alpha^2) = H_2 - \frac{1}{2} \left[u_{o_2}^2 + 2\alpha u_{o_2} u_{12} + 0(\alpha^2) \right]$$

Setting

$$H = h_o + \frac{u_o^2}{2} \qquad = \text{conditions where mixing begins}$$

And substituting, we obtain

$$h_{o_1} + \alpha h_{11} = h_{o_1} - \alpha u_{o_1} u_{11}$$

and (72)

$$h_{o_2} + \alpha h_{12} = h_{o_2} - \alpha u_{o_2} u_{12}$$

Now substitution of the expansions into the transformed momentum and energy equation we may set up an ordered solution process for the individual forms.

(a) Zeroeth Order Problem; $0(\alpha^\circ)$

Momentum

$$u_o u_{o_{x_*}} + v_o u_{o_{y_*}} = (\epsilon_{o_*} u_{o_{y_*}})_{y_*} \tag{73}$$

Energy

$$u_o h_{o_{x_*}} + v_o h_{o_{y_*}} = \left(\frac{\epsilon_{o_*}}{Pr_T} h_{o_{y_*}}\right)_{y_*} \tag{74}$$

(b) Boundary Conditions

$$u_o(x_*, \infty) = u_{o_1},\ u_o(x_*, -\infty) = u_{o_2},\ u_o(x_*, o) = \frac{1+\lambda_o}{2}$$

or

$$\phi_o(x_*, o) = 0 \tag{75}$$

$$h_o(x_*, \infty) = h_{o_1},\ h_o(x_*, -\infty) = h_{o_2} \tag{76}$$

where

$$\lambda_o = \frac{u_{o_2}}{u_{o_1}}$$

and

$$u_o = \phi_{o_{y_*}}$$

(b) First Order Problem; $0(\alpha)$

Momentum

$$u_o u_{1_{x_*}} + u_1 u_{o_{x_*}} + v_o u_{1_{y_*}} + v_1 u_{o_{y_*}} =$$

$$\frac{u_{o_1} u_{11_{x*}}}{h_{o_1}} \left(h_o - \frac{1}{2} \frac{\gamma}{\gamma - 1} \phi_o u_{o_{y_*}}\right) + \frac{1}{\rho_*}\left[\rho_* \left(\epsilon_{o*} u_{1_{y_*}} + \epsilon_{1*} u_{o_{y_*}}\right)\right]_{y_*} \tag{77}$$

Energy

$$u_o h_{1_{x_*}} + u_1 h_{o_{x_*}} + v_o h_{1_{y_*}} + v_1 h_{o_{y_*}} =$$

$$- \frac{u_{o_1} u_{11x*}}{h_{o_1}} \left(h_o u_o + \frac{1}{2} \frac{\gamma}{\gamma - 1} \phi_o h_{o_{y_*}}\right) + \frac{1}{\rho_*}\left[\frac{\rho_*}{Pr_T} \left(\epsilon_{o_*} h_{1_{y_*}} + \epsilon_1 h_{o_{y_*}}\right)\right]_{y_*} \tag{78}$$

Boundary Conditions

$$u_1(x_*, \infty) = u_{11}(x_*),\ u_1(x_*, -\infty) = u_{12}(x_*),\ u_1(o, y_*) = 0 \qquad (79)$$

or

$$\phi_1(x_*, o) = 0$$

$$h_1(x_*, \infty) = h_{11}(x_*),\ h_1(x_I, -\infty) = h_{12}(x_*) \qquad (80)$$

(c) General Solution for Zeroth Order Problem - Enthalpy Field in Velocity Space

Before proceeding to the solution of these order of approximation problems, we note the similarities between the momentum and energy equations in the "zeroth" order equations.

If it is assumed that $h_o = h_o(u_o)$, in place of equation (74) we may write:

$$u_o u_{o_{x_*}} + v_o u_{o_{y_*}} = \left(\frac{\epsilon_{o*}}{Pr_T} u_{o_{y_*}}\right) + \frac{\epsilon_{o*}}{Pr_T} u^2_{o_{y_*}} \left(\frac{h_{o_{u_o}} u_o}{h_{o_{u_o}}}\right) \qquad (81)$$

Then subtracting the ($\alpha°$) momentum equation from the above equation yields:

$$0 = (\epsilon_{o_*} u_{o y_*})_{y_*} \left(\frac{1}{Pr_T} - 1\right) + \frac{\epsilon_{o*}}{Pr_T} u^2_{o_{y_*}} \left(\frac{h_{o_{u_o}} u_o}{h_{o_{u_o}}}\right) \qquad (82)$$

Both well known incompressible eddy viscosity models may be represented by

$$\epsilon_* = \ell(x)\, u^n_{o_{y_*}}$$

Substitution into equation (82) yields

$$(n+1)\, u_{o_{y_* y_*}} \left(\frac{1}{Pr_T} - 1\right) + \frac{1}{Pr_T} u^2_{o_{y_*}} \frac{h_{o_{u_o}} u_o}{h_{u_o}} = 0 \qquad (83)$$

or

$$\frac{h_{o_{u_o u_o}}}{h_{o_{u_o}}} du_o = \frac{u_{o_{y_* y_*}}}{u_{o_{y_*}}} \frac{}{2} (n+1)\,(Pr_T - 1)\, u_{o_{y_*}} dy_*$$

Yielding

$$h_{o_{u_o}} = B_1 (u_{o_{y_*}})^{(n+1)(Pr_T - 1)} \tag{84}$$

and

$$h_o(u_o) = B_1 \int_o^{y_*} (u_{o_{y_*}})^{(n+1)\,Pr_T - n} dy_* + B_2 \tag{85}$$

Thus, we have a general solution for the zeroth order enthalpy as a function of the zeroth order velocity distribution.

(d) Solution of the Zeroth Order Problem for the Gortler Type Eddy Viscosity Model

In order to illustrate the method of solution of the problem, it is necessary to be specific with regard to the eddy viscosity model, the general approach, however, is applicable no matter which model is assumed.* Because of its simplicity we will use the Gortler model of eddy viscosity to demonstrate the solution procedure.

Let us recall that

$$\epsilon = Kx\,(u_1 - u_2)$$

For zero pressure gradient flow.

---

* If one chooses to work with the mixing length eddy viscosity ($\epsilon = \ell^2 u_y$) model it will be found more convenient to specify the relation between the mixing lengths $\frac{\ell}{\ell^*} = (\frac{\rho_*}{\rho})^{3/2}$ rather than between the eddy viscosities.

Extending this formulation to pressure gradient in a general manner but in such a way as to preserve the general approach of the original development one obtains

$$\epsilon_* = \frac{1}{2} \frac{u_{o_1} x_*}{\sigma_*} \left\{ K_o (1 - \lambda_o) + \alpha \left[K_o \left(\frac{u_{11} - u_{12}}{u_{o_1}} \right) K_1(x_*) (1 - \lambda_o) \right] + 0(\alpha^2) \right\} \tag{86}$$

Let

$$\eta = \frac{\sigma_* y_*}{x_*} \tag{87}$$

and

$$\phi = u_{o_1} \frac{x_*}{\sigma_*} f(\eta) \tag{88}$$

Then we note

$$u_o = \phi_{y_*} = u_{o_1} f'(\eta)$$

and

$$v_o = - \phi_{x_*} = - \frac{u_{o_1}}{\sigma_*} (f - \eta f')$$

Substitution of (86), (87) and (88) into the momentum equation (73) yields

$$\frac{u_{o_1}^2}{x_*} ff'' = \frac{1}{2} \frac{u_{o_1}^2 \sigma_*}{x_*} K_o (1 - \lambda_o) f''' + 0(\alpha)$$

Then by letting

$$\sigma_* = \frac{1}{K_o (1 - \lambda_o)} \tag{89}$$

gives the well known Gortler problem

$$f''' + 2ff'' = 0 \tag{90}$$

With boundary conditions

$$f'(\infty) = 1,\ f'(-\infty) = \lambda_o,\ \frac{1+\lambda_o}{2} = f(o)$$

Which is the Gortler problem for zero pressure gradient mixing. Thus,

$$\frac{u_o}{u_{o_1}} = f'(\eta) = \frac{1+\lambda_o}{2}\left[1 + \frac{1-\lambda_o}{1+\lambda_o}\,\mathrm{erf}(\eta) + 0\left(\frac{1-\lambda_o}{1+\lambda_o}\right)^2\right] \qquad (91)$$

The corresponding zeroth order energy equation is then solved by substitution of (91) into equation (85) with n = 0, yielding the zeroth order ($\frac{dp}{dx} = 0$) enthalpy field:

$$h_o(\eta) = u_{o_1}\,\frac{1-\lambda_o}{2}\,B_1\,\frac{2}{\sqrt{\pi}}\int_o^{\eta} e^{-Pr_T\,\xi^2}\,d\xi + B_2 \qquad (92)$$

where

$$\mathrm{erf}(\eta) = \frac{2}{\sqrt{\pi}}\int_o^{\eta} e^{-\xi^2}\,d\xi$$

Then, by a change of variables under the integral it is found that:

$$h_o(\eta) = u_{o_1}\,\frac{1-\lambda_o}{2}\,B_1\,\mathrm{erf}\left(\frac{\eta}{\sqrt{Pr_T}}\right) + B_2$$

with boundary conditions given by:

$$h_o(\infty) = h_{o_1} = u_{o_1}\,\frac{1-\lambda_o}{2}\,B_1 + B_2$$

$$h_o(-\infty) = h_{o_2} = -u_{o_1}\,\frac{1+\lambda_o}{2}\,B_1 + B_2$$

Thus:

$$B_1 = \frac{h_{o_1} - h_{o_2}}{u_{o_1}(1-\lambda_o)} \qquad B_2 = \frac{h_{o_1} + h_{o_2}}{2}$$

Then

$$h_o(\eta) = h_{o_1} \frac{1 + \frac{h_{o_2}}{h_{o_1}}}{2} \left[1 + \frac{1 - \frac{h_{o_2}}{h_{o_1}}}{1 + \frac{h_{o_2}}{h_{o_1}}} \operatorname{erf}\left(\frac{\eta}{\sqrt{Pr_T}}\right)\right] \tag{93}$$

Which indicates that the degree of spreading of enthalpy at η corresponds to the degree of spreading of velocity at $\frac{\eta}{\sqrt{Pr_T}}$. Which is as one would expect.

(e) Solution of the First Order Problem with the Gortler Eddy Viscosity Model

Using the same transformation used for the zeroth order problem but setting

$$\phi_1 = u_{o_1} \frac{x_*}{\sigma_*} \ell(x_*)\, g(\eta) \tag{94}$$

$$u_1 = \phi_{1_{y_*}} = u_{o_1} \ell\, g' \tag{95}$$

$$v_1 = -\phi_{1_{x_*}} = -\frac{u_{o_1}}{\sigma_*} \left[\frac{d(x_* \ell)}{dx_*} g - \ell \eta g'\right]$$

The first order momentum equation is then transformed to:

$$x_* \frac{d\ell}{dx_*} f' g' - \frac{d(x_* \ell)}{dx_*} f'' g - \ell f g'' = x_* \frac{u_{1_{1_{x_*}}}}{u_{o_1}} \left(\frac{h_o}{h_{o_1}} - \frac{\gamma}{\gamma - 1} \frac{u_{o_1}^2}{2h_{o_1}} f f''\right) + \frac{1}{2}\left\{\left[\frac{u_{11} - u_{12}}{u_{o_1}(1 - \lambda_o)} + \frac{K_1(x_*)}{K_o}\right] f''' + \ell g'''\right\} \tag{96}$$

Before proceeding with the solution of this equation, let us examine several terms in order to determine their form and possible further simplifications.

(1) Relations Between Free Stream Properties

Let us investigate the form of $u_{11} - u_{12}$. We approach the investigation by first examining the isentropic nature of the free stream flows.

$$\frac{p_\infty}{\rho_\infty^\gamma} = \frac{p_{t_\infty}}{\rho_{t_\infty}^\gamma} = \text{Const. and } \frac{p_{-\infty}}{\rho_{-\infty}^\gamma} = \frac{p_{t_{-\infty}}}{\rho_{t_{-\infty}}^\gamma}$$

Therefore, since $p_1 = p_2$:

$$\frac{\rho_2}{\rho_1} = \frac{\rho_{t_2}}{\rho_{t_1}} \left(\frac{p_{t_1}}{p_{t_2}}\right)^{\frac{1}{\gamma}} = \text{Constant} \tag{97}$$

Now examine the free stream momentum equations

$$\rho_1 \frac{u_1 du_1}{dx} = -\frac{dp}{dx} = \rho_2 u_2 \frac{du_2}{dx}$$

This equation may be put in the form

$$\frac{d\frac{1}{2}u_1^2}{dx} = \frac{\rho_2}{\rho_1} \frac{d\frac{1}{2}u_2^2}{dx} = \frac{h_{o_1}}{h_{o_2}} \frac{d\frac{1}{2}u_2^2}{dx}$$

which may be integrated directly, since $\frac{\rho_2}{\rho_1}$ is independent of x.

$$\frac{1}{2}(u_1^2 - u_{o_1}^2) = \frac{h_{o_1}}{h_{o_2}} \frac{1}{2}(u_2^2 - u_{o_2}^2)$$

Introducing the expansions for u_1 and $u_{-\infty}$ yields:

$$\alpha u_{o_1} u_{11} + 0(\alpha^2) = \frac{h_{o_1}}{h_{o_2}} \alpha u_{o_2} u_{12} + 0(\alpha^2) \tag{98}$$

Thus, $u_{11} - u_{12}$ may be determined in terms of the stagnation conditions of the two streams and their velocities at the point of initial encounter.

$$u_{12} = u_{11} \frac{u_{o_1}}{u_{o_2}} \frac{h_{o_2}}{h_{o_1}} \tag{99}$$

Then

$$u_{11} - u_{12} = \left(1 - \frac{h_{o_2}}{h_{o_1}}\right) \frac{1}{\lambda_o} \tag{100}$$

(2) Exponential Streamwise Velocity Gradient Form

If we let the free stream velocity gradient vary as some power of x_*, thus

$$u_{11} = u_{o_1} a x_* \tag{101}$$

Then

$$u_{11} - u_{12} = \left(1 - \frac{1}{\lambda_o} \frac{h_{o_2}}{h_{o_1}}\right) u_{o_1} a_N x_*^N \tag{102}$$

It is noted that the form of the resultant pressure gradient is similar to (101)

$$\frac{dp}{dx} = -\alpha \frac{\gamma - 1}{\gamma} p_o M_{o_1}^2 N a_N x_*^{N-1} + 0(\alpha^2) \tag{103}$$

(3) Dependence of ϵ_{*o} on X_N from Dimensional Considerations

We also set $K_1(x) = a_N k_N K_o x^N$ in the eddy viscosity formula.

If $$u(x_N, \eta) = \phi_{1_{y_*}} = u_{o_1} \ell(x_*) g'(\eta)$$

Then $$\ell(x_*) = a_N x_*^N$$

Substitution of these relations into the momentum equation yields after simplification:

$$(N+1) f'' g - N f' g' + f g'' + \frac{1}{2}(N+1) f'' g''' = -N \left(\frac{h_o}{h_{o_1}} - \frac{\gamma}{2} M_{o_1}^2 f f''\right) - \frac{1}{2}\left[\frac{1 - \frac{h_{o_2}}{h_{o_1}\lambda_o}}{1 - \lambda_o} + k_N\right] f''' \tag{104}$$

A solution may now be constructed in the form

$$g_N = g_{N_1} + \frac{\gamma}{2} M_{o_1}^2 g_{N_2} + \left[\frac{1 - \frac{h_{o_2}}{h_{o_1} \lambda_o}}{1 - \lambda_o} + k_N \right] g_{N_3} \tag{105}$$

Then we may state the problem in an operator notation:

$$\left[\frac{1}{2} D^3 + f D^2 - N f' D + (N+1) f'' \right] \begin{pmatrix} g_{N_1} \\ g_{N_2} \\ g_{N_3} \end{pmatrix} = \begin{pmatrix} - N \frac{h_o}{h_{o_1}} \\ f f'' \\ - \frac{1}{2} f''' \end{pmatrix} \tag{106}$$

where

$$D^n(\ ) \equiv \frac{d^n (\ )}{d \eta}$$

With boundary conditions:

$$\begin{aligned} g_{N_i}(0) &= 0 \qquad i = 1, 2, 3 \\ g'_{N_2}(+\infty) &= g'_{N_3}(\pm \infty) = 0 \\ g'_{N_1}(+\infty) &= 1 \\ g'_{N_1}(-\infty) &= \frac{h_{o_2}}{\lambda_o h_{o_1}} \end{aligned} \tag{107}$$

Recalling that:

$$\frac{h_o(\eta)}{h_{o_1}} = \frac{1 + \frac{h_{o_2}}{h_{o_1}}}{2} \left[1 + \frac{1 - \frac{h_{o_2}}{h_{o_1}}}{1 + \frac{h_{o_2}}{h_{o_1}}} \operatorname{erf} \left(\frac{\eta}{\sqrt{Pr_T}} \right) \right]$$

and

$$f(\eta) = \frac{1 + \lambda_o}{2} \left[1 + \frac{1 - \lambda_o}{1 + \lambda_o} \operatorname{erf}(\eta) \right]$$

The equations may be solved by quadrature or numerical methods.

Note, however, that the functions g_{N_i} will depend on λ_o through f, and therefore they are not universal functions. The functions g_{N_2} and g_{N_3} are, however, independent of $\frac{\gamma}{2} Mo_1^2$, and all other boundary conditions i.e., $\frac{ho2}{ho1}$, and k_N so the problem does not have to be completely resolved for each particular case.

Should we wish to represent the case where the free stream velocity is of the form:

$$u_{11} = u_{o_1} \sum_{N=1}^{M} a_N x^N \tag{108}$$

we may merely superpose the individual solutions with $u_{11} = u_{o_1} a_N x_*^N$, since the differential equation for g_N is linear. The first order stream function will then be of the form:

$$\phi_1(x,\eta) = \sum_{N=1}^{M} a_N x^{N+1} g_N(\eta) \tag{109}$$

(4) Solution of the First Order Energy Equation

Having the solution for the velocity field, we now, turn to the matter of determining the enthalpy field. The same techniques are applicable here as were employed in the solution for the velocity field.

Recalling equation 72

$$h_\infty = h_{o_1} - \alpha u_{o_1} u_{11} + 0(\alpha^2)$$

We set

$$h_1(x,\eta) = -u_{o_1}{}^2 a_N x^N r(\eta) \tag{110}$$

Substitution of this into the first order energy equation and transforming as in the case of the velocity field yields a similar equation.

$$\left[\frac{1}{2Pr_T} D^2 + f D - Nf'\right] r_N = -N\left(\frac{h_o}{h_{o_1}} f' + \frac{\gamma}{2(\gamma-1)} f \frac{h_o'}{h_{o_1}}\right)$$

$$+ \frac{N+1}{(\gamma-1)M_{o_1}{}^2} g_N \frac{h_o'}{h_{o_1}} + \frac{\frac{h_{o_2}}{h_{o_1}} \frac{1}{\lambda_o}}{2 PR_T(\gamma-1)M_{o_1}{}^2} \left[\frac{}{1-\lambda_o} + k_N\right] \tag{111}$$

Again we set

$$r_N = r_{N_1} + \frac{\gamma}{2\gamma - 1} r_{N_2} + \frac{1}{(\gamma - 1) M_{o_1}^2} r_{N_3} + \left[\frac{1 - \frac{h_{o_2}}{h_{o_1}} \frac{1}{\lambda_o} + k_N}{1 - \lambda_o} \right] r_{N_4} \qquad (112)$$

$$2 Pr_T (\gamma - 1) M_{o_1}^2$$

Then

$$\left[\frac{1}{2 Pr_T} D^2 + f D - N f' \right] \begin{pmatrix} r_{N_1} \\ r_{N_2} \\ r_{N_3} \\ r_{N_4} \end{pmatrix} = \begin{pmatrix} - N \frac{h_o}{h_{o_1}} f' \\ - f \frac{h_o'}{h_{o_1}'} \\ (N + 1) g \frac{h_o'}{h_{o_1}} \\ \frac{h_o''}{h_{o_1}} \end{pmatrix} \qquad (113)$$

With boundary conditions

$$r_{N_1}(\infty) = 1, \quad r_{N_1}(-\infty) = \frac{h_{o_2}}{h_{o_1}}$$

$$r_{N_i}(\pm\infty) = 0, \quad i = 2, 3, 4 \qquad (114)$$

These equations may be solved by the same procedures utilized for the velocity field. Note, however, that in addition to being dependent on λ_o through f, r_{N_3} is dependent on the other boundary conditions through g_N.

(f) Physical Flow Field Evaluation

The flow field has now been determined in the transformed plane. Its evaluation in the physical plane requires merely that the transformation be inverted. This is relatively straightforward and is accomplished directly through the integration of the $y - y^*$ relation

$$\int_o^y dy' = \left(\frac{p}{p_o}\right)^{\frac{1}{2}} \int_o^{y_*} \frac{\rho_*}{\rho}\, dy_*' = \left(\frac{p}{p_o}\right)^{\frac{1}{2}} \frac{\rho_*}{\rho_{o_1}} \int_o^{y_*} \frac{\rho_{o_1}}{\rho}\, dy_*' \quad (115)$$

But,

$$\frac{\rho_{o_1}}{\rho} = \frac{p_o}{p(x)} \frac{h(x_*, \eta)}{h_{o_1}} \quad (116)$$

The integration does not involve x^*, therefore we may multiply through by $\frac{\sigma^*}{x_*} = \frac{\sigma^*}{x}$, yielding

$$\frac{\sigma_* y}{x} = \left(\frac{p_o}{p}\right)^{\frac{1}{2}} \frac{\rho_*}{\rho_{o_1}} \left\{ \int_o^{\eta} \frac{h_o(\eta)}{h_{o_1}}\, d\eta' + (\gamma - 1) M_{o_1}^2 \sum_{N=1}^{M} a_N x^N \cdot \int_o^{\eta} r_N(\eta')\, d\eta' \right\} \quad (117)$$

which may be integrated to obtain

$$\frac{\sigma_* y}{x}(x, \eta) \quad (118)$$

where the density ratio $\frac{\rho_*}{\rho_{o_1}}$ is identical to the reference density ratio for zero pressure gradient mixing.

The velocity field is then

$$u(x, \eta) = u_{o_1} \left[u_o(\eta) + \alpha \sum_{N=1}^{M} a_N x^N g_N(\eta) \right] + 0(\alpha^2) \quad (119)$$

and the enthalpy field is

$$h = h_{o_1} \left[h_o(\eta) + \alpha(\gamma - 1) M_{o_1}^2 \sum_{N=1}^{M} a_N x^N r_N(\eta) \right] + 0(\alpha^2) \quad (120)$$

Equation (119) and (120) coupled with Equation (118) provide a complete description of the flow field.

It is interesting to note that throughout the analysis α has remained arbitrary. Thus, it appears possible to represent any small and continuous velocity gradient arbitrarily closely in the first order by the polynomial $\alpha = \sum_{N=1}^{M} a_N x^N$. The solution given above should, therefore, approximate the mixing of compressible streams under such conditions arbitrarily closely.

(h) Dissimilar Gases in a Pressure Gradient

It is noted that the method used in the preceding section may be applied directly to the mixing of dissimilar gases as long as their respective ratio of specific heats, γ, are equal. Methods similar to those used above may be included to account for molecular weight and specific heat variations. However, the restriction must be placed that the Lewis number is unity, otherwise the solution to the energy equation is no longer available. Such restriction appears to be minor in the light of much evidence that mass and energy (temperature) appear to diffuse at the same rate.

3.2 Experimental Studies

3.2.1 Experimental Background

This section covers the description of the experimental hardware and test instrumentation, the experimental procedure and results of the specific experiments. The design of the major hardware components spanned approximately 9 months of the total program. Detail hardware design fabrication and assembly, as well as assembly of major hardware, instrumentation and control systems, spanned approximately the next 5 months of the program. Installation of the test hardware and preliminary checkout occupied the next month and an additional 4 weeks was required in "debugging" instrumentation and controls, fabricating and installing modifications. Performance of the final experiments themselves required only about 2 weeks. Final experiments consisted of three combinations of Mach number in the cold flow, constant pressure mixing case and two combinations of Mach number in the cold flow positive pressure gradient case. Complete reduction of the data required another 2 weeks. As will be pointed out in the following sections, although only the cold flow air to air data were obtained,

complete hardware and instrumentation were assembled for performance of hydrogen mixing tests, as well as high temperature air mixing tests.

3.2.2 Test Hardware and Facility Description

The design, description and capabilities of hardware developed and used in performance of this program were described in the following paragraphs.

(A) Pebble Bed Heater and Air Supply

This facility was not designed nor fabricated under the present contract. However, its capability as are pertinent to the present study will be described. A block diagram of the complete system is shown in Figure 1. It is seen from this diagram that this system consists of an air compressor, a storage system, an air flow control system and a regenerative gas fired heat exchanger. Additionally, there are the necessary facility protection and safety systems together with the instrumentation required for the operation of this facility.

The method of operation of this system is as follows: the air is compressed by two vertical four-staged compressors whose capacity is 30 cubic feet of compressed air per hour at 3000 psi. The compressed air is stored in a 104 cubic foot spherical pressure vessel with a 3000 psi working pressure. The gas fired regenerative heat exchanger, the pebble bed heater, is heated by a natural gas excess air burner positioned at the top of the heat exchanger. The hot gases are forced down to the storage bed and exhausted to atmosphere through an 8 inch diameter stack. The system is designed to operate at a maximum stagnation temperature of 4500°R. The pebble bed, the active part of the heat exchanger consists in the main of zirconium oxide spheres, contained in a cylindrical volume, 14 inches in diameter and 162 inches long. The containing wall for the bed is made from refractory and insulating brick. The entire heater vessel is a cylindrical shell of carbon steel 52-1/2 inches in outside diameter and 16 feet 9 inches long. The vessel was designed per appropriate ASME pressure code for a maximum internal pressure of 2100 psi and a maximum wall temperature of 650°F. When both the heating and compression cycles are completed the system is ready to operate. At this stage the gas burner system is sealed off from the gas fired heat exchanger and air is fed through from the storage vessel via the air flow control system to the pebble bed heat exchanger. From the heat exchanger the air passes into the test section.

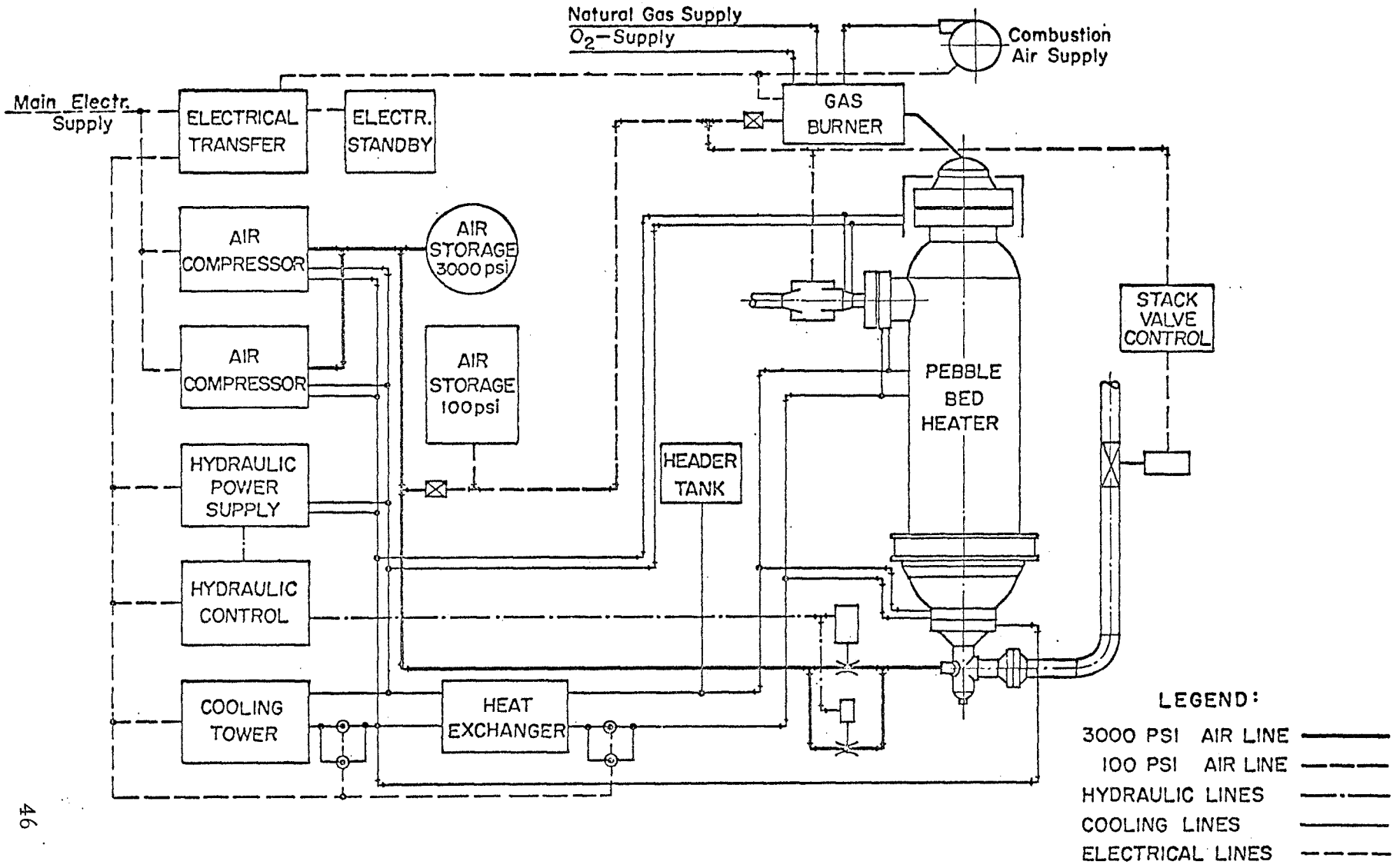

FIG. 1. BLOCK DIAGRAM OF COMPLETE SYSTEM

Since the temperature of operation of the bed may be as high as 4000°F and some operation may be carried on with hazardous gases, an ultravision flame detector was used. This type of detector can sense the difference between real flame and red hot refractory. It is actuated only by ultraviolet radiation in the wave band .20 to .26 microns which is present in all flames. Additionally, emergency water cooling and electrical power supply systems are available in the event of main power failure. All controls are designed such that in the event of power failure the system will automatically be shut down.

The air flow control system for supplying test air through the pebble bed heater is electro-hydraulically operated. Air is admitted by alternatively a 1-inch or 2-inch diameter hydraulically operated servo-valve. The servo-valve hydraulic motor is controlled electrically by a four-stage proportional and differential control feed back system. This system receives valve position and flow system pressure feed back. The latter is compared to the existing set point for the desired flow system pressure. The set point pressure is manually adjustable by means of a dial potentiometer.

The flow control system for the second stream extends from either the high pressure sphere in the event that the secondary is air or from gas storage bottles, in the event another gas is being used, through a dome type pressure regulator then on to the test section. The dome pressure regulator is rated at over 3000 psi and delivers over 5 lbs per sec mass flow rate. The dome pressure is controlled by a manual pressure regulator.

In the present series of tests the primary flow was not routed through the furnace but came directly from the controlled servo-valves to the test section.

(B) The Test Section

The test section is defined as that unit of the system in which the primary and secondary flows are accelerated to the desired Mach number, brought together and allowed to mix according to the desired streamwise pressure distribution. The total test section is shown schematically in Figure 2.

(a) Nozzle Section

In this section the gases of both the primary and secondary stream are accelerated to the supersonic Mach number desired and

NOZZLE BLOCK COVER PLATE

TEST SECTION TOP VIEW
NOZZLE BLOCK-SUPPORT BLOCK AND TOP PLATE OMITTED

TYPICAL PLATE DEFLECT SYSTEM

13.750

NOZZLE BLOCK REPLACABLE

FIXED SCHLIEREN WINDOW ⚠

"O" RING

TYPICAL CUTOUT FOR WINDOW AND PROBE ⚠

CENTER WEDGE

TEST SECTION SIDE VIEW
TEST SECTION SIDE PLATE OMITTED

3½

18.200

NOZZLE BLOCK REPLACABLE

20.325

NOZZLE BLOCK SUPPORT 'T'

THERMAL EXPANSION ROLLER

TOP SURFACE OF 12" x 3" CHANNEL

TEST SECTION TOP VIEW
NOZZLE BLOCK-SUPPORT BLOCK AND TOP PLATE OMITTED

TYPICAL PLATE DEFLECTION SYSTEM

TEST SECTION SIDE VIEW
TEST SECTION SIDE PLATE OMITTED

HINGE POINT

THERMAL EXPANSION ROLLER

⚠ SEE DETAILS, DRAWING NO 010-0

UNLESS OTHERWISE SPECIFIED DIMENSIONS ARE IN INCHES TOLERANCES ON: FRACTIONS ± 1/16 .X ± .1 ANGLES ± 1° .XX ± .03 SURFACE FINISH √ .XXX ± .010	DRAWN / DATE	CETEC MOUNTAIN VIEW, CALIFORNIA
	CHECKED	TEST SECTION GENERAL ASSEMBLY, DESIGN OF NOZZLE BLOCKS
	DESIGN SUPERVISOR	
	ANALYSIS	
	PROJECT ENGR	
	APPROVED	SIZE H · CODE IDENT NO. 29559 · DRAWING NO. 003-2
	APPROVED	SCALE HALF WEIGHT · SHEET 1 OF 1

are brought together as two uniform streams at the exit of this section. The streams are separated by a central wedge configuration of 10° included angle. The tip section of the wedge slowly turns the flows parallel to one another through circular arcs of approximately 38.6 in. radius. The tip section continues for another 0.30 inches. The thickness of the tip at this point is .020 inches as shown in figure 3. The main body of the wedge is fabricated from OFHC copper and has manifolding and flow passages provided for water cooling. The tip section is fabricated from high temperature inconel steel.

The wedge is supported by four 3/8 inch diameter harden steel pins inserted two from each side through one-inch thick steel at the head end. Two one quarter inch diameter harden steel pins likewise support the wedge at approximately center span. These pins are inserted through one-inch thick steel doors covering the nozzle section. Approximately four inches from the tip in the inconel section one eighth inch diameter harden steel pins also extend through the doors and provide the final support for the center wedge.

The center wedge has been constructed in this manner in order to provide maximum rigidity under load and temperature and a high degree of thermal isolation of the streams as well as minimum flow discontinuity at the tip where the flows join.

The primary and secondary streams are accelerated to uniform Mach numbers by means of two-dimensional nozzles positioned above and below the center wedge. The nozzle contours were determined by means of the method of characteristic using a computer program capable of accounting for a changing ratio of specific heats as the flow expands through the nozzle. The nozzle contours are constructed in two steps. First, the method of characteristics determines the necessary contour for expansion of the gases to a uniform flow opposite the straight wall of the center wedge. This flow is at an intermediate Mach number below that desired at the exit of the nozzle section. This Mach number is related to the final Mach number through the 5° turn required to bring the flow parallel to the axis of the test section. The final contour is constructed on the basis of Prandtl-Meyer wave cancellation with a 38.6 inch radius turn at the tip of the center wedge. Note that this requires axial (longitudinal) as well as vertical alignment of the nozzles with the center wedge. Thus, an expansion wave generated on the nozzle surface intersects and cancels a compression wave generated by the circular arc contour on the center wedge.

Flow exits and nozzle section from both the primary and secondary sides through a 3 inch wide by 1.758 inch high flow channel

① INCONEL TIP SECTION TO BE AS CUTS ARE MADE
①② TRANSITION SURFACE TO BE 3
③ COOLING PASSAGES TO BE DI
①④ INCONEL TIP TO BE

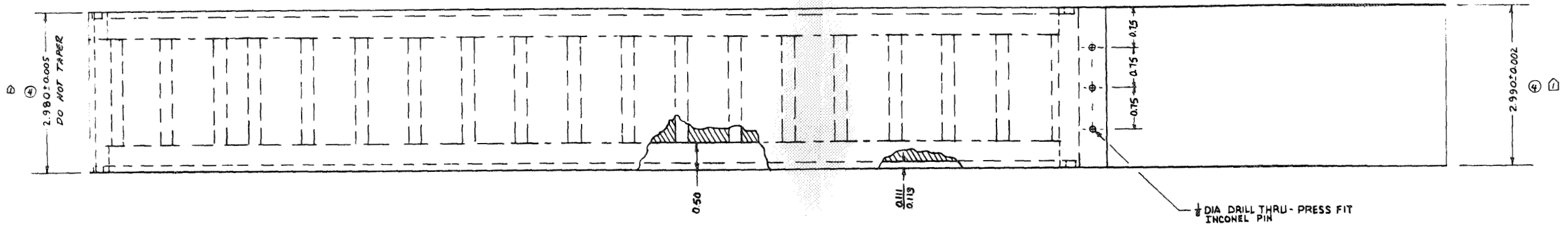

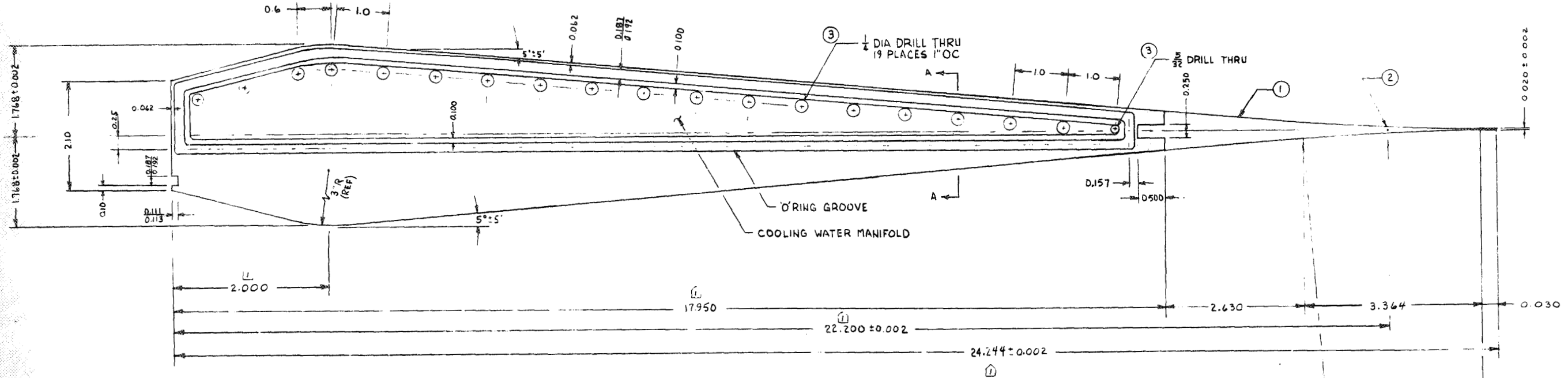

UNLESS OTHERWISE SPECIFIED DIMENSIONS ARE IN INCHES TOLERANCES ON: FRACTIONS = ±1/16 .XX=±.10 ANGLES = ± 1° .XXX=±.01 SURFACE FINISH √ .XXXX=±.002	DRAWN C. DATE
	CHECKED
	DESIGN SUPER
	ANALYSIS
	PROJ ENGR
	APPROVED
	APPROVED

① INCONEL TIP SECTION TO BE ASSEMBLED WITH COPPER MAIN SECTION BEFORE FINAL SURFACE CUTS ARE MADE

①② TRANSITION SURFACE TO BE 38.599 INCH RADIUS CIRCULAR ARC

③ COOLING PASSAGES TO BE DRILLED THRU FLUSH WITH SIDEWALL

①④ INCONEL TIP TO BE 0.010 WIDER THAN COPPER BODY

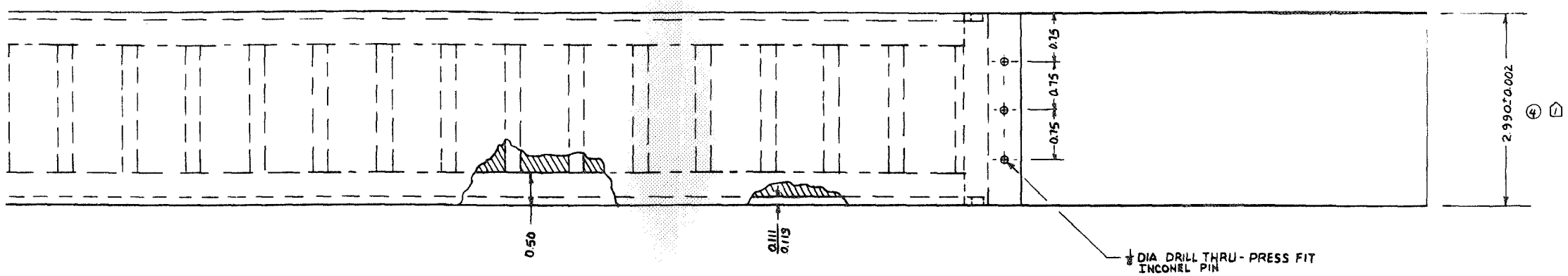

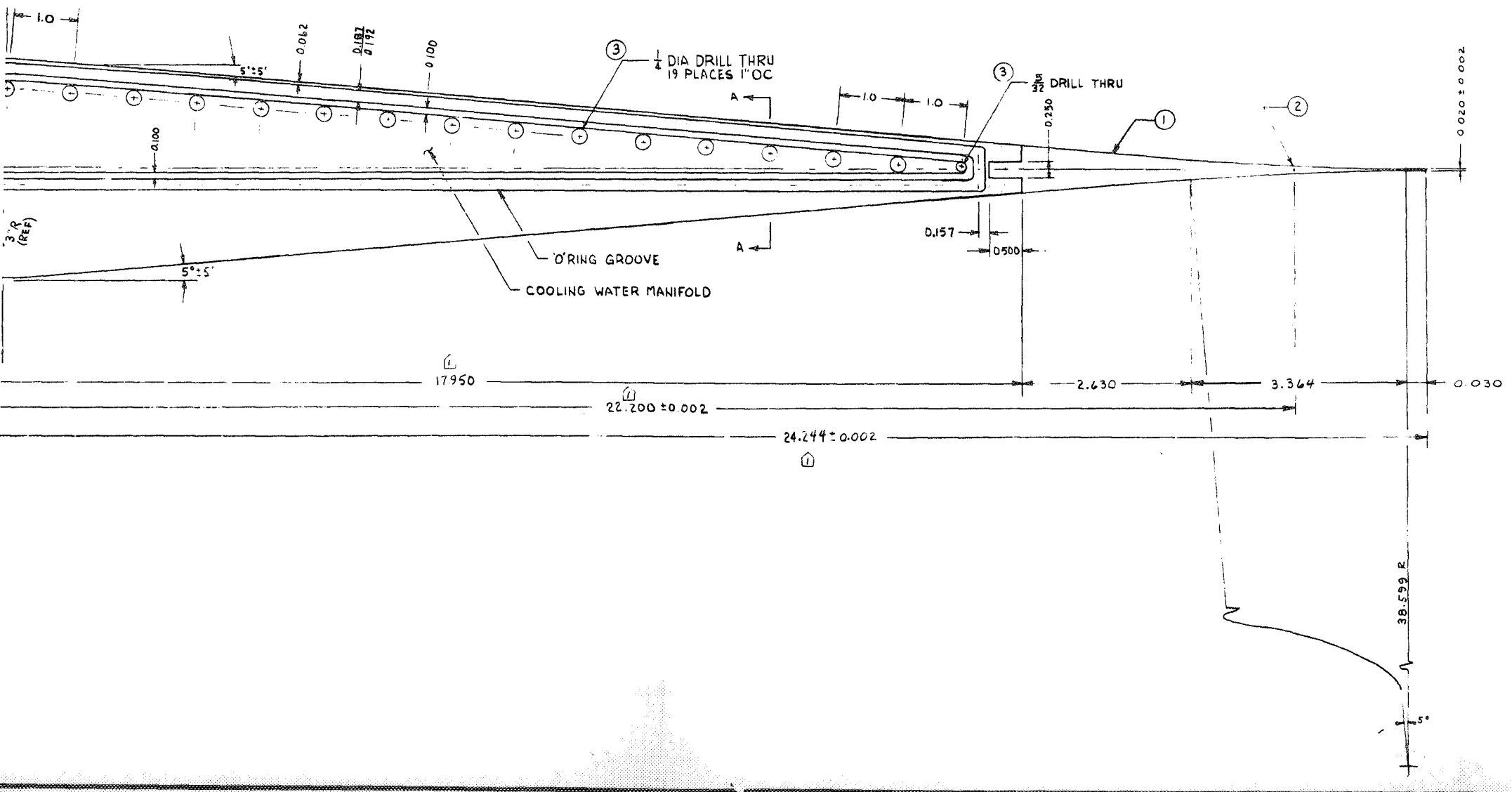

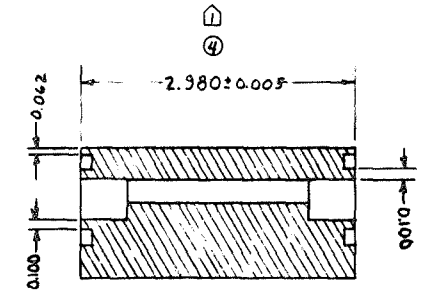

SECTION A-A

UNLESS OTHERWISE SPECIFIED DIMENSIONS ARE IN INCHES TOLERANCES ON: FRACTIONS ±1/16 .XX±.10 ANGLES ±1° .XXX±.01 SURFACE FINISH √ .XXXX±.002	DRAWN C. DATE	CETEC MOUNTAIN VIEW, CALIFORNIA	
	CHECKED	CENTER WEDGE NEAR FIELD NOZZLES	
	DESIGN SUPER		
	ANALYSIS		
	PROJ ENGR		
	APPROVED	SIZE D	CODE IDENT NO 29559
	APPROVED	SCALE FULL	SHEET 1 OF 1

DRAWING NO 1-051

immediately after leaving this section the .020 tip thickness is added to the total flow channel height yielding a 3.536 inch high flow channel for the two streams combined.

A total of six nozzles were fabricated, four low temperature nozzles and two high temperature nozzles. All nozzles were fabricated from OFHC copper and water cooling channels were provided in all but one nozzle which would not be used under any condition of elevated temperature.

The low temperature nozzles were to be used for ambient 500° and 1000°F total temperature streams. Design exit Mach numbers of 4, 2.5 and 1.75 were provided. Two Mach 1.75 nozzles were fabricated in order that two Mach 1.75 streams could be flowed simultaneously. One of these nozzles was not provided with water cooling passages since it would only perform under ambient total temperature conditions.

Upon study of the variation of the specific heat ratio for air and hydrogen it was found that these cold flow nozzle contours would supply uniform flow for both gases over the temperature range indicated and within the expected experimental tolerances. Air flow at 2500°F total temperature would, however, require significantly different nozzle contours. It was expected to investigate Mach 4 and a Mach 1.75 air flow with this high stagnation temperature. These two high temperature nozzle contours were then fabricated.

The overall length of the nozzles are 20.20 inches. A 1-inch ledge on either end of the nozzle block is provided for positioning. The nozzles are held in place by set screw clamps at each end and in the center. The set screws are threaded to top and bottom channels which provide the frame for the nozzle section. (See Figure 4).

Figure 4 shows the transition section from air supply to the nozzle section as well as the mounting of the nozzles and the center wedge. The framework section is fabricated of high grade steel. Close tolerances machining and ground surfaces allowed accurate positioning of the component. Once the component parts were positioned relative to one another, they were match drilled and oversized 1/2 inch harden steel pins were inserted. The assembly was then bolted together with 1/2, 3/8 and 1/4 inch, high tensile strength steel bolts.

(b) The Mixing Section

The mixing section extends out from the nozzle section a distance of 60 inches with two 1/2 thick by 3-inch wide blades forming the upper

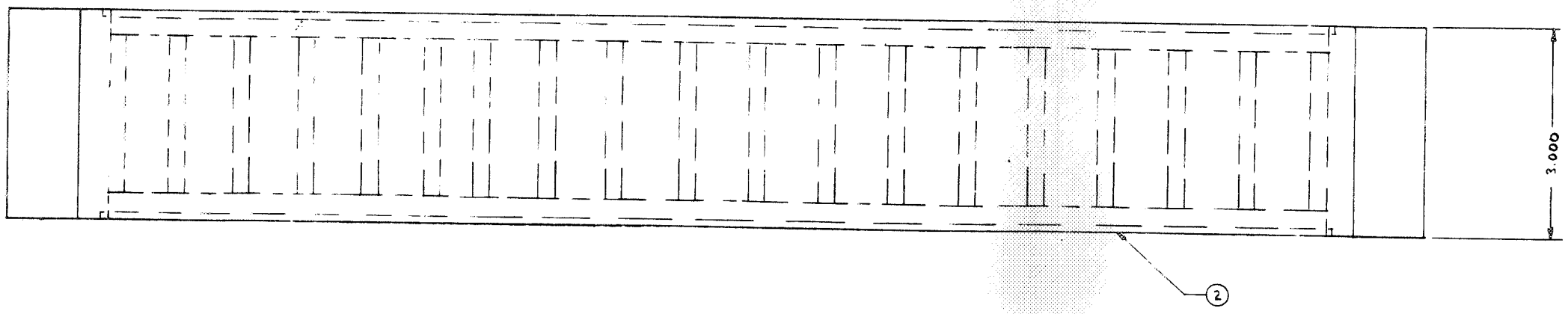

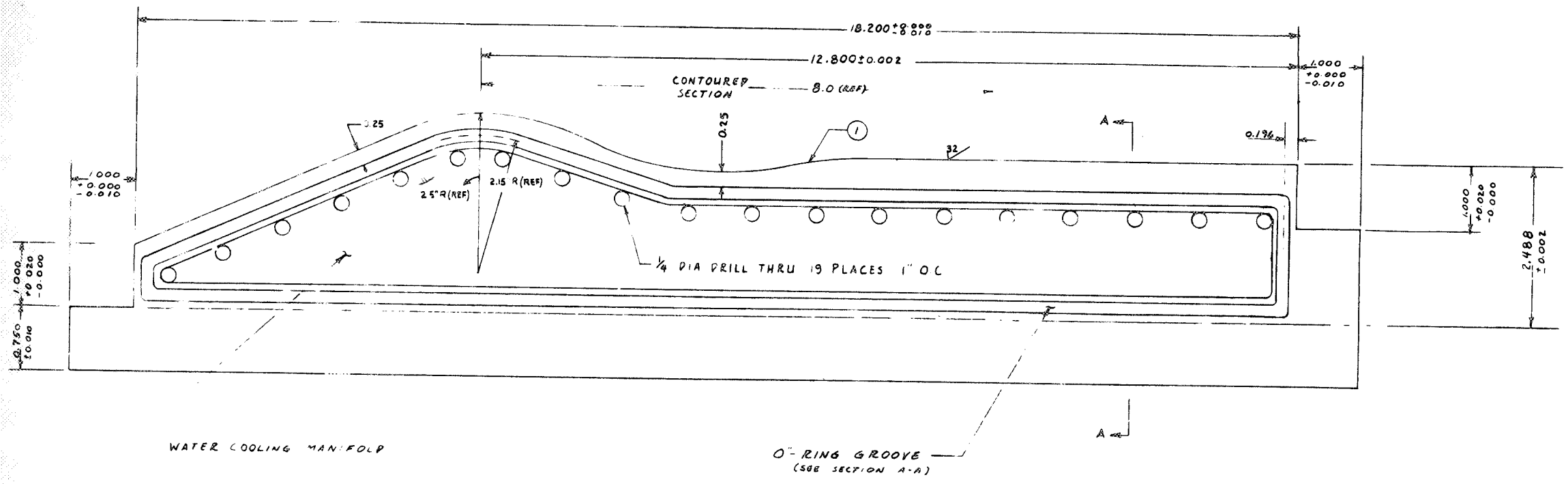

TYPICAL REPLACABLE

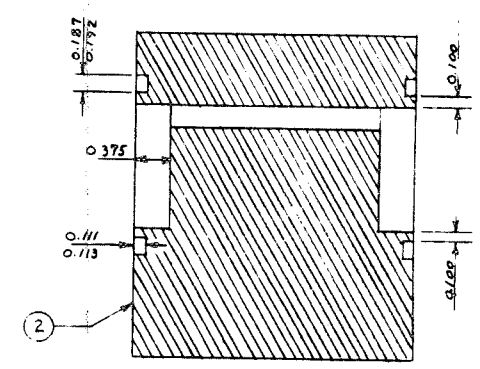

SECTION A-A

UNLESS OTHERWISE SPECIFIED DIMENSION ARE IN INCHES TOLERANCES ON: FRACTIONS ±1/16 .X= ± 10 ANGLES ±1° .XX= ± .05 SURFACE FINISH √ XXX= ± 010	DRAWN DATE CHECKED DESIGN SUPER ANALYSIS PROJ ENGR
	APPROVED
	APPROVED

(1) SURFACE TO BE CONTOURED IN ACCORDANCE WITH TABULATED COORDINATES ±0.003.

(2) SIDE SURFACE NOT TO BE MACHINED

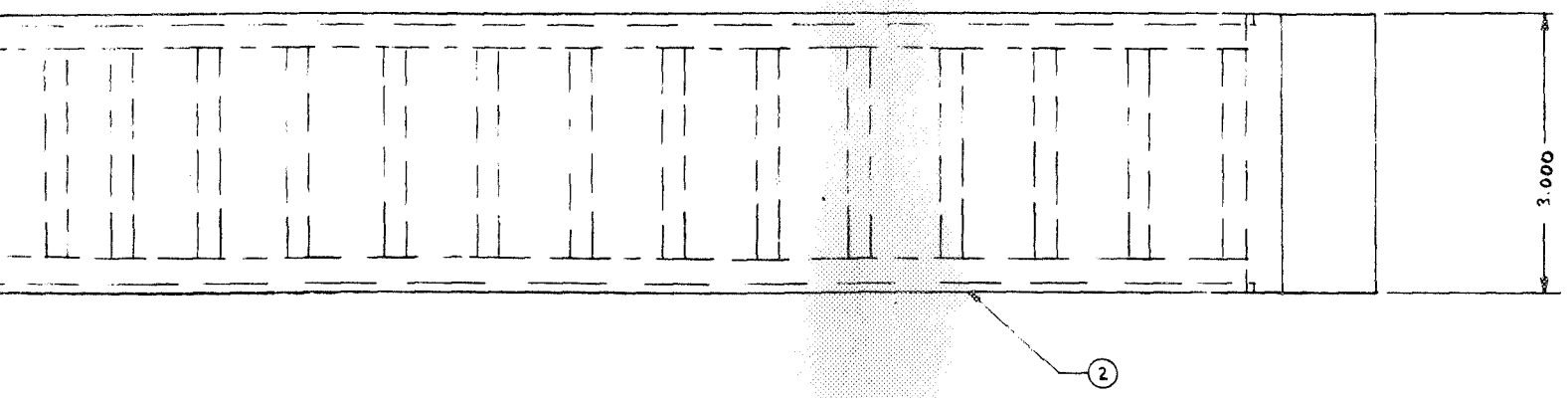

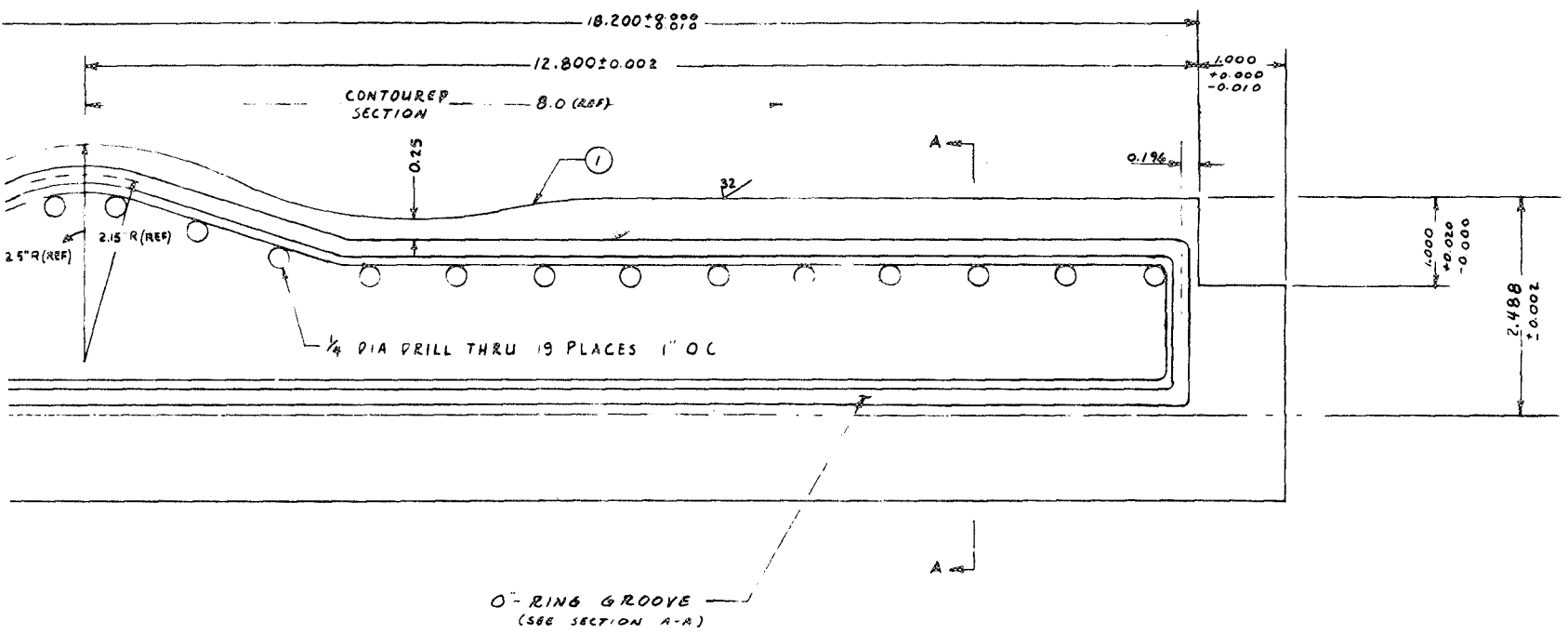

TYPICAL REPLACABLE

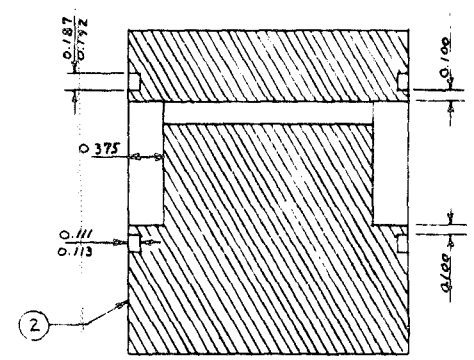

SECTION A-A

UNLESS OTHERWISE SPECIFIED DIMENSION ARE IN INCHES TOLERANCES ON: FRACTIONS ±1/16 .X= ± 10 ANGLES ±1° .XX= ± .05 SURFACE FINISH ✓ .XXX= ± 010	DRAWN DATE CHECKED DESIGN SUPER ANALYSIS PROJ ENGR	CETEC MOUNTAIN VIEW, CALIFORNIA MACH 4 NOZZLE BLOCK - NEAR FIELD
	APPROVED APPROVED	SIZE D | CODE IDENT NO 29559 | DRAWING NO. 1-052 SCALE FULL | WEIGHT | SHEET 1 OF 1

and lower walls of the flow channel and two 1-inch thick by 13.9 inches wide by 78 inches long steel plates forming the vertical walls. (See Figure 5).

Each side wall contains five ports to receive three inch diameter schlieren observation windows. The left hand side wall (facing in the flow direction) contains five ports to receive instrumentation boxes for measurement of pressure temperature and gas concentration profiles. However, only three pairs of schlieren windows and three instrumentation ports are used at any one time. The remaining ports are closed by appropriately fitted blanks.

Hangars for adjusting the position of the upper and lower walls are attached to the side wall double nut threaded rod extend through the hangars to the adjustable wall. The wall position is then determined by screwing the center rod up or down and locking the two nuts. The walls are held fixed at the nozzle exit by bolts and pins. The flow channel area and, therefore, the streamwise pressure gradient is controlled by deflection of the blades with the adjustable hangars at three locations downstream of the nozzle exit.

The pressure seal between the vertical and horizontal walls is provided by a silicon rubber "O" ring running the length of the horizontal wall and mating against the ground surface (between 16 and 8 micro-inches per inch surface finish) of the vertical wall.

At the end of the top and bottom blades which is 60 inches from the nozzle exit, the diffuser section begins. The vertical walls extend beyond the mixing region into the diffuser area. The top and bottom diffuser blade are butted against the blades from the mixing section. The diffuser blades stand the 18 inches from the ends of the mixing section blades to the end of the side wall plus an additional 24 inches. One inch thick steel side walls mating to the mixing section side walls are provided to complete the flow channel in the diffuser area.

Flow exhausts from the diffuser exit into a 30 inch ID, 40 inch OD, 20 ft. tall safety tower which conducts the gases up and away from the test area and building. A replaceable deflector plate is provided inside the tower. To turn the gases upward, the region between the 30 and 40 inch diameter pipes which compose the safety tower is filled with insulation. The insulation provides some sound attenuation but primarily serves to insure that the outer pipes will not be burned through in the event of combustion of the exhaust gases, and as an energy absorber medium in the event a projectile (such as a pebble from the heater bed or broken probe) should pierce the deflector plate and the 30 inch diameter pipe.

77.885
77.865

6.495
6.485

12.010
11.990

12.010
11.990

12.010
11.990

12.010
11.990

TAPPED HOLES
TYP. 5 PLACES

3/4

3/4

3/4

1/2

2 1/2

3/4

DIMENSIONS FOR REF ONLY
SEE DETAILS 1 & 2

2.945
2.935

12.010
11.990

12.010
11.990

12.010
11.990

12.010
11.990

SIDEWALL CUTOUTS

SCALE: 1/2 FULL SIZE NO REQ'D 2 SEE NOTE ①

0.005 R MAX

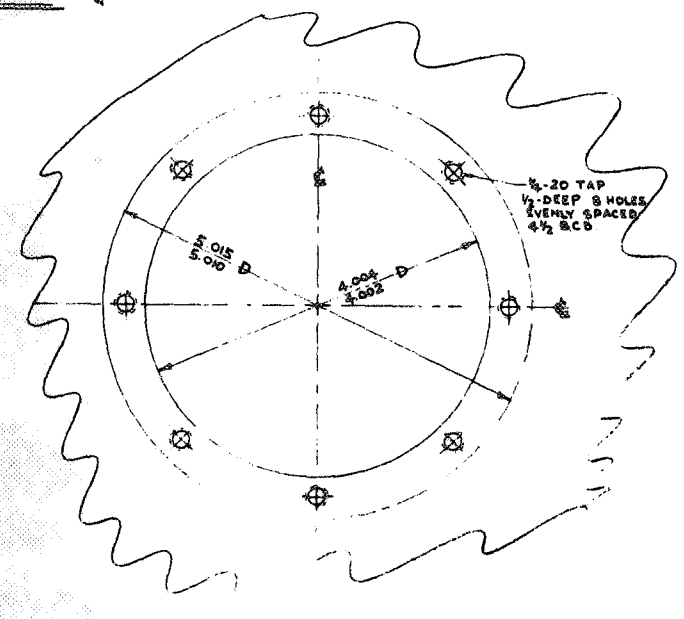

DETAIL 1
WINDOW CUTOUT
TYP. 5 PLACES
SCALE: FULL SIZE

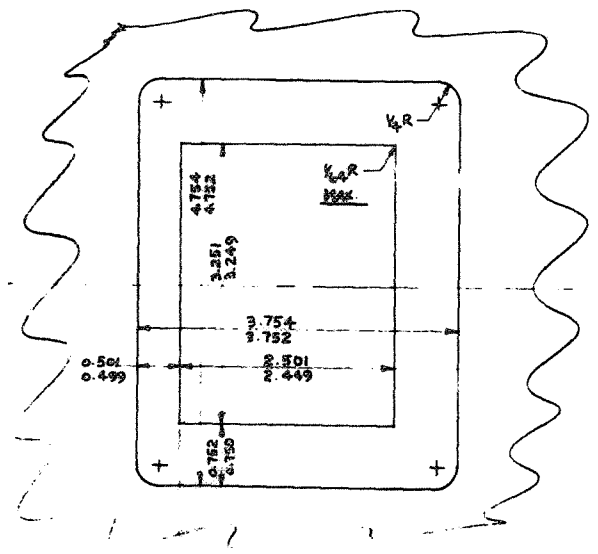

DETAIL 2
INSTRUMENT CUTOUT
TYP. 3 PLACES
SCALE: FULL SIZE

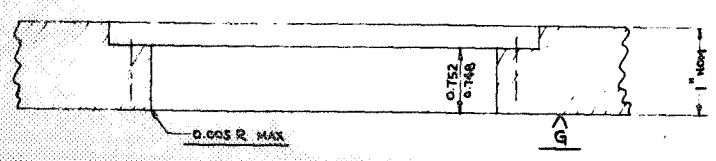

REF. EDGE

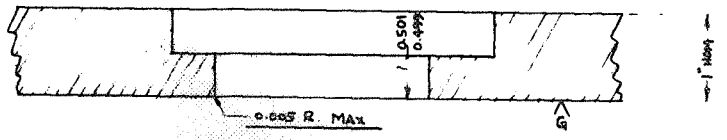

NOTES
① CIRCULAR CUTOTS ON BOTH PIECES
RECTANGULAR CUTOUTS ON 1 SIDEWALL PCE ONLY

UNLESS OTHERWISE SPECIFIED DIMENSIONS ARE IN INCHES TOLERANCES ON:			
FRACTIONS ± 1/16	.X ±.1	DRAWN	DATE
ANGLES ° ± 1°	.XX ±.03	CHECKED	
SURFACE FINISH 32	.XXX ±.005	DESIGN SUPERVISOR	
		ANALYSIS	
		PROJECT ENGR.	
APPROVED		MOUNTAIN	
APPROVED		SIZE D	CODE 2
		SCALE AS	

77.885
77.865

12.010
11.990

12.010
11.990

12.010
11.990

12.010
11.990

1.000
1.000

13.992
13.898

12.010
11.990

12.010
11.990

12.010
11.990

12.010
11.990

SIDEWALL CUTOUTS
SCALE: ½ FULL SIZE NO REQ'D 2 SEE NOTE ①

1" NOM

G

0.506
0.494

¼-20 TAP
½-DEEP 8 HOLES
EVENLY SPACED
4½ B.C.D

DETAIL 1
WINDOW CUTOUT
TYP. 5 PLACES
SCALE: FULL SIZE

¼R

1/64R MAX

4.754
4.122

3.251
3.249

3.754
3.752

0.501
0.499

2.501
2.449

0.752
0.750

DETAIL 2
INSTRUMENT CUTOUT
TYP. 3 PLACES
SCALE: FULL SIZE

REF. EDGE

0.752
0.748

1" NOM

0.501
0.499

0.005 R. MAX

G

NOTES
① CIRCULAR CUTOUTS ON BOTH PIECES
RECTANGULAR CUTOUTS ON 1 SIDEWALL PCE ONLY

UNLESS OTHERWISE SPECIFIED DIMENSIONS ARE IN INCHES TOLERANCES ON:	DRAWN DATE	CETEC MOUNTAIN VIEW, CALIFORNIA
FRACTIONS ± 1/16 .X ±0.1	CHECKED	DETAILS OF TUNNEL SIDEWALL
ANGLES ± ½° .XX ±0.03	DESIGN SUPERVISOR	
SURFACE FINISH 32 √ .XXX ±0.005	ANALYSIS	
	PROJECT ENGR.	
	APPROVED	SIZE D / CODE IDENT NO. 29559 / DRAWING NO. 010-0
	APPROVED	SCALE AS NOTED / SHEET 1 OF 1

(c) The Schlieren System

The schlieren system was constructed to obtain qualitative information regarding the nature of the flow inside the mixing channel. In particular, the flow immediately after the nozzle exit and immediately before each active instrumentation port. The schlieren system was mounted on an I-beam frame. The frame was floated over the test bay floor by air filled rubber tubes. The flotation served to isolate the system from external vibration such as pumps and compressors operating in other parts of the building. The optical system was composed of (1) a light source furnished with a type 110, 21.8 volts 4.5 amp lamp, (2) a condensing lens of approximately 6 inch focal length, (3) two 12-inch spherical mirrors of approximately 12 foot focal length, (4) six 1/4 wave lengths optical flat mirrors, (5) a micrometer adjusted knife edge, (6) a translucent viewing screen and polaroid camera.

The system was set up as shown in Figure 6. The light source and condensing lens, one 12-inch mirror and three of the optical flat mirrors were set up on one side of the test section. The three remaining optical flats were set up directly across the viewing ports.

Light is emitted from the light source and focused on an aperture by means of the condensing lens. The aperture is placed at the focal links of the 12-inch diameter mirror. Thus, representing an approximation to a point source. Light continuing from the aperture strikes the mirror and is reflected as a beam of parallel light. This parallel light is then intercepted by the optical flat and directed through the schlieren port across the flow channel and then strikes the optical flat mirror on the opposite side. This mirror directs the light to the second spherical mirror which then focuses the parallel light at its focal point. The schlieren knife edge is located at this point. All three beams coming through the flow channel from each of the three optical flat are focused in a horizontal line enabling the use of a single knife edge to obtain the schlieren effect. From the focal point the beams again expand and are projected on the translucent screen where the schlieren image of the flow field in the test section may be observed and photographed.

(d) Pressure - Velocity Probe System

Instrumentation is broken into two parts, the first that necessary for control of the flow which was described in section 3.2.2A and that which gives the indication that required operating conditions

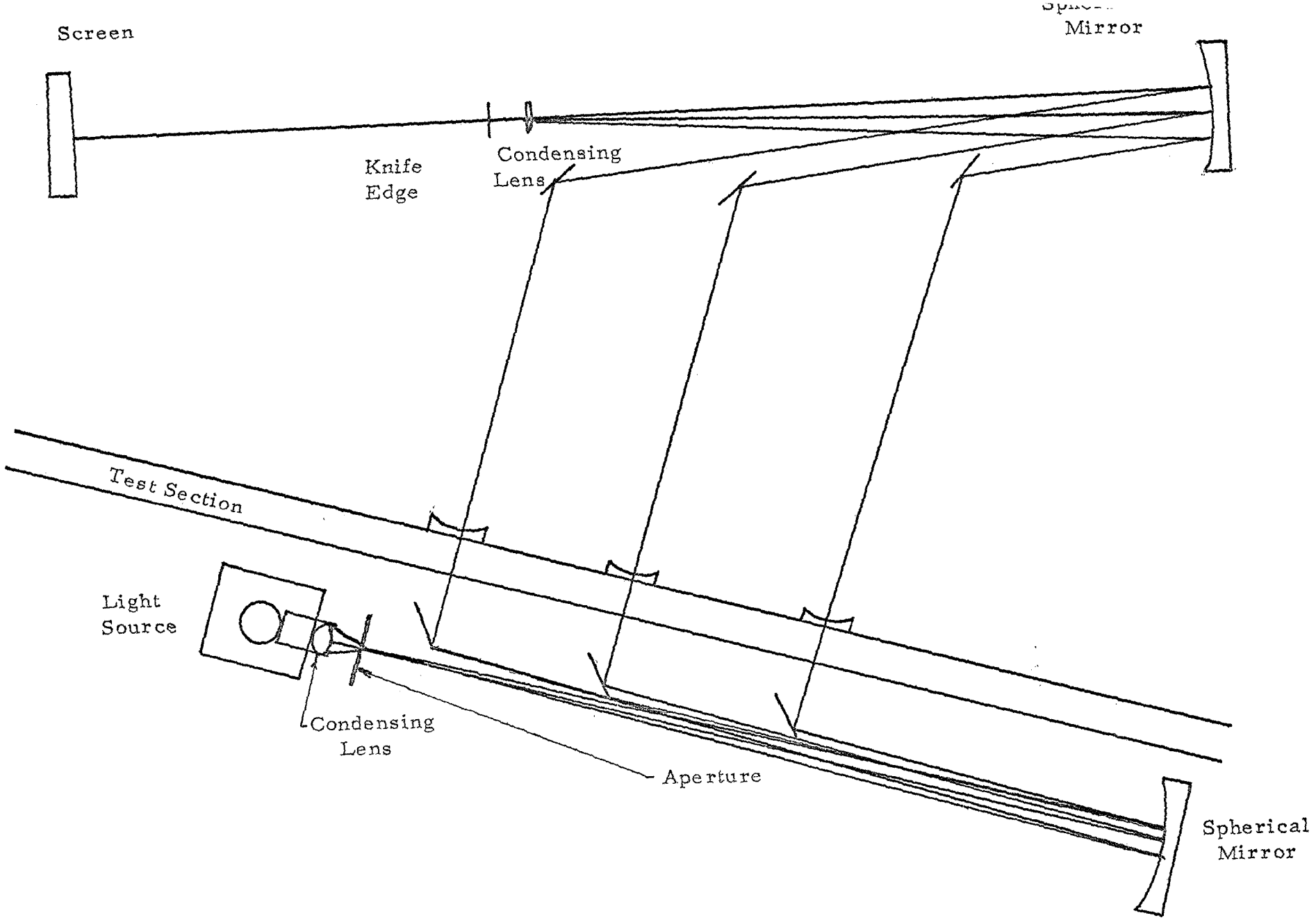

Figure 6. Schematic Layout of Schlieren System

have been obtained. The second consists of probes injected into the stream to supply information for description of the local flow field.

The first group consists primarily of pressure measurement, the flow control pressures are described in section 3.2.2. The flow condition pressure consists of static taps located opposite each instrumentation port. There are five side wall static taps at each station. One tap is located on the geometric center of the side wall. The remaining four are placed at .55 and 1.0 inches above and below the centerline tap. There are two static taps on each of the bottom and top blades. These taps are located 1/2 inch either side of the geometric center of the blade. Four additional static pressure taps were added at the noxzle exit. There were located on either side of the test section at the geometric centers of the top primary and bottom secondary flow channel. These static pressure taps were connected to an assembly of 40 mercury manometers since all static pressures to be measured were sub-atmospheric, the monometer board was of the commonwell variety. The data were recorded by a series of photographs taken during the run in which the manometer deflection as well as the level of the well were visible. Other control pressures were also recorded by these photographs.

In order to determine the local flow properties in the mixing region, the system was designed to inject pressure, temperature and gas sample probes into the flow stream at three separate locations or stations along the flow channel link. Briefly, the system consisted of a gas sampling rig (Figure 7) which formed part of the flow channel side when the probe was withdrawn. A shielded stagnation temperature and impact pressure probe which traverse flow field on a common arm.

The pressure probe is a simple .040 OD, .028 ID stainless steel tube projecting .250 inches in front of the tapered traverse arm. The tube extends through the steel body of the traverse arm, makes a 90° bend and extends on out of the sealed instrumentation box to be connected to the pressure transducer. The pressure transducer, Model No. PA769TC-200-350, is an absolute pressure gage of the strain gage type with temperature compensated elements in the interval of -65 to +250°F. The pressure range for these gases is from 0 - 150 psia.

The total temperature probe was of in-house manufacture and design. Its components are the thermocouple element which is steel encased and insulated and contains a chromel alumel thermocouple junction for temperature not exceeding a 1000°F and a platinum

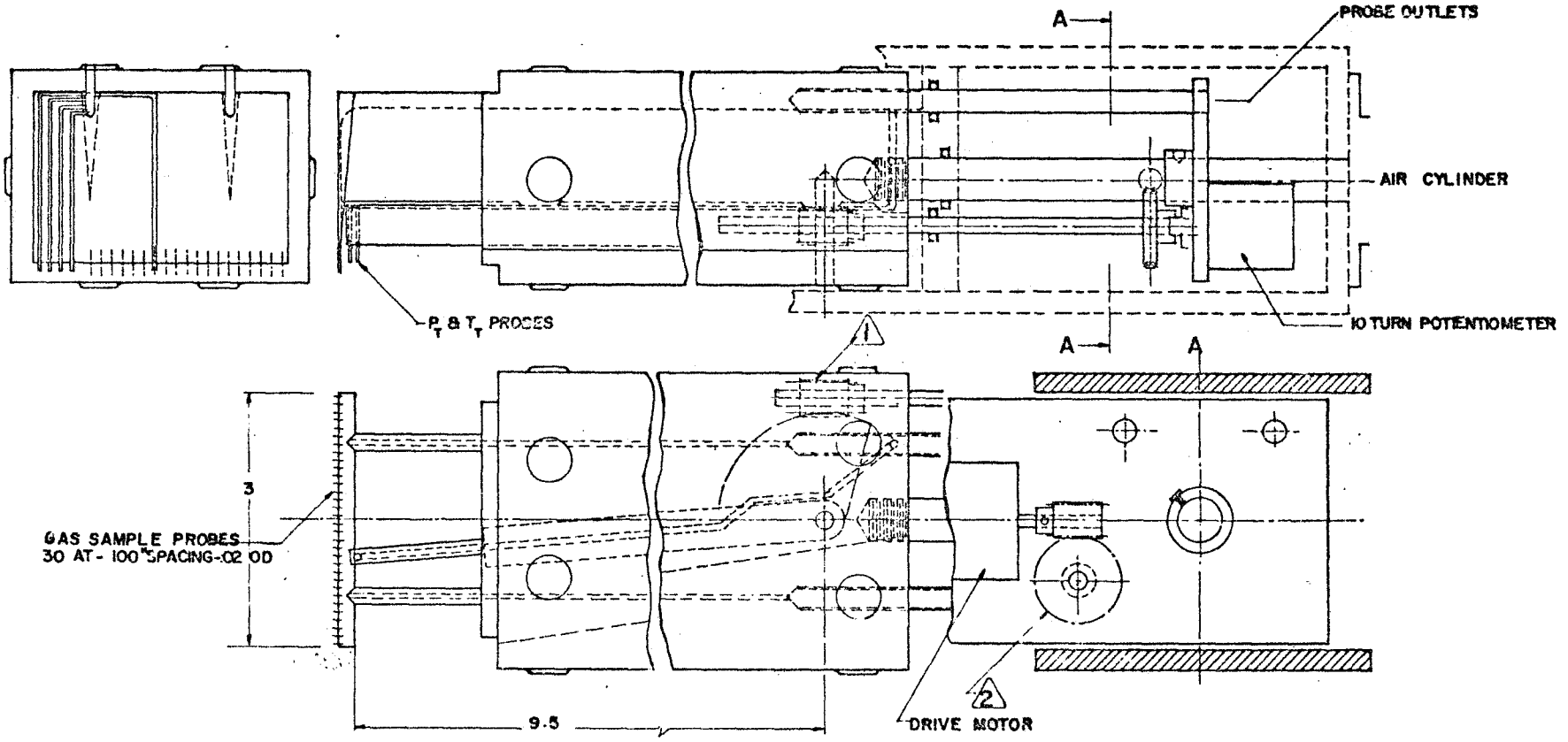

NOTES:

1. FASTENERS NOT SHOWN FOR CLARITY
2. WORM GEAR - PIC # Q7-28, WORM # Q 8-2
   GEAR REDUCTION = 120:1
   20° ARM SWEEP 6.7 TURNS ON INPUT SHAFT
3. WORM GEAR - PIC # Q 7-5, WORM # Q 8-2
   GEAR REDUCTION = 50:1
   MOTOR SPEED FOR 10 SECOND SWEEP = 200 rpm

UNLESS OTHERWISE SPECIFIED DIMENSIONS ARE IN INCHES TOLERANCES ON: FRACTIONS = ± 1/16 .x = ± .1 ANGLES = ± 1°, .xx = ± .05 SURFACE FINISH √ .xxx = ± .005	DRAWN / DATE		MOUNTAIN VIEW, ESTEC CALIFORNIA
	CHECKED		PROBE CARRIER ASSEMBLY
	DESIGN SUPERVISOR		
	ANALYSIS		
	PROJECT ENGR.		
	APPROVED		SIZE C / CODE IDENT NO 29559 / DRAWING NO. 100-1
	APPROVED		SCALE FULL SIZE / SHEET 1 OF 1

rhodium junction for temperatures above that range. The second component is the shield (See Figure 8). The shield has a .040 inch diameter opening with two vent ports of .020 inch diameter located just aft of the thermocouple junction.

In order to obtain the local flow field description, the pressure and temperature traverse measurements were accompanied by a traverse position measurement. This measurement was accomplished by the linkage of a linear potentiometer with a total resistance of 10,000 ohms and a linear travel of .44 inches.

(c) Gas Sampling System

The gas sample rake is made up of .020 inch OD stainless steel tubes mounted in a stainless steel wedge as shown in Figure 9. The spacing of the probes is nominally 0.1 inch. Seven tubes are selected at each station and connected to the sampling system shown in Figure 10. The remaining tubes are then blocked off to prevent unwanted fluid transfer into or out of the tunnel. The gas sample collection system shown in Figure 10 consists of a collector box sealed off by a surgical rubber membrane. Each collector chamber is pierced by two hypodermic needles. One needle leads to the sample probe itself, the other to a vacuum pump. When the rake is injected into the stream, the dynamic pressure of the flowing gases as well as the suction of the vacuum pump tend to purge the collector chamber. The collector chamber is partitioned such that the entire volume will be swept during this purge cycle. Immediately on injection of the sample rake into the flow stream, the pressure and temperature traverse is begun. When this traverse is completed, the solenoid valve is actuated which withdraws the hypodermic needles from the membrane in the sample collector. The sample then consists of gases trapped in the collector chamber at this time (probe injection to completion of pressure temperature sweep spans approximately 15 seconds). Seven such samples are obtained at each measurement station, allowing a construction of the gas composition profile across the mixing region as well as longitudinally.

The injection of the probes is sequenced such that minimum disturbance to the flow in the channel is obtained. Under high temperature conditions, water cooling is required for the probes when they are injected into the flow stream. This cooling must be coordinated to also satisfy the minimum disturbance criteria. After flow conditions have been established, the aft most probe is injected into the stream. Cooling water is circulated through the gas sample

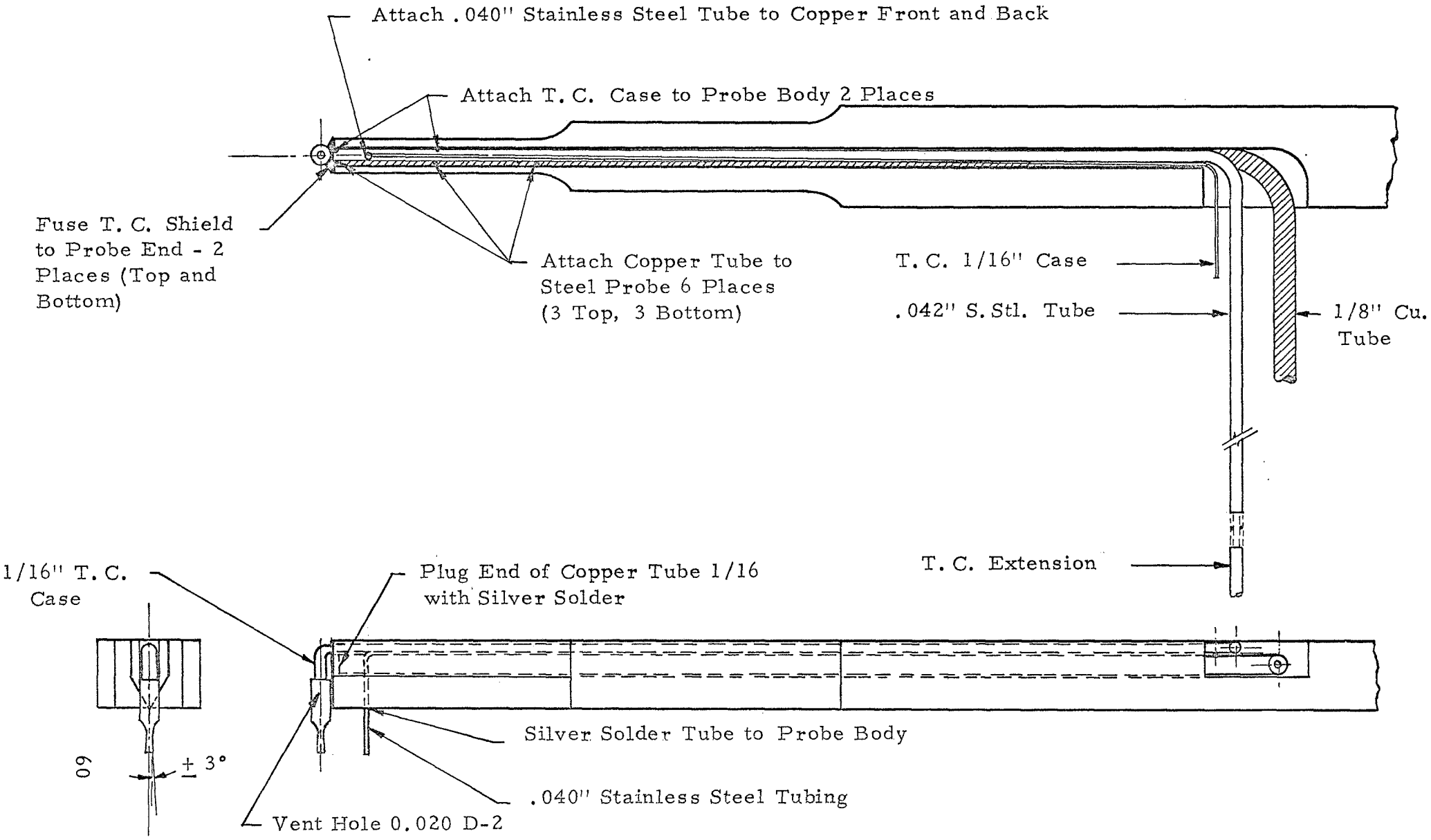

Figure 8. Pressure Temperature Probe Assembly

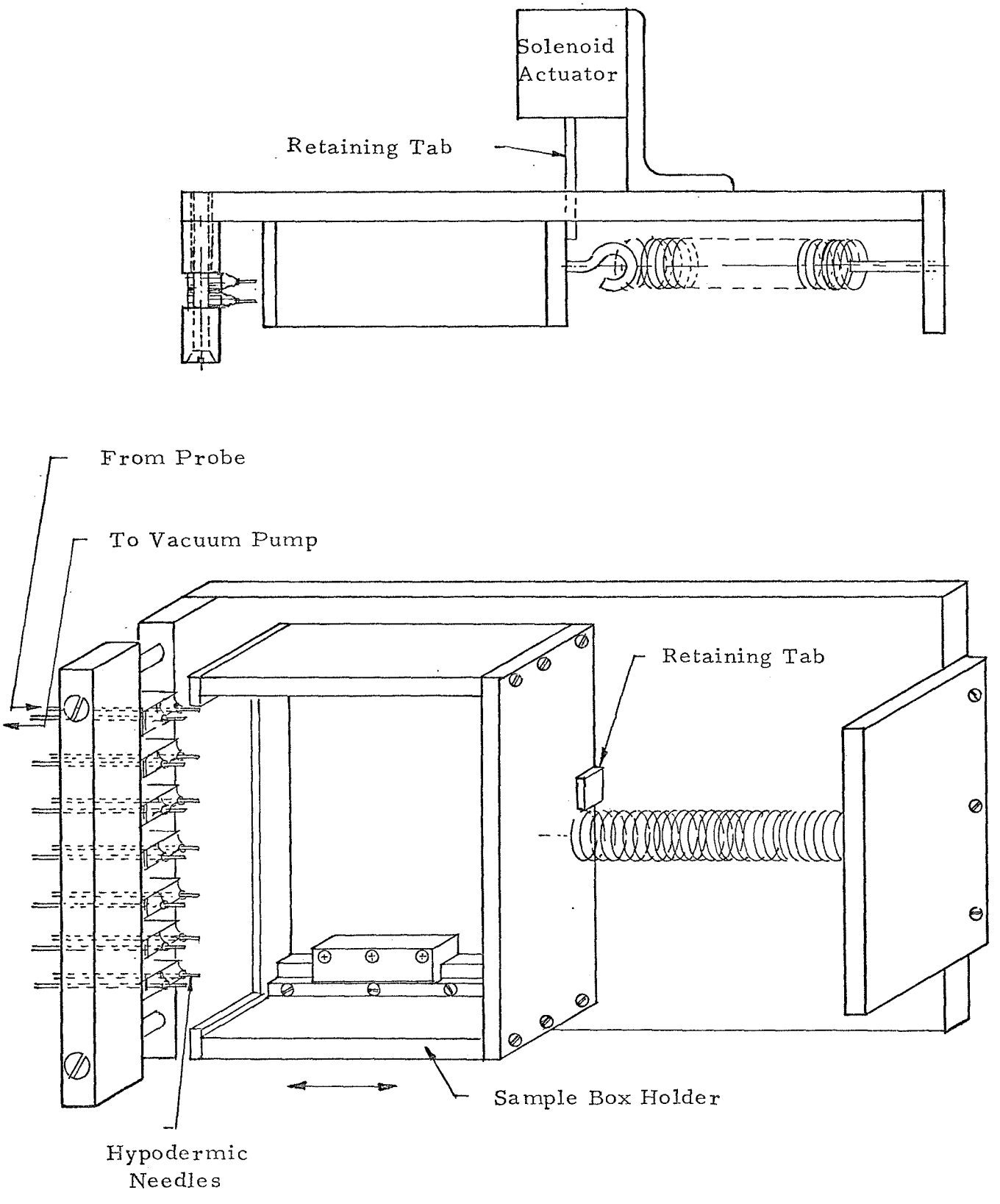

Figure 9. Gas Sample Collection System

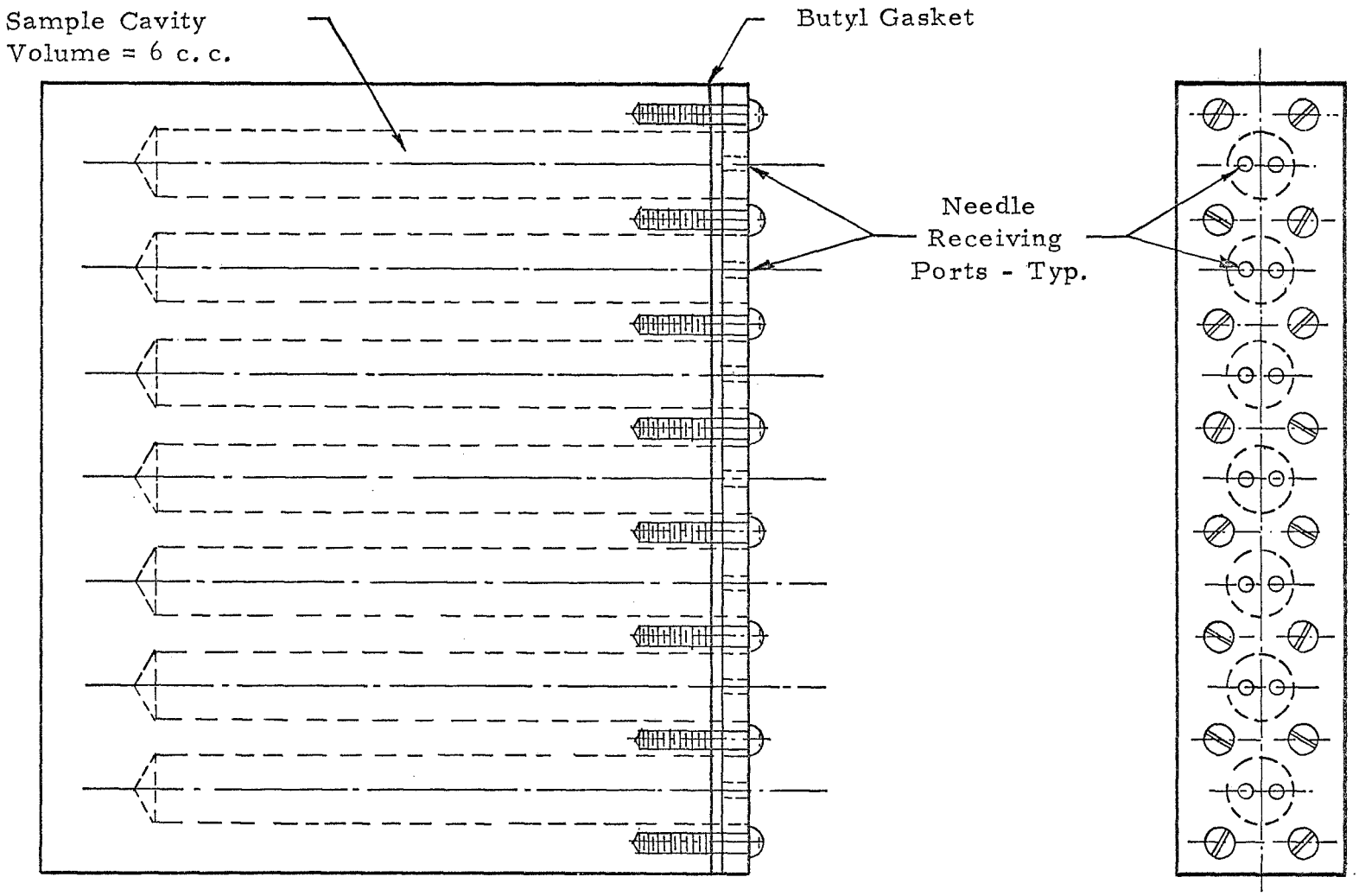

Figure 10. Sample Collector Box

rake and is injected into the traversing probe. Cooling water from the traversing probe passes out through a 1/8 inch copper tube and is sprayed onto the back of the probe through a series of .040 diameter holes drilled in the tube. Upon completion of this traverse, the probe is withdrawn and the probe just ahead of it is inserted. Residual water from the probe cooling system will not disturb measurements at this forward station and if the probe should, through some malfunction, remain in the stream, the forward measurements would not be disturbed providing the tunnel did not unstart due to choking. This sequence is then repeated for the third and forward most probe.

(f) Gas Analysis System

The analysis of gas samples obtained from the test section is accomplished with the gas chromatograph. The chromatograph unit employed is Model 90-P3 employing a 20 inch silica gel column and a 6 foot, 5X molecular sieve column in series. The carrier gas employed was argon rather than the usual helium. The chormatograph output was recorded on a 6 inch strip chart recorder with a disc integrator attachment.

The gas sample was inserted into the chromatograph by means of a gas sampling valve which injects a .25 milliliter sample into the columns. The volume of each test sample obtained from the gas sample probes in the test section is approximately 7 milliliters.

Each test sample is normalized to atmoshperic pressure with argon carrier gas using a U-tube water manometer and a 50 milliliter gas burette. The amount of argon necessary to normalize the sample is determined by means of the burette and U-tube. This, together with the knowledge of the volume of the sample, enables the sample dilution to be determined. The chromatograph output was calibrated using prepared samples with hydrogen to air ratios from 9:1 to 1:9 with argon to sample ratios from 1:1 to 20:1. In general, the response of the instrument was more linear in the range of the more highly diluted sample. Instrument sensitivity is such that more accurate results could be obtained using very dilute samples. However, preparation of these samples in such large number as would be required would be more laborious than using the calibration curves with respect to dilution. The accuracy of the overall experimental measurements is in the neighborhood of $\pm$ 5 percent. Gas composition measurements obtained by this method is well within that accuracy.

With the columns at approximately 150 degrees Centigrade and carrier gas flow rate at approximately 160 milliliters per minute, the sample passes through the columns and the analysis is completed in approximately 2 minutes. The gas sample system is shown schematically in Figure 11.

3.2.3 Experimental Program

This section is devoted to describing the conduct of the experimental program, observations during the check out runs leading to the final test procedure, as well as the test procedure itself.

A. Experimental Objectives

The experimental program was set up to obtain quantitative measurements of impact, pressure, concentration and temperature distributions in the region between two uniform parallel two-dimensional supersonic streams with constant cross sectional static pressure. Streamwise pressure gradients in the form of simple polynomials:

$$\frac{dp}{dx} = \begin{cases} ax + b \\ c \end{cases}$$

where a, b and c are small constant numbers and x is the distance in the streamwise direction - were to be investigated. Mixing of air and hydrogen streams with stagnation temperature ratios of 2:1 and 1:1 were to be investigated as well as mixing of two air streams with stagnation temperature ratios up to 6:1. Six contoured two dimensional nozzles with nominal design mach numbers of 1.7, 2.5 and 4.0 were to be combined in such a manner that velocity ratios of .18 to .53 are obtained in the hydrogen air mixing and velocity ratios of .36 to .83 are obtained in the air to air mixing.

Due to funding limitations all objectives of the experimental program were not accomplished. The experimental results encompassed isoenergetic mixing of the air streams over the designated Mach number range with 0 pressure gradient and specific investigations of constant and linearly varying streamwise pressure gradients.

B. Test Section and Instrumentation Checkout

During the checkout phase of the experimental program, the aerodynamic and mechanical characteristics of the test section and the instrumentation probes were determined. In the initial series of

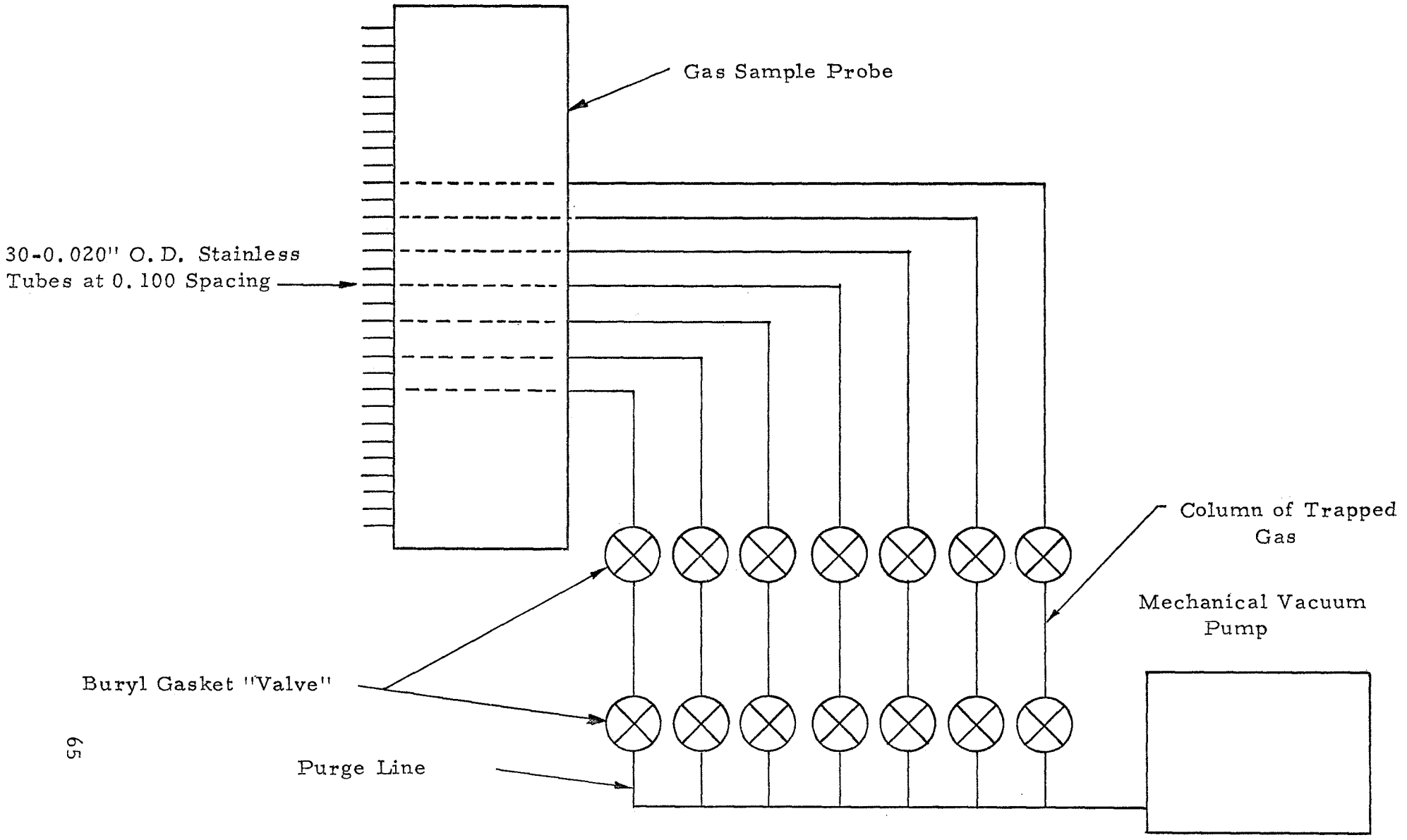

Figure 11. Schematic of Seven Point Gas Sampler

tests nominal Mach 1.7 nozzles were installed in both the primary and secondary streams. Boundary layer growth was found to be significantly greater than indicated by theoretical predictions. Total pressures of 60 psia and wall divergents of .350 of an inch were insufficient to obtain a uniform pressure along the lengths of the test section. However, after installing a Mach 2.5 nozzle in the secondary stream, uniform pressures were obtained with the wall deflection moderately uniform. This configuration resulted in adequate uniformity of pressure for all Mach numbers combinations in the isobaric mixing investigations. The diffuser was maintained at essentially wide open setting for all test conditions. A total pressure of 100 psi absolute for a Mach 2.5 stream mixing with the Mach 1.7 stream and a 350 psia total pressure for a Mach 4 stream mixing with a Mach 1.7 stream were found to give sufficiently small boundary layer growths and sufficiently long run durations to obtain satisfactory measurements in the mixing region.

During these initial checkout runs it was found that the aerodynamic forces were sufficient to cause the pressure and temperature traverse probes to oscillate as they swept across the stream. The phenumatic drive system for the traverse probe was then converted to a hydraulic drive which gave a positive displacement to the traverse actuator and eliminated the probe oscillation. Frequent purging of the hydraulic lines was necessary to maintain the lines clear of air and maintain their positive displacement nature. Adjustable two-way flow restrictors were installed at each traverse probe actuator to obtain the desired rate of traverse (approximately 10 seconds) and a fast rate return (less than 1 second).

After the test section aerodynamics were characterized to the extent that uniform constant pressure flow was obtained it was noted that the static to impact pressure and static to total pressure measurements did not yield the same free stream mach numbers. Measurements in the high Mach number flows indicated a definite interference of the gas sampling rake with the total temperature impact pressure probe. Such interference requires that a shock wave emanate from the tip of the gas sample probes at an angle greater than 70°. The wedge angle of the gas sample rake is 15°. A flow deflection of this magnitude at the lowest Mach number measured, approximately 1.65, would correspond to a 60° shock wave angle. Since care had also been taken in the design of the probes to avoid overall blockage of the test section it was concluded that there was a local flow blackage causing the shocks and the gas sample rake and the pressure temperature traverse probe to merge into a detached

bow shock. Since the gas sample probes were not necessary for the air mixing investigation they were removed from the instrumentation box. Static pressure readings along the test section indicated no adverse effects caused by the cavity in the side wall where the gas sample rates were removed. The test section static pressure remained constant and uniform. Agreement between the free stream Mach number as determined by the impact and by the total pressure measurement was greatly improved.

Uniformity of flow existing from the nozzle was investigated. Static pressure measurements at 1/4 inch intervals were taken at a distance 1 inch from the nozzle exit. These measurements indicated no more than a 5 per cent variation minimum to maximum of Mach number across the lowest Mach number nozzle. This variation includes the lip shock emanating from the .020 inch tip of the central divider. Schlieren records of the flow at the exit section indicate some flow nonuniformities but showed the lip shock to be by far the strongest. A typical example is shown in Figure 12.

3.2.4 Experimental Data and Results

Final experimental results were obtained for isoenergetic air to air mixing for 0, constant positive, and linearly increasing streamwise pressure gradients. Data were obtained for three combinations of primary and secondary stream Mach numbers under 0 streamwise pressure gradient conditions and a single combination of Mach numbers for each of the pressure gradient types.

Data from the experiments presented in three forms. The first is the particular velocity profile obtained by impact pressure surveys and local static pressure measurements. Three velocity profiles are presented for each run condition corresponding to measurements obtained at 3 axial stations along the mixing duct. The other forms in which the data are presented are derived from these velocity profiles. The second form is the effective spread parameter which is given by the divergence of the 10% and 90% velocity defect points in the mixing zone. The third is closely related, but is determined from the maximum slope of the velocity profile at a given station. It is found that the former, $\overline{\sigma}$, and the latter, $\sigma(0)$, are very nearly equal for the present experimental data.

The reduce data are tabulated in Appendix B. Velocity profile data appear in Tables B1. Spreading, rates, $\overline{\sigma}/\sigma_o$, and $\sigma(0)/\sigma_o$ are given in Table B2.

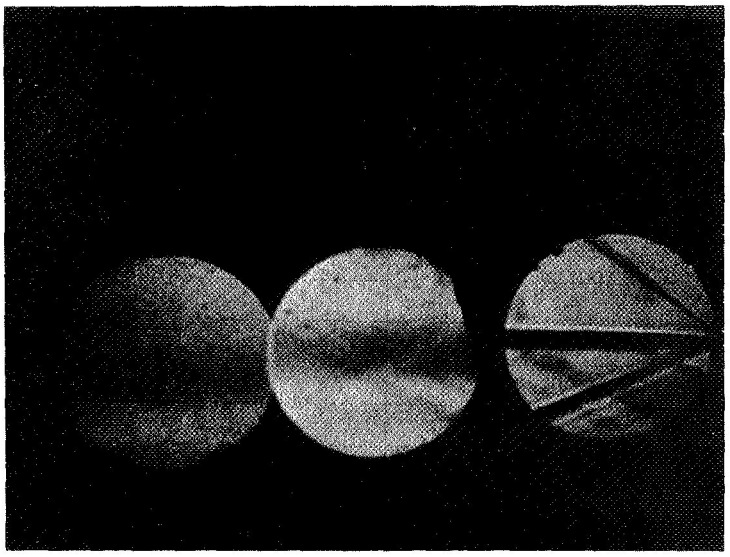

Figure 12. Typical Schlieren Picture from Run at M1 = 1.75 and M2 = 2.50. Pictures taken at window stations 0, 12 and 24" from Nozzle Exit.

The first form for the data allow an inspection of the detail of the mixing process while the second and third provides a means for comparing mixing zone spread rates under a wide variety of boundary conditions.

A. Velocity Profile Data

Velocity profiles were obtained from mean static pressure measurements and impact pressure measurements at each of three stations. The sensitivity of this technique appears to be affirmed by agreement with Mach number measurements in the free stream, as determined from static to total pressure measurements (within $\pm 2\%$). Displacement of the velocity point due to the velocity gradient across the probe is deemed to be minor since the opening on the pitot probe is less than .030 inches. This is well within the accuracy of the position measurement. Particularly since an accurate reference position was not obtainable from the position measurements apparatus. as it exists.

In general the velocity profiles obtained demonstrate the characteristics expected of flow configurations of this type. However, the appearance of boundary layer effects from the central divider was noted particularly in the low Mach number stream. These boundary layers were much thicker than design calculations had indicated. These effects manifested themselves as a dip in velocity below that of the lower speed stream in measurements taken near the divider tip. This strong effect washed out very rapidly and was never detected at the second measurement location which was approximately 18 inches from the divider tip. The effects were detectable far downstream, however, by the appearance of a ripple in the velocity profile at the outer edges of the mixing zone. That is, the velocity at the edge of the mixing zone would appear to have leveled off at a constant value but would then make a final adjustment to the order of 1% to the free stream velocity. The effects further manifested themselves in a lesser degree of similitude in the velocity profile than reported by some investigators.

The boundary layers on the upper and lower walls were detectable in some of the pitot traverses, however, their effects on the mixing region are nil. Since there was ample undisturbed free stream flow (a minimum of .3 inches) between the wall boundary layer and the edge of the mixing zone in all the final runs. To summarize the effects of the boundary layers we may neglect the wall boundary layer effects. The effects of the boundary layer on the central divider however, are definitely noticeable when this boundary layer is large,

as in the case of the low Mach number flow. (A thicker boundary layer was experienced in the lower total pressure in order to stay within the mass flow limitations of the facility). This initial boundary layer has two effects, the most apparent is an insulating effect which tends to decrease local velocity differences and, therefore, slow the mixing process in the initial region. The second effect is compensatory to the first, that is, the vorticity generated in the initial boundary layer may be significantly greater than that which would be generated by the velocity differences of the two streams. If this were the case then the initial mixing rates would be enhanced. The balance between these opposing effects will, therefore, shift depending upon the initial condition. For example, if the initial boundary layers were turbulent and the velocities of the two streams were very nearly equal, we would expect the latter effects to dominate and the mixing in the initial region to be enhanced. If on the other hand, the initial boundary layer were laminar and the velocity difference between the streams was large we would expect the insulating effect to dominate and the initial mixing rate would be lower than with the boundary layer absence.

B. The Spreading Rate of the Mixing Zone

The full spreading rate of the mixing zone is difficult to evaluate accurately. Since it is difficult to establish the exact boundaries of the mixing zone. One method commonly used is to determine the spreading of the 10% and 90% velocity defect points and define that as the spreading rate, $b_{.9}$.

$$b_{.9} \equiv y\left(\frac{\bar{u} - u_2}{u_1 - u_2} = .9\right) - y\left(\frac{\bar{u} - u_2}{u_1 - u_2} = .1\right) = y_{.9} - y_{.1}$$

Accordingly, this procedure was followed in reducing the present data.

The spreading rates, $b_{.9}$ for the zero pressure gradient conditions are shown in Figure 13a and those for the pressure gradient flows in Figure 13b. We note that none are particularly straight line variations as the zero pressure gradient theory would predict. This is a manifestation of the initial boundary layers.

C. The Jet Spread Parameters

Since the jet spread parameter varies across the mixing zone, it is necessary to pick a significant point to examine for comparative purposes. Two characteristic jet spread parameters have been referred to, $\bar{\sigma}$ and $\sigma(0)$, the effective spread parameter and the

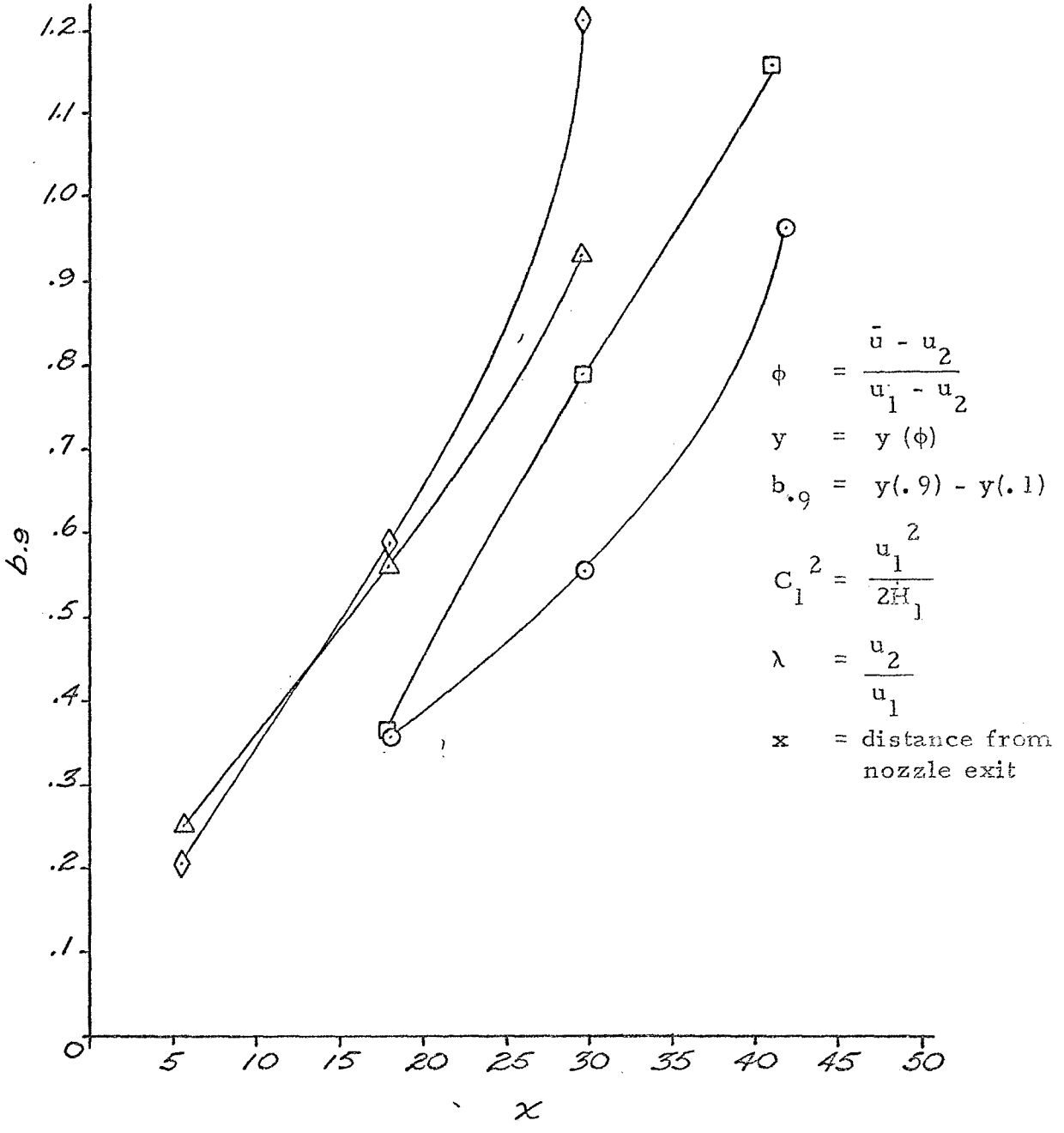

SYMBOLS

	C_1^2	λ
○	.691	.857
△	.691	.708
□	.694	.718
◇	.528	.818

FIG. 13 a. EXPERIMENTAL JET SPREADING RATES

$$\phi = \frac{\bar{u} - u_2}{u_1 - u_2}$$

$y = y(\phi)$

$b_{.9} = y(.9) - y(.1)$

$$C_1^2 = \frac{u_1^2}{2H_1}$$

$$\lambda = \frac{u_2}{u_1}$$

x = distance from nozzle exit

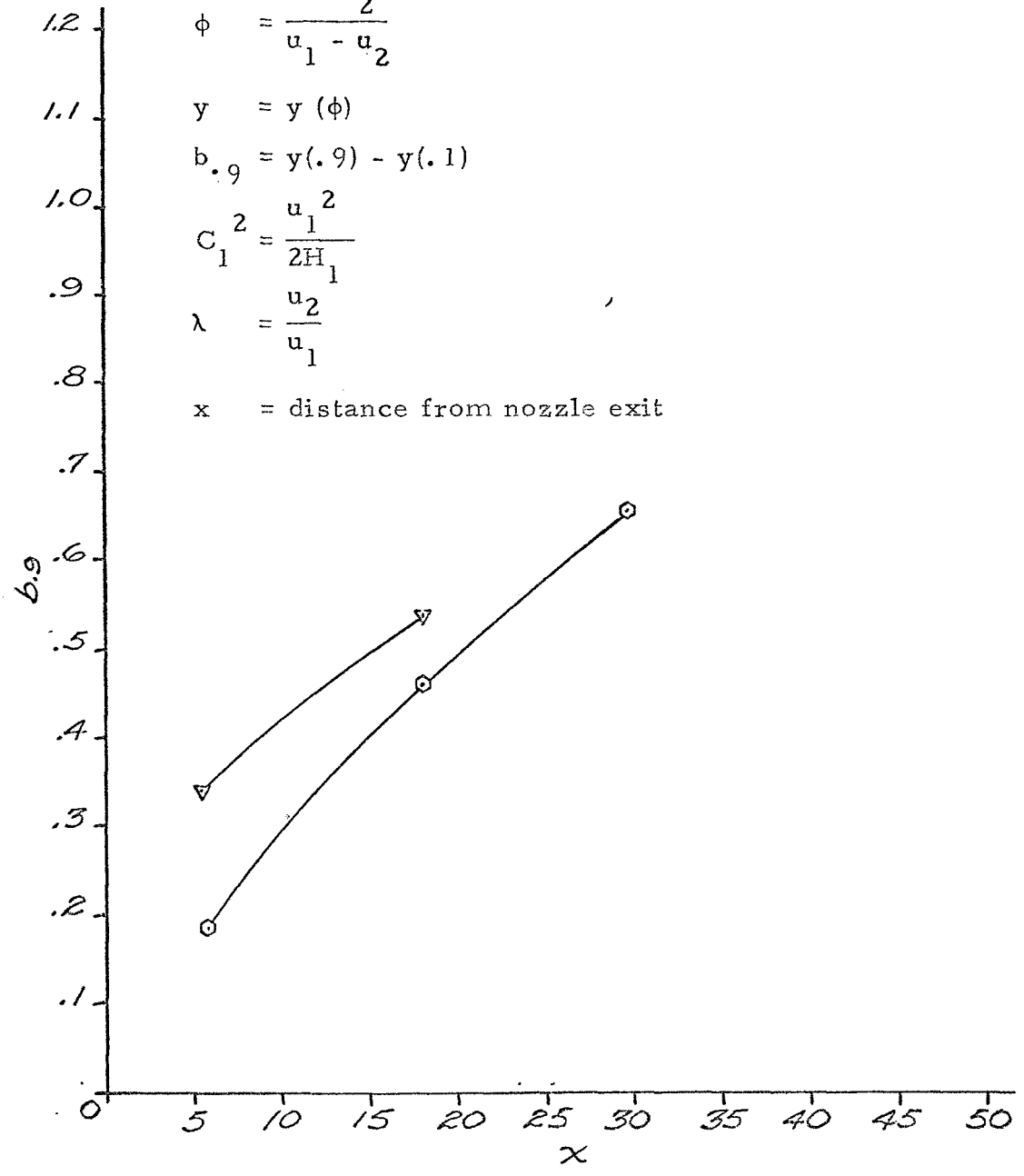

SYMBOLS

	C_1^2	λ	$\frac{dP}{dx}\left(\frac{PSI}{IN}\right)$
○	.735	.825	+.067
▽	.516	.773	+.03 + .0825 · X

FIG. 136 EXPERIMENTAL JET SPREADING RATES WITH PRESSURE GRADIENT

spread parameter evaluated at the point of maximum velocity gradient, respectively.

The effective spread parameter, $\bar{\sigma}$, is found experimentally from the spreading rate, $b_{.9}$ described above,

$$\frac{\bar{\sigma} b_{.9}}{x} \quad \frac{\sigma(y_{.9} - y_{.1})}{x} = \eta_{.9} - \eta_{.1}$$

It is found that for the error function profile, $\eta_{.9} \approx .9$, $\eta_{.1} \approx -.9$, therefore:

$$\frac{\bar{\sigma}}{\sigma_o} \approx \frac{1.8\, x}{11.0\, b_{.9}} ,$$

where: $\sigma_o = 11.0$ = the spread parameter for incompressible flow with $\lambda = 0$

The spread parameter ratio for the revised energy equation may be determined analytically to be:

$$\frac{\bar{\sigma}}{\sigma_o} = \frac{1 + \lambda}{1 - \lambda} \left[\frac{\rho_r}{\rho_1} \left(\frac{\beta - C_1^2 \lambda^2}{2(1 - C_1^2)} \right) \right]^{-1} \qquad (121)$$

Another likely candidate would be the point of maximum slope of the velocity profile, which is normally the average velocity point in the mixing region.

In the simple case of the error function velocity profile, this may be evaluated as follows:

$$\frac{u(\eta)}{u_1} = \frac{1 + \lambda}{2} \left[1 + \frac{1 - \lambda}{1 + \lambda} \operatorname{erf}(\eta) \right]$$

$$\frac{d\left(\frac{u}{u_1}\right)}{d\eta} = \frac{1 - \lambda}{2} \frac{2}{\sqrt{\pi}} e^{-\eta^2}$$

and noting that

$$\frac{d\eta}{d\left(\frac{y}{x}\right)} = \sigma + \frac{y}{x} \frac{d\sigma}{d\left(\frac{y}{x}\right)} \quad \text{and} \quad \frac{u(0)}{u_1} = \frac{1 + \lambda}{2} = \frac{1}{2}(u_1 + u_2)$$

Thus we evaluate the velocity gradient with respect to y/x at $\eta = \frac{\sigma y}{x} = 0$

$$\left.\frac{d(\frac{u}{u_1})}{d(\frac{y}{x})}\right|_{\frac{y}{x}=0} = \frac{1-\lambda}{\sqrt{\pi}}\,\sigma(0)$$

We may divide this expression by σ_o (= 11.0). The incompressible jet spread parameter, and rearrange to yield:

$$\frac{\sigma(0)}{\sigma_o} = \frac{\sqrt{\pi}}{(1-\lambda)\,\sigma_o}\left.\frac{d(\frac{u}{u_1})}{d(\frac{y}{x})}\right|_{\frac{y}{x}=0}$$

The right hand side of this expression may be determined by graphical differentiation of the measured velocity profile and by the measured velocity ratio.

The spread parameter ratio may be determined analytically from the definition of η and the relation derived in section 3.1.7 for $\frac{\sigma_o y}{x}$

$$\frac{\sigma(0)}{\sigma_o} = \lim_{\eta\to o}\frac{\eta}{\frac{\sigma_o y}{x}} = \lim_{\eta\to 0}\frac{\eta}{\frac{1-\lambda}{1+\lambda}\frac{\rho_r}{\rho_1}\int_0^{\eta}\frac{\rho_1}{\rho}\,d\eta'}$$

Which becomes:

$$\frac{\sigma(0)}{\sigma_o} = \frac{1}{\frac{1-\lambda}{1+\lambda}\frac{\rho_r}{\rho_1}\cdot\frac{\rho_1}{\rho(0)}} \qquad (122)$$

The two characteristic spread parameters for the present investigation are shown in Table B2 for the different cases. It is found that the difference between the two is slight. Yielding to the desire to predict the jet spreading rates we will use the effective spread parameter $\bar{\sigma}$ for our comparisons. Table I lists the available data for $\frac{\bar{\sigma}}{\sigma_o}$ from various investigators.

Table I

Summary of Experimental Values of Jet Spread Parameter

Crocco No. C_1^2	Velocity Ratio λ	Temperature Ratio β	Parameter Ratio $\bar{\sigma}/\sigma_o$	Reference	Data Set
0	0	1.0	1.0	19	
0.111	.5	.882	3.1	20	
0.284	0	.952	1.48	21	a
0.430	0	.930	1.42		b
0.152	0	.935	1.20		c
0.127	0	.935	1.06		d
0.338	0	1.014	1.40	22	
0	.36	1.0	2.58	23	a
0	.46	1.0	3.91		b
0	.61	1.0	4.05		c
0	.66	1.0	4.76		d
0.496	0	1.0	1.94	24	
0.69	0.86	1.0	7.7	Present	a
0.69	0.71	1.0	5.1	"	b
0.695	0.72	1.0	5.3	"	c
0.528	0.82	1.0	4.5	"	d
*0.735	*0.825	1.0	2.7	"	e
*0.698	*0.836	1.0	6.2	"	f
*0.686	*0.838	1.0	7.4	"	g
+0.516	+0.773	1.0	4.9	"	h
+0.487	+0.837	1.0	5.4	"	i

*Local values for $\frac{dp}{dx} = +0.067$ psi/inch

+Local values for $\frac{dp}{dx} = +0.03 + 0.0825x$ psi/inch

Turning again to the details of table B2, we note the spread parameter at the forward stations is somewhat different than at the latter stations. The spread parameter at the forward stations appears to be somewhat different from the spread parameter at the latter stations. Such can also be noted from the spread rate data in Figure 13. This is particularly pronounced in the low Mach number runs and tends to substantiate the boundary layer effects discussed earlier. If we assume the spread parameter approaches the value which would exist in the absence of the initial boundary layer effects and we may further assume the lack of similarity in the velocity profile to be due to these initial boundary layer effects. We may consider the limit values of spread parameters to be those for the mixing of ideal uniform streams. Agreement between these data and predictions for such uniform streams will be discussed in the following sections.

3.3 Comparison of Data with Theory

A reference density has been determined which reasonably correlates the mixing data obtained where severe, initial boundary layer effects were not present. The correlations of $\frac{\bar{\sigma}}{\sigma_o}$ appear to be valid for the compressible flow data of other investigators in the low velocity ratio range and for the present data in the high velocity ratio range. The latter being the only known measurements of this sort for compressible flows in the high velocity ratio range. The incompressible flow data of Sabin[23] throughout the velocity ratio range (high and low) is well correlated by the present expressions, since his excellent correlations of these data were used as the incompressible basis for the analysis in the compressible regime.

Data were obtained for two cases of mixing with a positive streamwise pressure gradient, and the analytical development completed. It was not possible, under the present contract, to assess the agreement between the data and theory, since funds for developing the computer program and making the necessary calculations were not available. However, the theory uses the zero pressure gradient solution as a basis and the reference density for this solution is apparently identical to that for the base solution. The experimental values for the spread parameter in these mild pressure gradient are not markedly different from the similar zero pressure gradient flows. These two facts lead us to believe the agreement for this more general situation will be essentially as good as for the case of isobaric mixing.

3.3.1 Comparison of Zero Pressure Gradient Data and Theory

The primary purpose of this combined analytical and experimental study of compressible turbulent mixing was to seek an evaluation of the reference density (arising in the analytical treatment) which will satisfy the requirements of the analysis and produce a correlation of mixing data. Such a correlation would allow the prediction of spread rates, through an appropriately defined spread parameter, and a prediction of velocity profile data, given the boundary conditions for the flow:

(1) Primary Crocco number, C_1^2
(2) Total enthalpy, H_1
(3) Velocity ratio, λ
(4) Total enthalpy ratio, β

An empirical representation of such a reference density has been obtained using these data and that of other investigators. This reference density is applicable except at values of the product $\lambda^2 C_1^2$ very near unity.

The general agreement between the theory and data is assessed in two ways. The first, and the method by which the reference density was formulated, is evaluated on the basis of the predicted effective spread parameter based on spreading rate and that obtained experimentally. The second is a comparison of the predicted and measured velocity profiles.

Substantial agreement was obtained except where significant initial boundary layer effects were present. These effects were significant primarily in the low Mach number cases, due to the low total pressures required under these conditions. As mentioned in section 3.2.4A the effects of the initial boundary layer appeared to be a function of the relative vorticity created by the gas interface versus that produced by the gas-wall interface. A simple Reynolds number correlation of those effects does not appear possible. That is, in some instances the initial boundary layer appeared to isolate the streams and retard mixing while in others, mixing was enhanced. The particular behavior is qualitatively predictable upon weighing the thickness of the initial boundary layer and the relative vorticity due to the gas-solid and gas-gas interface.

It was, therefore, necessary to consider the asymptotic values of the spreading rate in assessing the correlation. That is, as the mixing proceeds downstream, the effects of the initial conditions will diminish

and the pure gas-gas mixing mechanisms will dominate. Thus, the spreading rate far from the initial boundary layer should approach that for mixing in absence of an initial boundary layer. Based on this assumption, a correlation of the jet spread parameter for all available data was made.

The relation (121) may be compared to the experimental value when the appropriate relation for $\frac{\rho_r}{\rho_1}$ is substituted.

Conversely, this comparison will allow the reference density to be evaluated. Correlation of the present data and those of other investigators resulted in the following formulation for the reference density.

$$\frac{\rho_r}{\rho_1} = \frac{1 - C_1^2}{\frac{1}{2}(1 + \beta) + C_1^2 [1 - 2\lambda + .64\lambda^2 - \frac{1}{2}(1 + \lambda^2)]}$$

That is, referring to equations 37, $A = \frac{1}{2}$, $B = 1$, $D = -2$, and $E = .64$.

This relation is used in conjunction with the revised energy equation.

A reference density evaluated with the laminar form of the energy equation was considered to be inappropriate for the present turbulent mixing study and was not totally evaluated. It was found that considerable modification to the reference formula would be necessary to obtain agreement with a large part of the data. It has also been assumed that the reference state was a physical state somewhere within the mixing layer. As such, certain restrictions are placed upon the experimentally evaluated constants in the reference state equation for values of the parameters C_1^2, λ, and β of interest. A cursory examination of the equation constants necessary to provide reasonable correlation of the data available with the laminar relation, revealed that the parameter values for which the reference state would correspond to a physical state within the mixing region was unduly restrictive. Indeed, that problem is not altogether absent from the above relation, but these restrictions pertain only for values of C_1^2 and λ very near 1.

The correlation of the data for $\frac{\bar{\sigma}}{\sigma_o}$ with this formulation is shown in Figure 14.

Velocity profiles for four cases are shown in Figures 15 through 18 and as determined with the proposed reference density and as measured

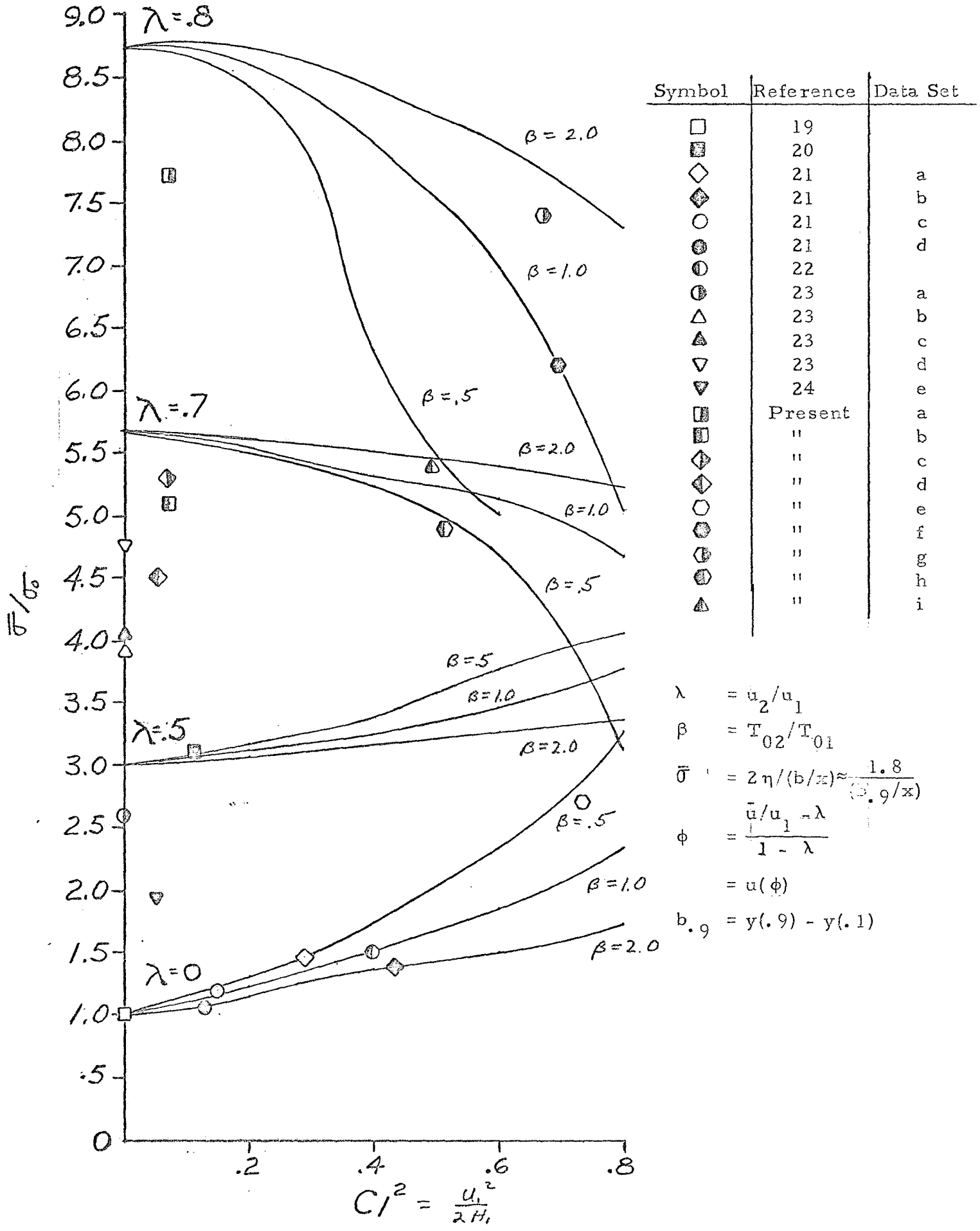

Symbol	Reference	Data Set
□	19	
■	20	
◇	21	a
◆	21	b
○	21	c
●	21	d
◐	22	
◑	23	a
△	23	b
▲	23	c
▽	23	d
▼	24	e
◧	Present	a
▣	"	b
◈	"	c
◈	"	d
⬡	"	e
⬢	"	f
◑	"	g
◍	"	h
▲	"	i

$\lambda = u_2/u_1$

$\beta = T_{02}/T_{01}$

$\bar{\sigma} = 2\eta/(b/x) \approx \frac{1.8}{(b_{.9}/x)}$

$\phi = \frac{\bar{u}/u_1 - \lambda}{1 - \lambda}$

$= u(\phi)$

$b_{.9} = y(.9) - y(.1)$

FIG. 14 EFFECTIVE JET SPREAD PARAMETER

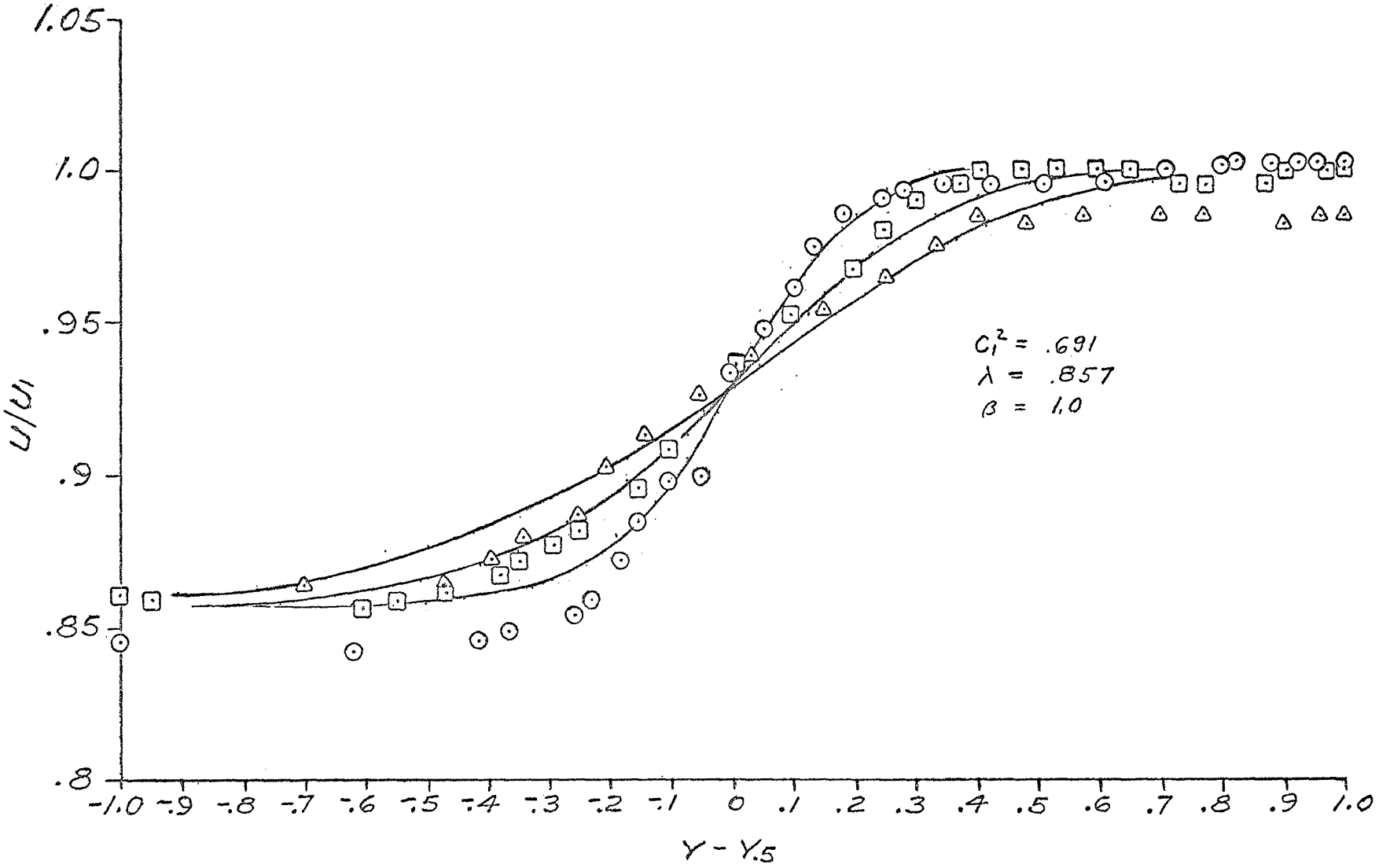

FIG 15 VELOCITY PROFILES FOR AIR-AIR MIXING

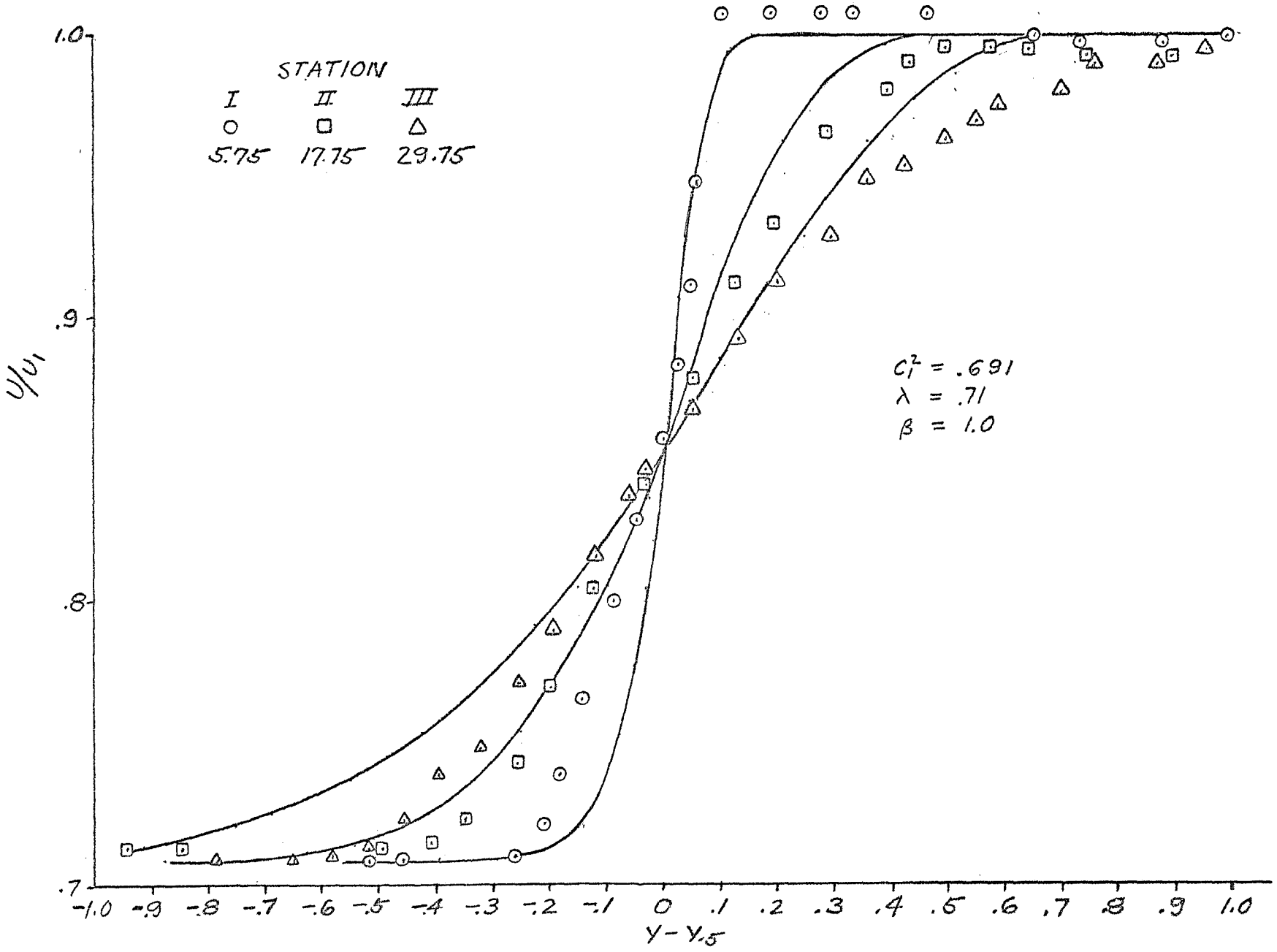

FIG. 16 VELOCITY PROFILES FOR AIR-AIR MIXING

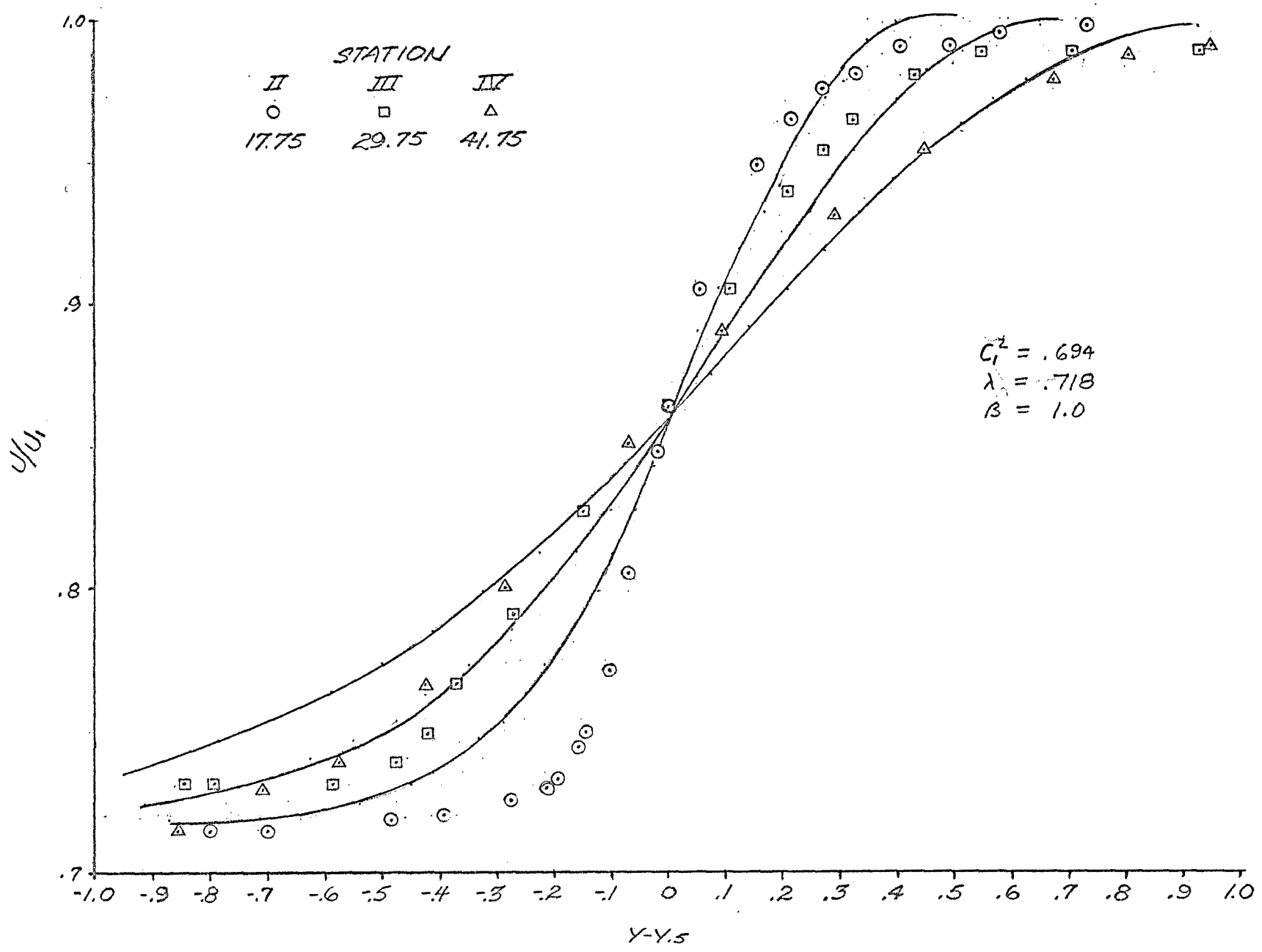

FIG. 17 VELOCITY PROFILES FOR AIR-AIR MIXING

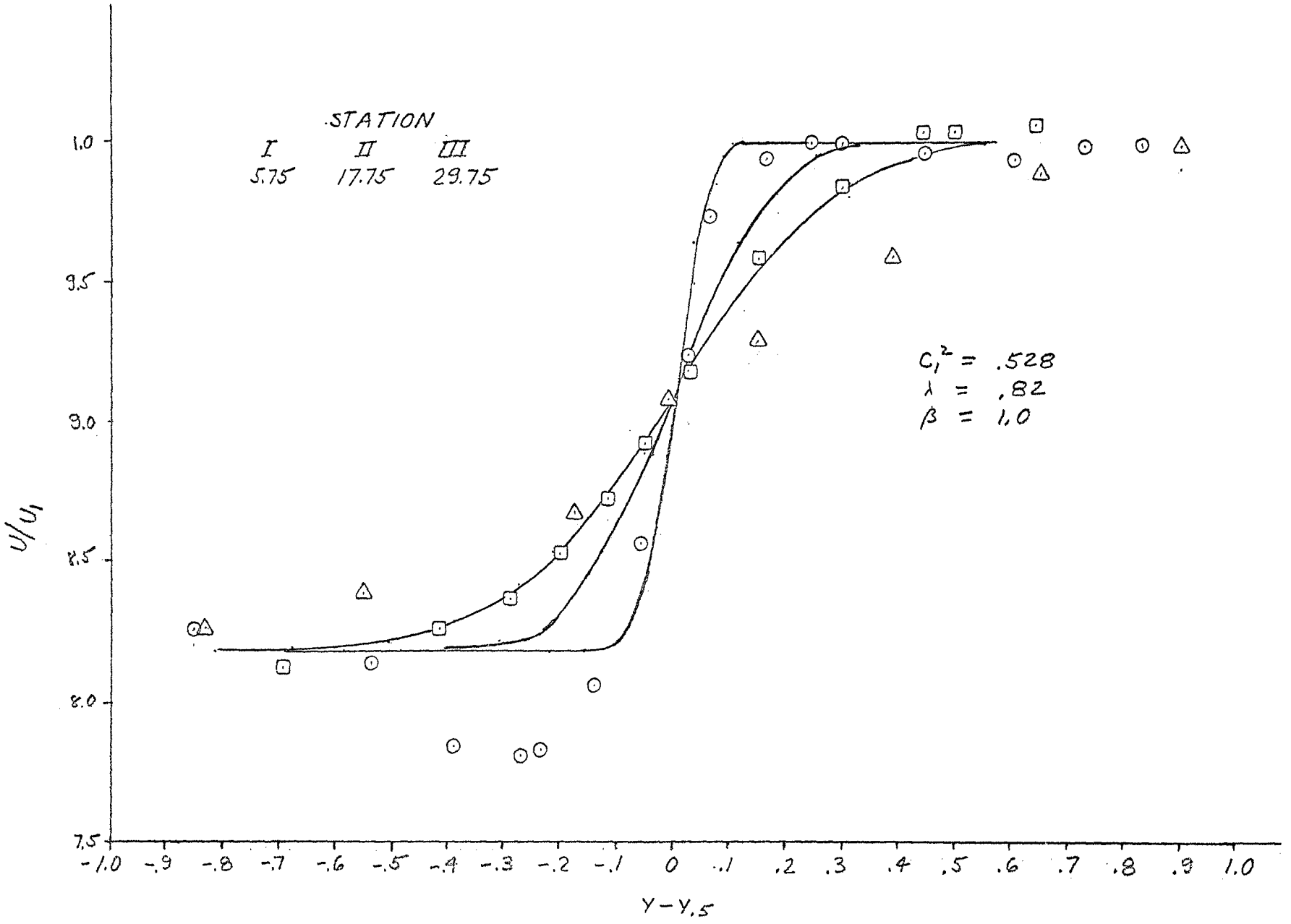

FIG. 18 VELOCITY PROFILES FOR AIR-AIR MIXING

at each of three stations for each case. The initial boundary layer effects are, of course, not reflected in the theoretical curves. However, the general asymptotic spread rate of the mixing zones is fairly represented for the available data.

3.3.2 Streamwise Pressure Gradient Comparison

Two sets of experimental velocity profiles have been obtained for mixing with positive streamwise pressure gradients (see Figure 19 and 20). These data may be compared to the theoretical relations of section 3.1.8 in the same manner as were the corresponding relations for the isobaric mixing investigation. However, these correlations will be a function of the streamwise coordinate, x.

The comparison of a theoretical and experimental jet spread parameter as a figure of merit for the mixing rate is quite similar to the isobaric case. The experimental value is determined locally in the same manner as the isobaric case with the boundary conditions replaced by local boundary conditions.

$$\frac{\sigma(o, x)}{\sigma_o} = \frac{1}{\sigma_o \left(1 - \frac{u_2(x)}{u_1(x)}\right)} \left(\frac{\Delta \frac{u}{u_1}}{\Delta \frac{y}{x}}\right)_{max.}$$

The theoretical value is obtained from equation (107) of section 3.1.8.

$$\frac{\sigma(o, x)}{\sigma_o} = \frac{\eta}{\sigma_y \left(\frac{o}{x}\right)} \Bigg|_{y = 0}$$

$$= \frac{1}{\frac{1 - \lambda}{1 + \lambda} \frac{\rho_r}{\rho_{0_1}} \left(\frac{p_o}{p}\right) \frac{1}{2} \left\{ \frac{h_0(o)}{h_{0_1}} + (\gamma - 1) M_{0_1}^2 \sum_{N=1}^{M} a_N x^N r_N(0) \right\}}$$

Where $\frac{\rho_*}{\rho_{0_1}}$ may be chosen to be equal to $\frac{\rho_*}{\rho_1}$ for the isobaric case, with ρ_{0_1} equal to the initial density of the primary stream. The pressure ratio $\frac{p}{p_o}$ is the ratio of local to initial pressure and the other terms are as defined in section 3.1.8.

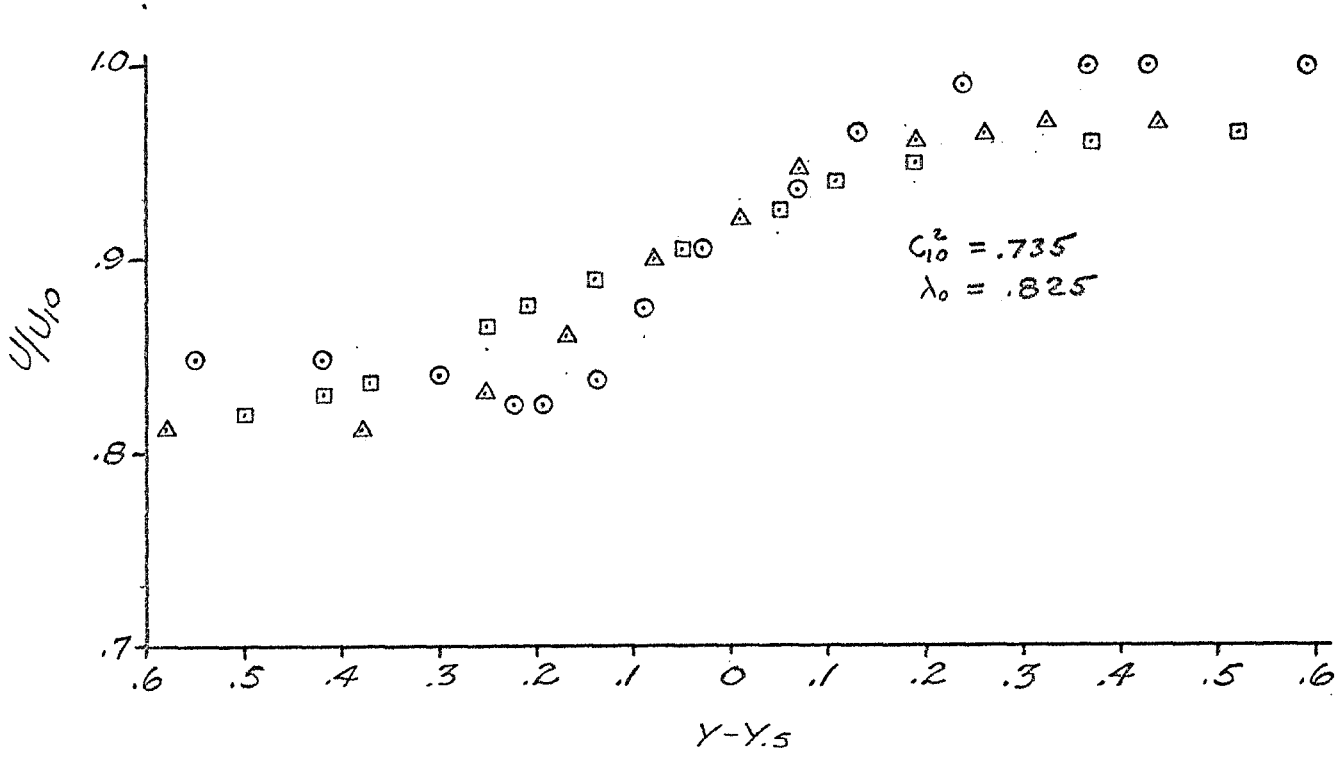

STATION

I	II	III
○	△	□
5.75	17.75	29.75

FIG. 19 VELOCITY PROFILES FOR AIR-AIR MIXING WITH PRESSURE GRADIENT

$$\frac{\Delta P}{\Delta X} = .067 \frac{PSI}{INCH}$$

$C_{10}^2 = \frac{U_0^2}{2H_1}$, INITIAL CROCCO NO.

$\lambda_0 = \frac{U_{20}}{U_{10}}$, INITIAL VELOCITY RATIO

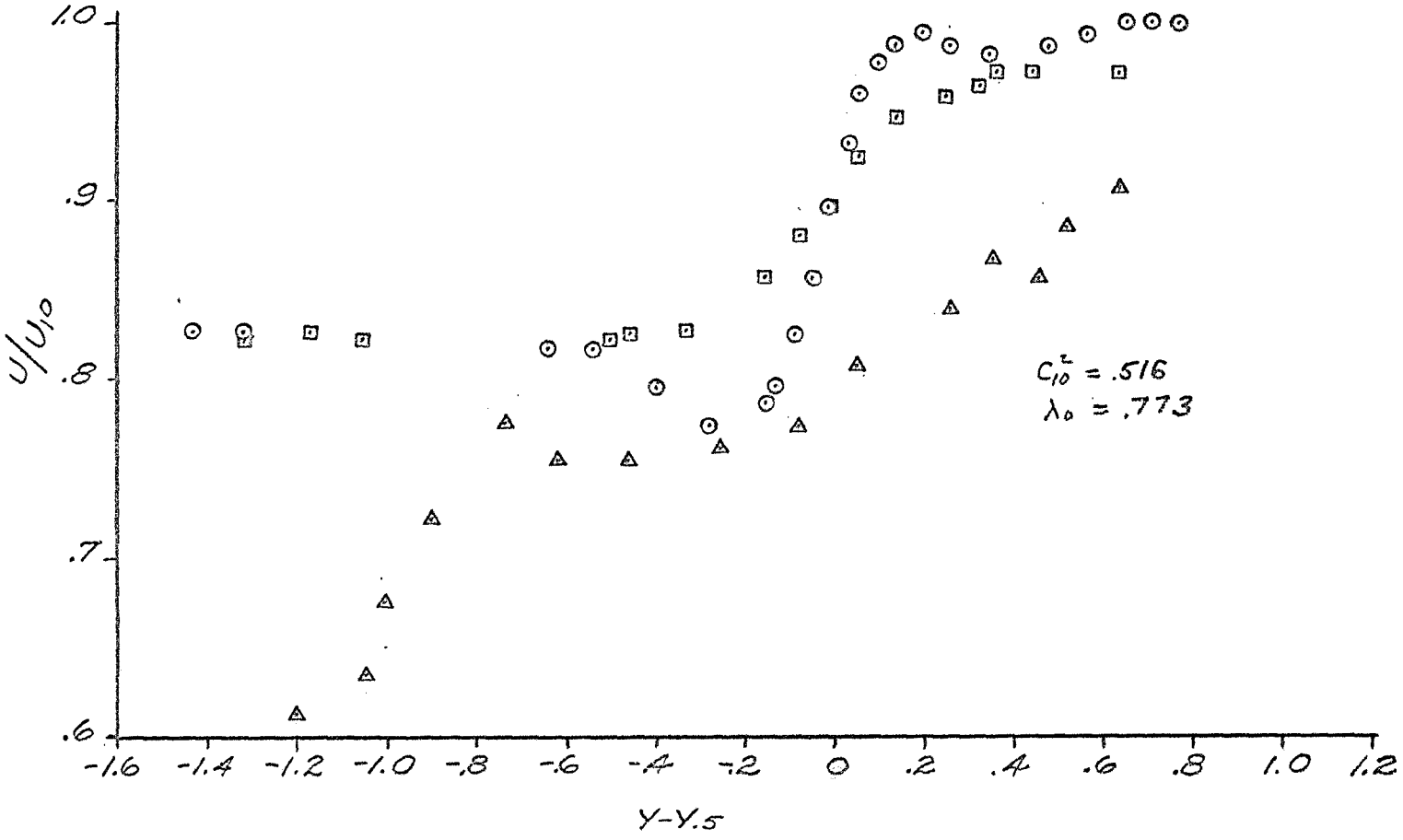

FIG. 20 VELOCITY PROFILES FOR AIR-AIR MIXING WITH PRESSURE GRADIENT

$$\frac{\Delta P}{\Delta x} = .03 + .0825 x \frac{PSI}{IN}$$

Actual comparison of results in terms of velocity profiles were not possible under the present funding due to the necessity for additional computer programming. However, general agreement appears to be good since variations in spreading rate from similar isobaric mixing measurements are small.

The mitigating effects of the initial boundary layer off the central flow divider are somewhat difficult to assess quantitatively, since both introduce an element of longitudinal variation of the parameters. The positive pressure gradient conditions for which the experiments were performed are particularly susceptible to the boundary layer disturbance since they tend to thicken the boundary layers.

3.4 Conclusions and Recommendations

The program, completed to its present stage, has five major accomplishments which should contribute significantly to the study and analysis of turbulent free shear layers.

1. A reference density for the first time has been obtained which allows prediction of isobaric turbulent mixing rates in the near field for compressible flow of similar gases. The unique reference density approach has been experimentally confirmed for isoenergetic streams.

2. This prediction method has been analytically extended to compressible flows with streamwise pressure gradients. The reference density for this condition is indicated to be that for the isobaric flow evaluated with conditions existing at the onset of mixing.

3. The relation between the enthalpy and velocity distribution in turbulent free shear flows has been shown to be analytically different from the relation for laminar flows and preliminary experimental confirmation of this has been obtained for the newly derived relation. The restriction of unity turbulent Prandtl number has been relaxed.

4. A hardware and instrumentation system has been developed and brought to working status which will enable the accurate experimental investigation of a wide range of free shear flow problems. Specifically, such problems which are of vital interest to design and optimization of SCRAMJET combustors as well as problems of a more fundamental nature.

5. Molecular weight effects have been included in the analysis. and the means to evaluate the reference state for dissimilar streams proposed.

REFERENCES

1. Channapragada, R. S., J. P. Woolley, "Turbulent Mixing of Parallel Compressible Free Jets" AIAA Paper 65-606 Presented at first Propulsion Joint Specialist Conference, Colorado Springs, Colorado, June 14-18, 1965.

2. Woolley, J. P., "The Time Mean Energy Equation for Turbulent Compressible Boundary Layers, and a Solution", submitted for publication as a technical note in AIAA Journal.

3. Low, G. M., "The Compressible Laminar Boundary Layer with Heat Transfer and Small Pressure Gradient", NACA TN 3028, October 1953.

4. Howarth, L., "Concerning the Effect of Compressibility on Laminar Boundary Layers and Their Separation," Proc. Royal Soc, (London), Vol. 194, p. 16, (1948).

5. Schlichting, H., "Boundary Layer Theory" 4th ed. McGraw Hill, 1960.

6. Tollmein, W., "Berechnung der Turbulenten Asubreitungsvorgaenge," ZAMM, 6, pp. 468-479, 1926 (Also NACA TM1985, 1945).

7. Keuthe, A. M., "Investigations of the Turbulent Mixing Regions Formed by Jets", Journal of Applied Mechanics, Vol. 2, No. 3, (1935).

8. Gortler, H., "Berechnung von Aufgaben der Freien Turbulenz auf Grund eines neuen Naeherungs-ansatzs," ZAMM, 22, pp. 244-254, (1942).

9. Crane, L. J., "The Laminar and Turbulent Mixing of Jets of Compressible Fluid-Part II the Mixing of Two Semi-Infinite Streams," Journal of Fluid Mechanics, Vol. 3, Part I, (October, 1957).

10. Eckert, E. R. G., "Survey on Heat Transfer at High Speeds," WADC TR 54-70, April, 1954 (Also Transactions of ASME, p. 1273, August, 1956).

11. Knuth, E. L., "Use of Reference States and Constant-Property Solutions in Predicting Mass.-Momentum-and Energy-Transfer Rates in High Speed Laminar Flows," Int. J. Heat Mass Transfer Vol. 6 pp. 1-22, Pergamon Press, 1963.

12. Knuth, E. L., Dershin, H., "Use of Reference States in Predicting Transport Rates in High Speed Turbulent Flows with Mass Transfer," Vol. 6 pp. 999-1018, Pergamon Press, 1963.

13. Scott, C. J., "The Application of Constant Property Solutions to Mass Transfer Cooling Calculations" Engineering Memo No. 76 University of Minnesota Institute of Technology, December, 1958.

14. Pai, S. I., "Fluid Dynamics of Jets," D. Van Nostrand, 1954.

15. Burggraf, O. R., "The Compressibility Transformation and the Turbulent Boundary Layer Equations," Journ, Aero. Sciences, Vol. 29, No. 2, (April, 1962).

16. Coles, D. E., "The Turbulent Boundary Layer in a Compressible Fluid," USAF Project Rand, Report R-403-PR, September, 1962.

17. Crocco, L., "A Transformation for the Compressible Turbulent Boundary Layer", AIAA Journal, 1, 12, December, 1963.

18. Wallace, J. E., "Hypersonic Turbulent Boundary-Layer Measurements Using an Electron Beam," AIAA Journal, 7 No. 4, April 1969 also, Report AN-2112-Y-1, June 1968, Cornell Aeronautical Lab., Buffalo, N. Y.

19. Liepmann, H. and Laufer, J., "Investigations of Free Turbulent Mixing," NACA TN 1257 (1947).

20. Szablewski, W., "Contributions to the Theory of the Spreading of a Free Jet Issuing from a Nozzle", Translation from the German NACA TM 1311, Nov. 1951.

21. Maydew, R. C. and Reed, J. F., "Turbulent Mixing of Axisymmetric Compressible Jets (In the Half-Jet Region) with Quiescent Air," Sandia Corp., Report SC-4764 (RR) Aerothermodynamics, (March 1963).

22. Gooderum, P., Wood, G., and Brevoort, M., "Investigation with an Interferometer of the Turbulent Mixing of a Free Supersonic Jet," NACA TR 9631 (1050).

23. Sabin, C. M., "An Analytical and Experimental Study of the Plane, Incompressible, Turbulent Free Shear Layer with Arbitrary Velocity Ratio and Pressure Gradient," Research Grant AFOSR 136-63 (Stanford Univ. Dept. of Mech. Engr. Report MD-9), October, 1963.

24. Eggers, J. M., "Velocity Profiles and Eddy Viscosity Distributions Downstream of a Mach 2.22 Nozzle Exhausting into Quiescent Air", NASA Technical Note NASA TN D-3601, Sept. 1966.

APPENDIX "A"

COMPUTER PROGRAM FOR EVALUATION OF PRESSURE GRADIENT FUNCTIONS IN THE MIXING ANALYSIS

AN EXPLANATION OF PROGRAM

I. Input

The following variables are given with their Fortran names and an explanation of their significance.

(1) XLAMO = λ_0 = initial velocity ratio of streams.

(2) H10 = h_{10} = enthalpy of primary stream.

(3) H20 = h_{20} = enthalpy of secondary stream.

(4) PRT = Prt = Prandtl no. of primary stream.

(5) KN(I) = k_n = eddy viscosity coefficient where the eddy viscosity formula is given by $k_1(X) = a_N k_N k_0 X^N$.

(6) GAMMA = γ = specific heat ratio.

(7) U10 = u_{10} = velocity of primary stream.

(8) EM01 = m_{01} = Mach no. of primary stream.

(9) R = distance from the origin to where the mixing disturbance is negligible.

(10) ND = number of elements into which the mixing zone is divided from the origin to distance R. It must be small enough to bring about stability in the Runge-Kutta method of integration of the differential equations. Also, it is desirable to have ND = 4I, where I is large enough so that R/I is a satisfactory incrementation for integration of the resulting functions r_N and h_0/h_{01}, and a small enough interval for a complete description of the functions.

(11) NM = the number of functions to be considered in the first order mixing process. This is the highest power of X in the polynomial representation of the pressure.

II. Output

The output is given in several listings of the functions computed from -R to +R over the domain of η. The listings shown in any given case are described below:

(1) For each N there is a listing in increments of $2 \cdot (R/ND)$ of g_{N1}, g_{N2}, r_{N1}, r_{N2}, r_{N3}, r_{N4} versus η.

(2) Next, a listing in increments of $4 \cdot (R/ND)$ of η, u_0/u_{01}, g_1, g_{NM} is given where

$$g'_N = g'_{N1} + \left[\frac{\gamma}{\gamma-1} \frac{u_{01}^2}{2h_{01}} + \left\{ \frac{1 - \frac{h_{02}}{h_{01}} \frac{1}{\lambda_0}}{1 - \lambda_0} + k_n \right\} \right] g'_{N2}$$

This comprises the description of the velocity field.

(3) The enthalpy field is next listed in increments of $4 \cdot (R/ND)$. This listing gives:

η, h_0/h_{01}, r_1, r_{NM} where

$$r_N = r_{N1} + \frac{\gamma}{\gamma-1} r_{N2} + \frac{1}{(\gamma-1)m_{01}^2} r_{N3} + \frac{\left[1 - \frac{h_{02}}{h_{01}} \frac{1}{\lambda_0} + k_N \right]}{2 Prt (\gamma-1) m_{01}^2 (1 - \lambda_0)} r_{N4}$$

(4) Finally, the listing is given of the functions for the transformation of an η value to the compressible plane in terms of y, X. They are:

$$\eta,\ \frac{\rho_*}{\rho_{01}} \int_o^\eta h_0/h_{01}\, d\eta,\ \frac{\rho_*}{\rho_{01}} \int_o^\eta r_1(\eta)\, d\eta, \ldots\ldots,\ \frac{\rho_*}{\rho_{01}} \int_o^\eta r_{NM}(\eta)\, d\eta$$

Summarial Flow Chart for First
Order Mixing Analysis

I. Main Program

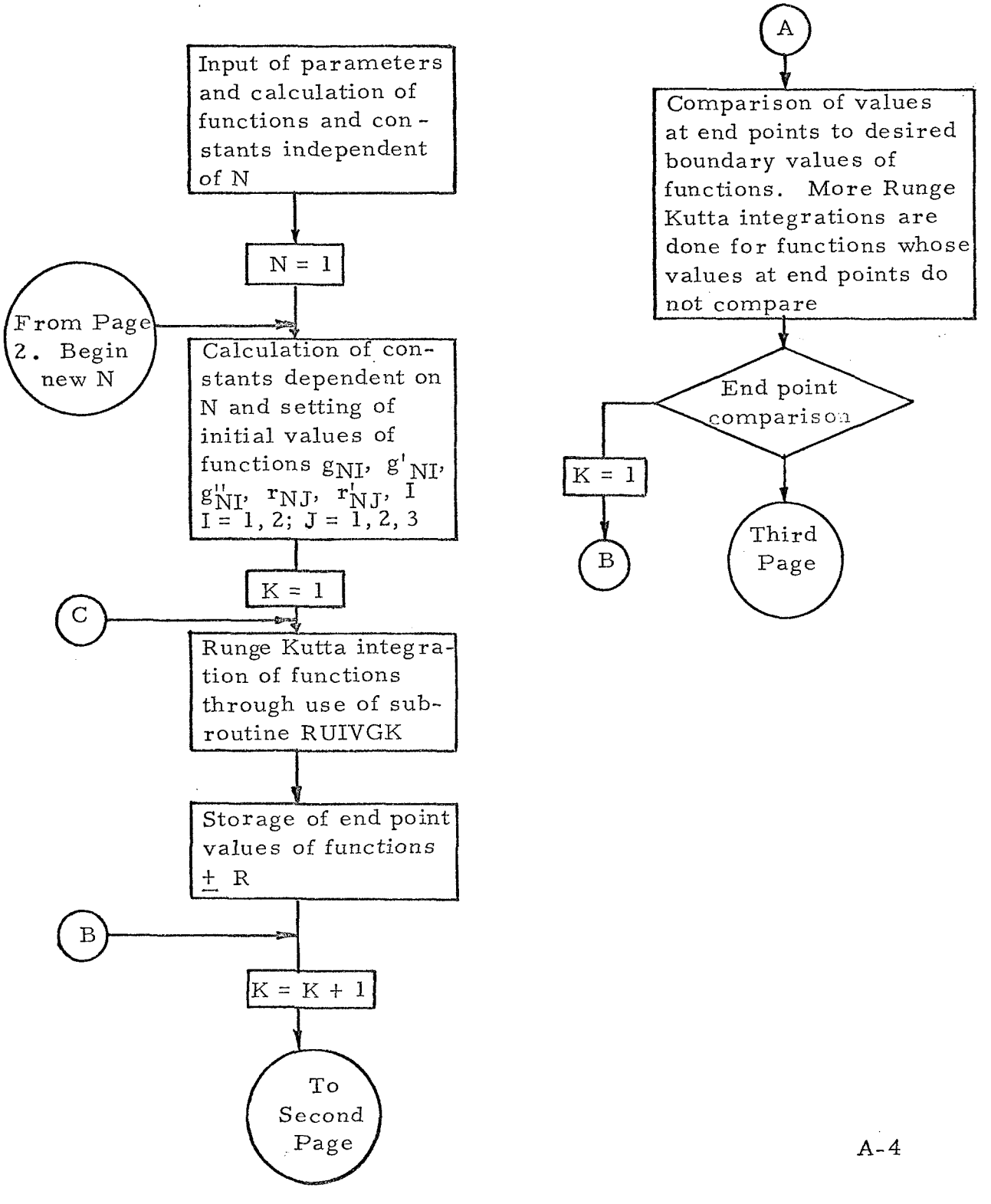

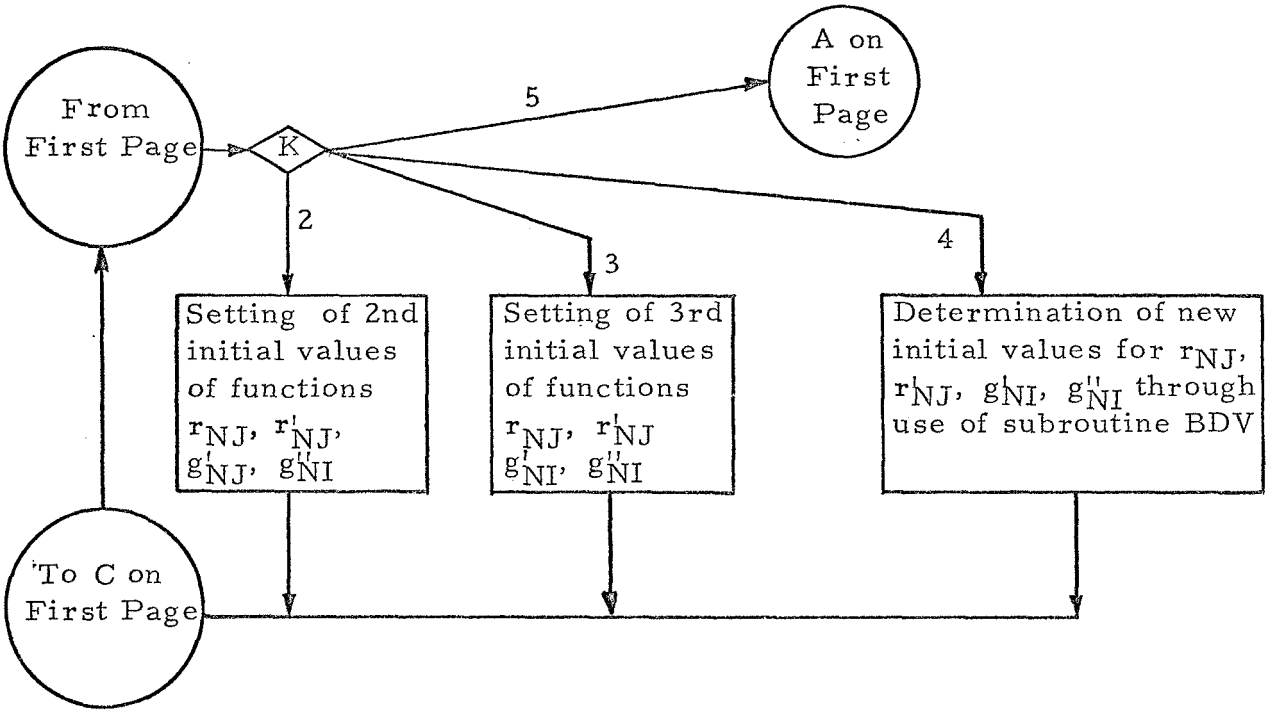
From First Page
K
5
A on First Page
2
3
4
Setting of 2nd initial values of functions r_{NJ}, r'_{NJ}, g'_{NJ}, g''_{NI}
Setting of 3rd initial values of functions r_{NJ}, r'_{NJ} g'_{NI}, g''_{NI}
Determination of new initial values for r_{NJ}, r'_{NJ}, g'_{NI}, g''_{NI} through use of subroutine BDV
To C on First Page

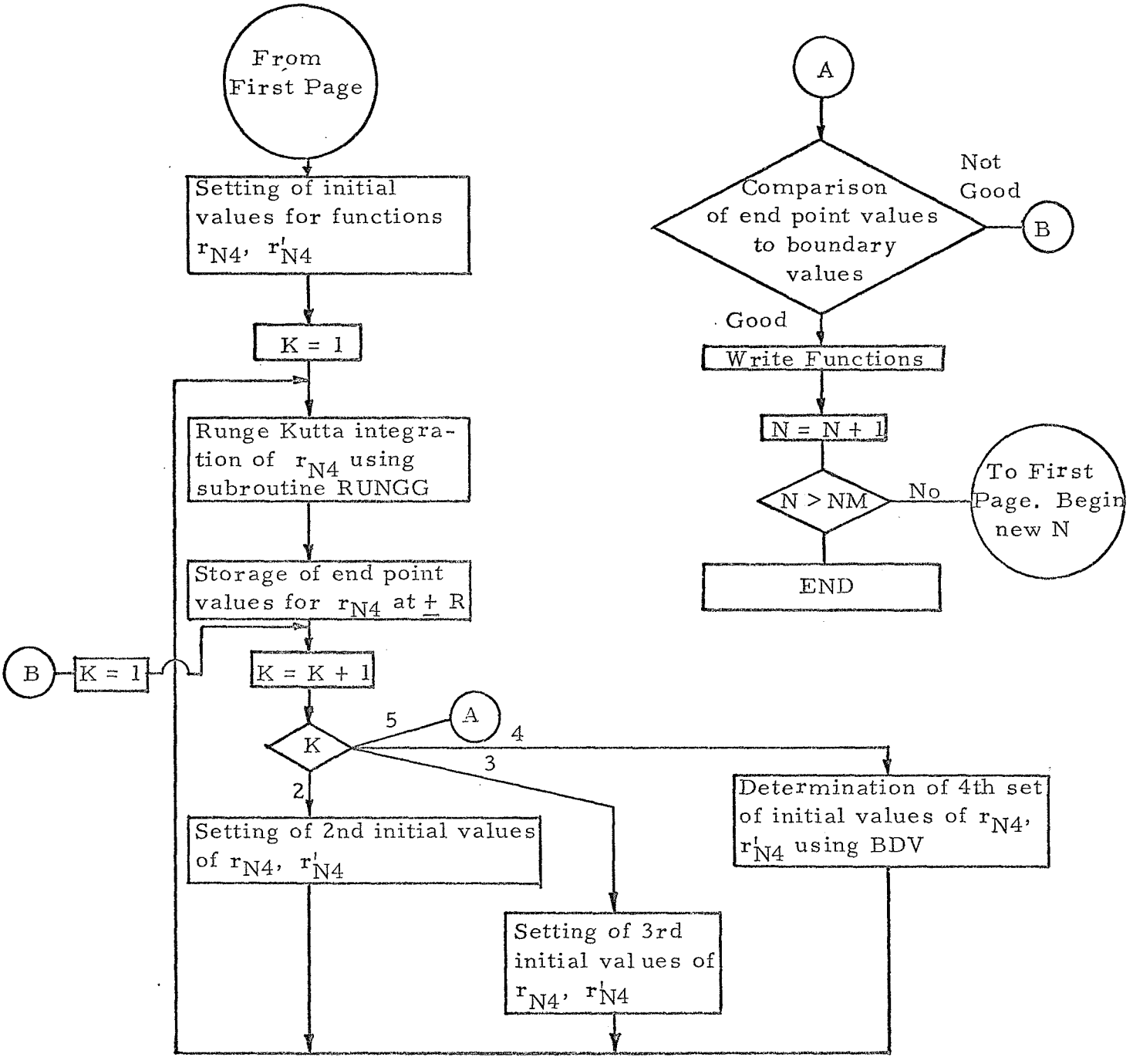
From First Page
Setting of initial values for functions r_{N4}, r'_{N4}
K = 1
Runge Kutta integration of r_{N4} using subroutine RUNGG
Storage of end point values for r_{N4} at ± R
B
K = 1
K = K + 1
K
5
A
4
3
2
Setting of 2nd initial values of r_{N4}, r'_{N4}
Setting of 3rd initial values of r_{N4}, r'_{N4}
Determination of 4th set of initial values of r_{N4}, r'_{N4} using BDV
A
Comparison of end point values to boundary values
Not Good
B
Good
Write Functions
N = N + 1
N > NM
No
To First Page. Begin new N
END

FLOW CHART FOR TRANSFORMATION FUNCTIONS AND FINAL OUTPUT

The following is a suggested form for calculation of transformation functions. At the end of each computation of the functions g_{Ni}, r_{Ni}, the values of the functions g'_N, r_N are stored in arrays so that, at the end of the calculation of boundary value, problems for all N up to NM, all functions g_N, r_N have been developed. Starting from here, the following is done. Note:

$$TRO(I) = \frac{\rho_*}{\rho_{01}} \int_o^\eta h_0/h_{01} d\eta ; \quad TR(I,K) = \frac{\rho_*}{\rho_0} \int_o^\eta r_k \, d\eta$$

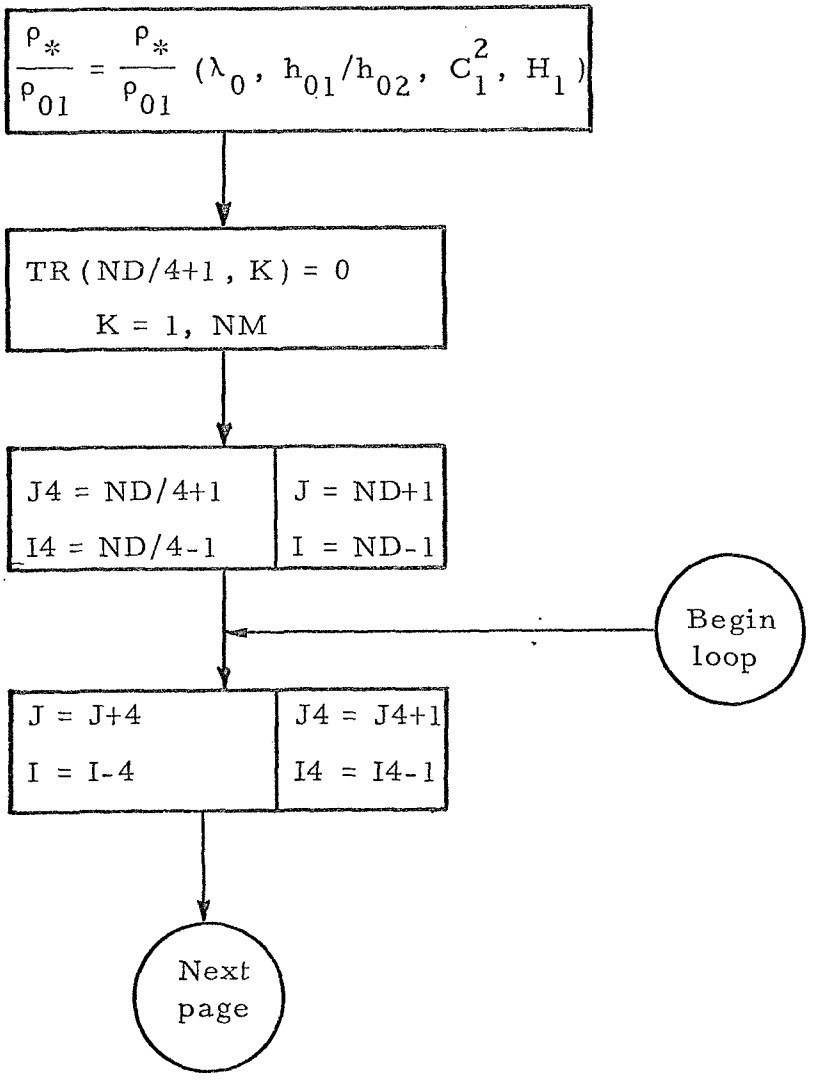

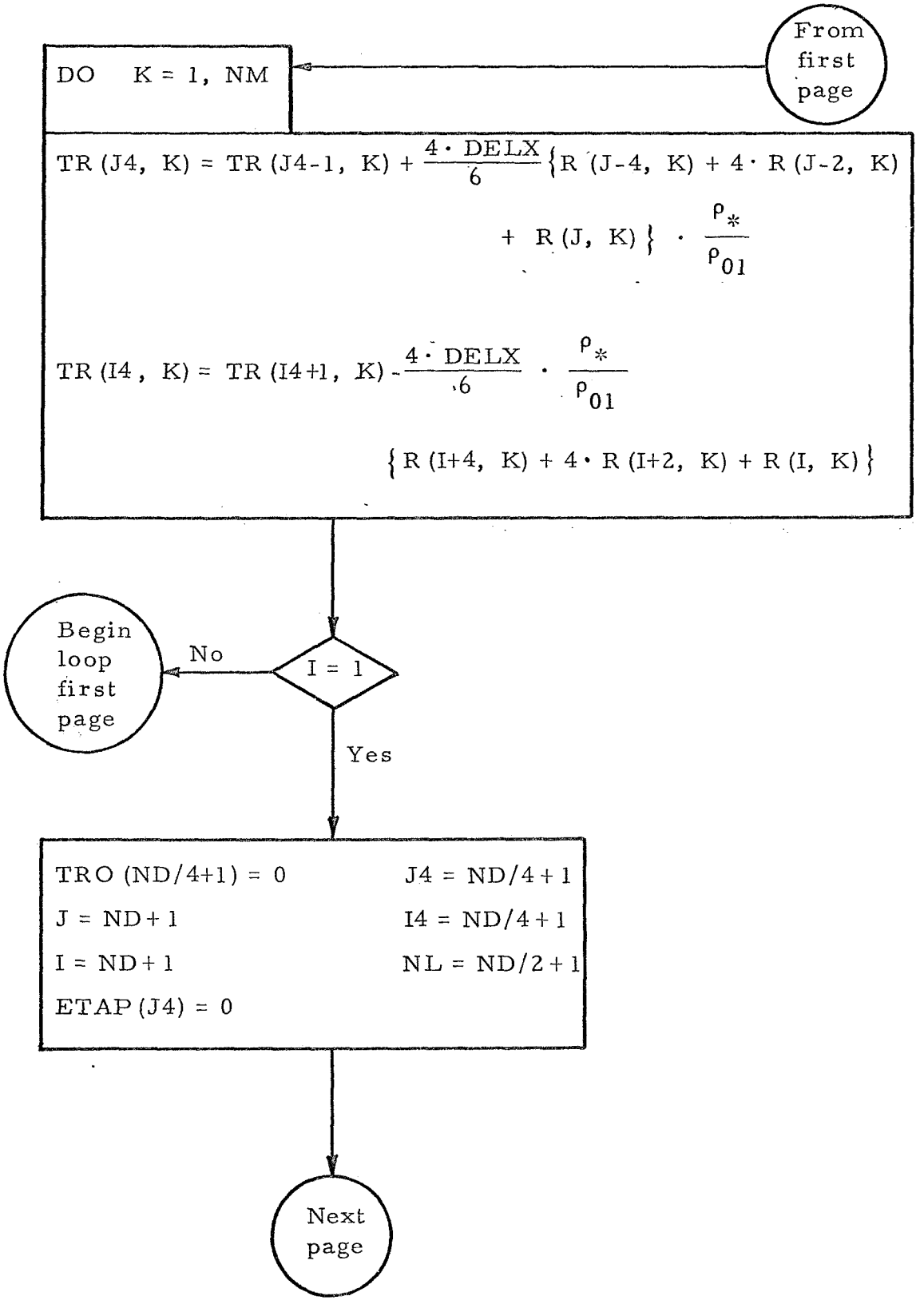
From first page
DO K = 1, NM
TR (J4, K) = TR (J4-1, K) + 4 · DELX / 6 { R (J-4, K) + 4 · R (J-2, K) + R (J, K) } · ρ* / ρ01
TR (I4, K) = TR (I4+1, K) - 4 · DELX / 6 · ρ* / ρ01 { R (I+4, K) + 4 · R (I+2, K) + R (I, K) }
I = 1
No
Begin loop first page
Yes
TRO (ND/4+1) = 0
J = ND+1
I = ND+1
ETAP (J4) = 0
J4 = ND/4+1
I4 = ND/4+1
NL = ND/2+1
Next page

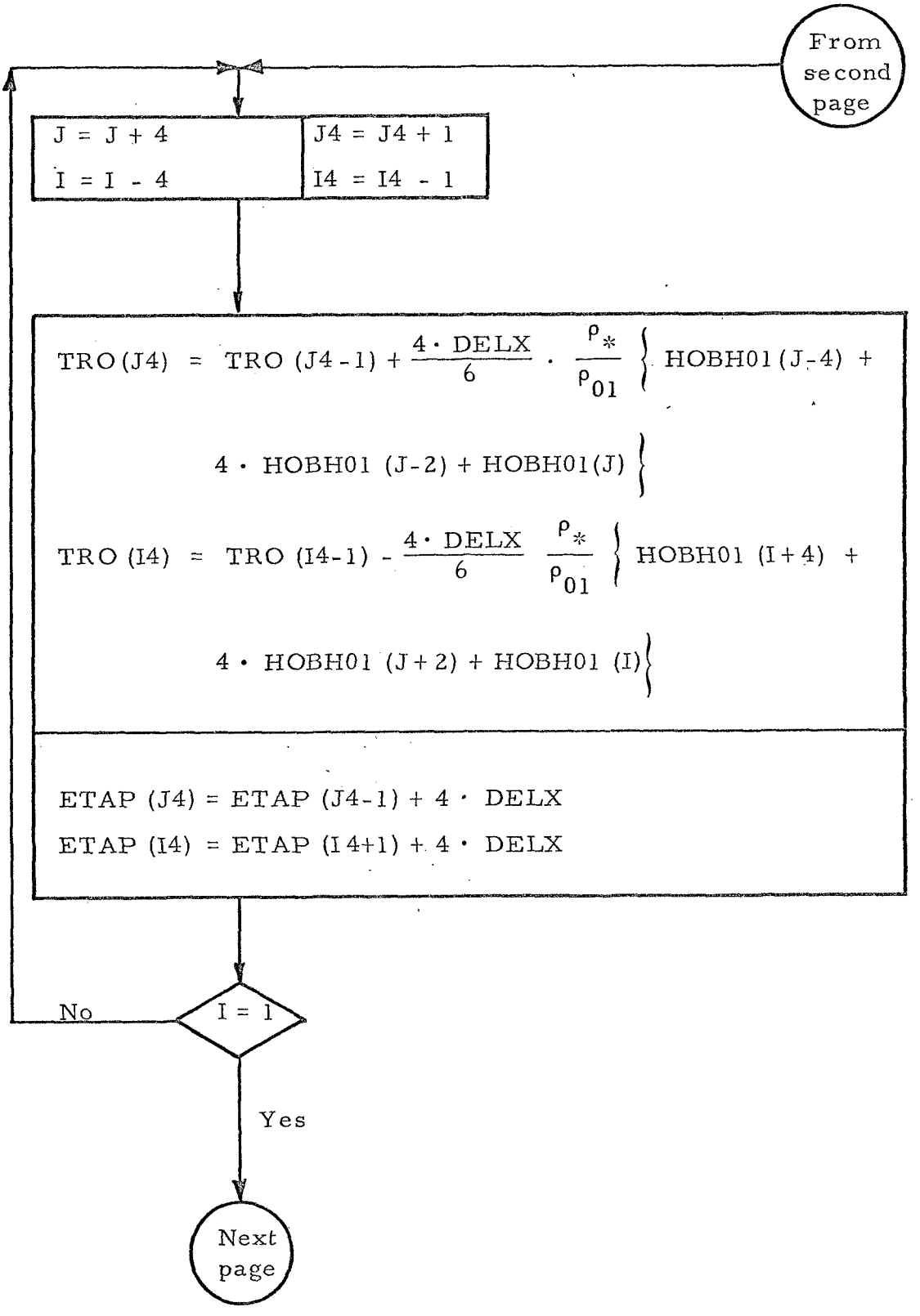
From second page
J = J + 4
I = I - 4
J4 = J4 + 1
I4 = I4 - 1
TRO(J4) = TRO (J4-1) + 4 · DELX / 6 · ρ* / ρ01 { HOBH01(J-4) + 4 · HOBH01 (J-2) + HOBH01(J) }
TRO (I4) = TRO (I4-1) - 4 · DELX / 6 · ρ* / ρ01 { HOBH01 (I+4) + 4 · HOBH01 (J+2) + HOBH01 (I) }
ETAP (J4) = ETAP (J4-1) + 4 · DELX
ETAP (I4) = ETAP (I4+1) + 4 · DELX
No
I = 1
Yes
Next page

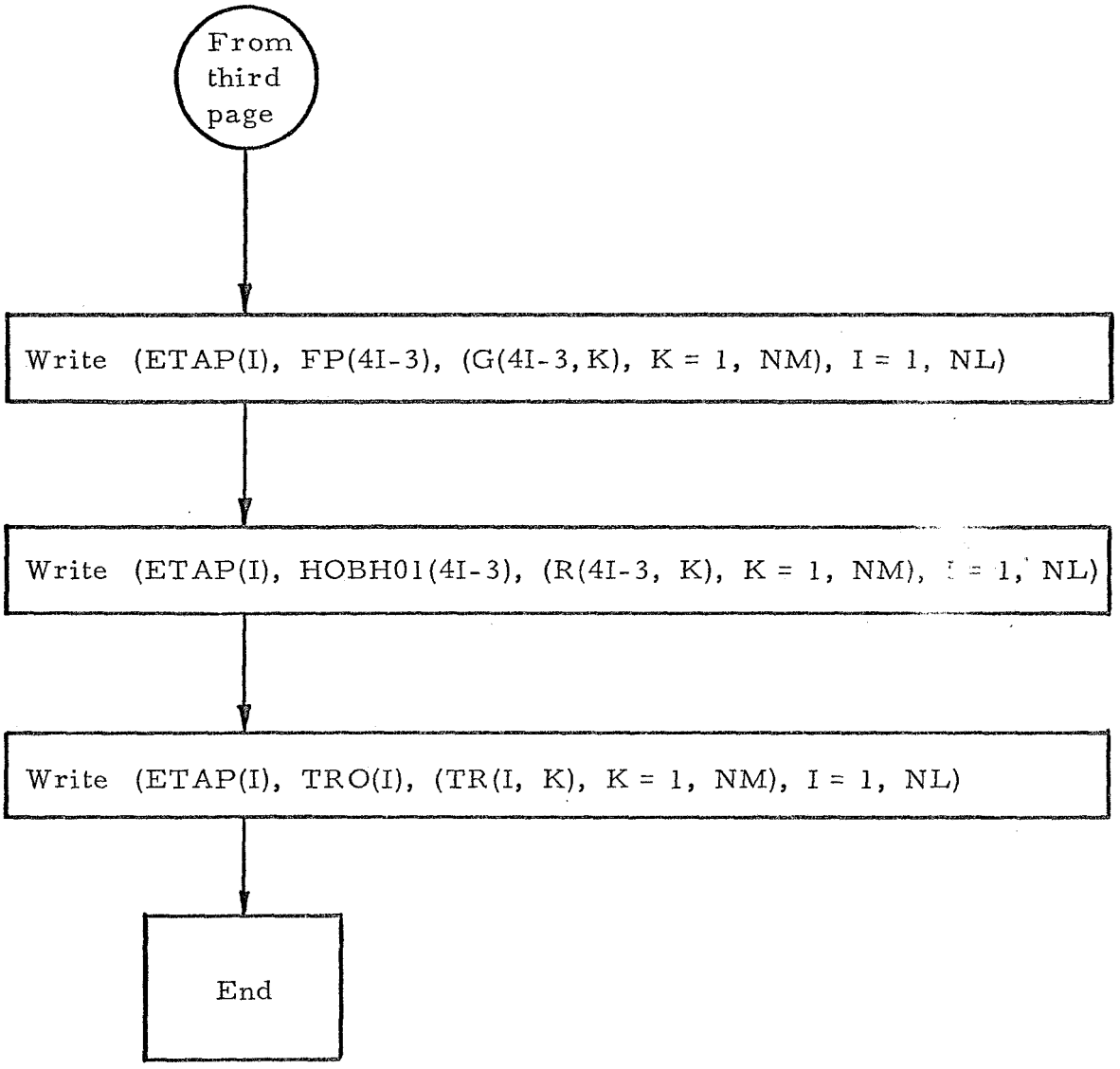
From third page
Write (ETAP(I), FP(4I-3), (G(4I-3,K), K = 1, NM), I = 1, NL)
Write (ETAP(I), HOBH01(4I-3), (R(4I-3, K), K = 1, NM), I = 1, NL)
Write (ETAP(I), TRO(I), (TR(I, K), K = 1, NM), I = 1, NL)
End

III. Subroutine BDV

The purpose of this subroutine is to make use of the three initial value guesses first made. Then any following three initial value guesses are treated in the same manner. The theory is below.

Let the boundary value problem on y be given as below.

$$y''' = f_1(x)\, y'' + f_2(x)\, y' + f_3(x)\, y + f_4(x)$$

$$y'(+R) = b_1$$
$$y'(-R) = b_0$$
$$y(O) = y_0$$

To solve this problem, one makes guesses as to the values of $y'(O)$, $y''(O)$, integrates the differential and obtains the results $y'(+R)$ and $y'(-R)$ for these guesses. In order to find what guesses should be made we suppose a Taylor series' expansion exists for y'. Let $y'(O) = s$, $y''(O) = t$. Then,

$$y'''(O) = f_1(O)\, t + f_2(O)\, s + f_3(O)\, y_0 + f_4(O)$$

$$y^{(4)}(O) = f_1(O)\, y'''(O) + f_1'(O)\, t + f_2(O)\, t + f_2'(O)\, s + f_3'(O)\, y_o$$

$$+ f_3(O)\, s + f_4'(O)$$

Note that $y^{(4)}(O)$ can be expressed as:

$$y^{(4)}(O) = A_4 + B_4\, s + C_4\, t$$

Any further derivative of y can be similarly expressed:

$$y^{(n)} = A_n + B_n\, s + C_n\, t$$

The expression for y' at $\pm R$ can then be reduced to:

$$(1) \qquad y'(R) = \sum_{n} \frac{y^{(n)}(O)}{(n-1)!} R^n = G_1 + G_2 s + G_3 t$$

$$(2) \qquad y'(-R) = G'_1 + G'_2 s + G'_3 t$$

Hence, for a finite interval, the values at the end points are linearly related to the guesses s & t for the initial value problem. If one has three guesses for s, t, and integrates to obtain $y'(\pm R)$ for these guesses, (1) & (2) provide three equations for the unknowns: G_1, G_2, G_3, G'_1, G'_2, G'_3. With these once calculated, the values for s, t satisfying (1) & (2) with $y'(R) = b_0$, and $y'(-R) = b_1$ can be obtained.

There are two questions: how are the s, t for the finite interval problem related to the s, t for the $\pm \infty$ boundary value problem? how large are the values G_2, G_3, G'_2, G'_3 - these may be small enough to make the dependency on s, t insenstivie in the regions around $\pm R$, but the function around the origin may be considerably changed.

The BDV subroutine assumes that for a large R the s, t are nearly those for the $\pm \infty$ problem and that sensitivity on s, t is sufficient to allow these values to be calculated using (1) & (2). It does so in these steps

A. Using $y'(\pm R)$ for 3 previous guesses G_1, G_2, G_3 and G'_1, G'_2, G'_3 are calculated using (1) & (2).

B. Using these G's one has these equations for s & t

$$G_2 s + G_3 t = b_1 - G_1$$

$$G'_2 s + G'_3 t = b_0 - G'_1$$

These are solved and the initial values s, t are returned the main program.

III. The Runge-Kutta Subroutines

The RUNGK subroutine integrates g_{N1}, g_{N2}, r_{N1}, r_{N2}, r_{N3}. After the 4th integration of these functions is made, their endpoint values are compared to the desired boundary values. If the comparison is within the desired tolerance for some function, an integer variable is set so that if further integration for other functions is needed, the integration for the function whose comparison is good is avoided. A further feature of the RUNGK routine is its capability of integrating in two directions. Tests are set up within the subroutine to determine if the independent variable is positive or negative and integration takes place accordingly.

The RUNGG subroutine is similar to RUNGK except that it is for the function r_{N4} alone. (Note that r_{N4} depends upon g_N.)

Table B1. Reduced Data for Velocity Profiles for Air-Air Mixing

Figure 15. $C_1^2 = .691$, $\lambda = .857$, $\beta = 1.0$

x = 17.75		x = 29.75		x = 41.75	
$y - y_{.5}$	u/u_1	$y - y_{.5}$	u/u_1	$y - y_{.5}$	u/u_1
-1.000	.8465	-1.000	.8618	-.700	.8644
-.620	.8439	-.950	.8593	-.470	.8644
-.415	.8465	-.610	.8567	-.390	.8721
-.370	.849	-.550	.8593	-.340	.8798
-.260	.8541	-.460	.8618	-.260	.8875
-.210	.8593	-.380	.8670	-.185	.9029
-.180	.8721	-.350	.8721	-.140	.9132
-.160	.8849	-.290	.8772	-.060	.9262
-.110	.8978	-.250	.8824	.030	.9390
-.055	.9006	-.160	.8952	.150	.9544
-.005	.9399	-.110	.9080	.250	.9646
.050	.9488	.010	.9364	.335	.9749
.100	.9611	.090	.9518	.400	.9852
.130	.9749	.190	.9672	.480	.9826
.180	.9852	.240	.9800	.575	.9852
.240	.9903	.300	.9903	.695	.9852
.280	.9929	.370	.9954	.770	.9852
.340	.9954	.410	1.0006	.900	.9826
.420	.9954	.470	1.0031	.965	.9852
.520	.9954	.530	1.0059	1.000	.9852
.620	.9954	.590	1.0006		
.710	1.0005	.650	1.0006		
.750	1.0057	.730	.9954		
.800	1.0108	.770	.9954		
.825	1.0150	.870	.9954		
.880	1.0160	.910	1.0006		
.925	1.0185	.970	1.0057		
.960	1.0185	1.000	1.0082		
1.000	1.0185				

Table B1 (continued)

Figure 16. $C_1^2 = .691$, $\lambda = .7077$, $\beta = 1.0$

x = 5.75		x = 17.75		x = 29.75	
$y - y_{.5}$	u/u_1	$y - y_{.5}$	u/u_1	$y - y_{.5}$	u/u_1
-.515	.708	-.940	.713	-.780	.708
-.460	.708	-.845	.713	-.650	.708
-.265	.710	-.495	.713	-.580	.710
-.220	.723	-.410	.715	-.520	.713
-.180	.739	-.340	.723	-.460	.723
-.140	.766	-.260	.744	-.390	.739
-.085	.800	-.200	.770	-.320	.749
-.045	.828	-.125	.805	-.250	.772
0	.857	-.030	.841	-.190	.790
.025	.884	0	.857	-.120	.816
.040	.913	.065	.877	-.060	.838
.060	.949	.125	.913	-.030	.846
.105	1.008	.190	.944	0	.857
.180	1.008	.280	.966	.050	.867
.275	1.008	.395	.980	.130	.893
.335	1.008	.435	.990	.200	.913
.465	1.008	.490	.995	.290	.929
.650	1.000	.575	.995	.360	.949
.730	.997	.640	.995	.430	.954
.875	.997	.740	.992	.490	.964
.990	1.000	.890	.992	.550	.970
		1.140	1.000	.580	.975
				.700	.980
				.760	.990
				.870	.990
				.950	.995
				1.040	.997

Table B1 (continued)

Figure 17. $C_1^2 = .694$, $\lambda = .718$, $\beta = 1.0$

x = 17.75		x = 29.75		x = 41.75	
$y - y_{.5}$	u/u_1	$y - y_{.5}$	u/u_1	$y - y_{.5}$	u/u_1
-.800	.715	-.840	.731	-1.040	.708
-.700	.715	-.790	.731	- .869	.715
-.480	.718	-.580	.731	- .712	.728
-.390	.720	-.475	.739	- .575	.739
-.275	.725	-.420	.749	- .420	.766
-.215	.728	-.370	.766	- .290	.800
-.195	.731	-.270	.790	- .070	.852
-.165	.739	-.150	.826	0	.864
-.145	.749	0	.864	.090	.890
-.105	.772	.110	.905	.290	.931
-.070	.805	.215	.939	.460	.954
-.020	.849	.275	.954	.675	.977
0	.864	.330	.964	.810	.982
.055	.905	.435	.980	.960	.990
.160	.949	.550	.987	1.110	.990
.220	.970	.710	.987		
.270	.980	.930	.987		
.335	.985	1.065	.990		
.430	.992				
.500	.992				
.580	.995				
.730	.997				
1.020	1.000				

Table B1 (continued)

Figure 18. $C_1^2 = .528$, $\lambda = .8182$, $\beta = 1.0$

x = 5.75		x = 17.75		x = 29.75	
$y - y_{.5}$	u/u_1	$y - y_{.5}$	u/u_1	$y - y_{.5}$	u/u_1
-1.270	.826	-1.260	.837	-1.060	.826
- .855	.813	-1.020	.813	- .830	.820
- .530	.811	- .690	.811	- .550	.839
- .395	.783	- .410	.826	- .180	.867
- .270	.781	- .290	.837	- .005	.908
- .235	.783	- .200	.852	.150	.928
- .140	.806	- .110	.872	.385	.958
- .055	.857	- .050	.892	.650	.989
.020	.923	.030	.918	.900	.999
.070	.973	.150	.958	1.000	.999
.165	.994	.300	.984		
.240	1.000	.440	1.004		
.300	1.000	.500	1.004		
.440	.996	.640	1.006		
.605	.993				
.730	.999				
.835	.999				

Table B1 (continued)

Figure 19. $C_{10}^2 = .735$, $\lambda_0 = .825$

x = 5.75		x = 17.75		x = 29.75	
$y - y_{.5}$	u/u_1	$y - y_{.5}$	u/u_1	$y - y_{.5}$	u/u_1
-.651	.843	-.720	.814	-.880	.813
-.550	.845	-.580	.813	-.615	.815
-.420	.845	-.380	.814	-.700	.820
-.300	.840	-.275	.855	-.420	.827
-.225	.827	-.165	.860	-.370	.837
-.195	.827	-.090	.900	-.250	.857
-.143	.837	+.005	.920	-.210	.875
-.090	.873	+.065	.945	-.140	.890
-.030	.905	.190	.957	-.050	.908
+.070	.935	.260	.965	+.050	.927
.130	.965	.322	.972	.110	.940
.235	.987	.441	.968	.190	.950
.365	1.00	.620	.970	.370	.960
.590	1.00	.740	.966	.520	.967
.720	1.00	.860	.970	.740	.975
.850	1.00	.950	.972		
.915	1.00	.970	.972		
		.990	.973		

Table B1 (continued)

Figure 20. $C_{10}^2 = .516$, $\lambda_0 = .773$

x = 5.75		x = 17.75		x = 29.75	
$y - y_{.5}$	u/u_1	$y - y_{.5}$	u/u_1	$y - y_{.5}$	u/u_1
-1.440	.829	-1.320	.824	-1.300	.608
-1.320	.829	-1.180	.818	-1.280	.585
-.680	.818	-1.060	.812	-1.200	.613
-.560	.818	-.560	.812	-1.140	.636
-.400	.795	-.460	.824	-1.060	.676
-.280	.772	-.350	.829	-.900	.721
-.160	.784	-.180	.858	-.760	.750
-.140	.795	-.080	.880	-.620	.755
-.080	.824	0	.897	-.460	.755
-.050	.858	.050	.926	-.240	.761
-.020	.897	.140	.948	-.080	.772
.020	.932	.240	.960	.040	.807
.050	.960	.340	.966	.240	.840
.100	.977	.380	.971	.380	.869
.150	.988	.440	.971	.460	.858
.200	.994	.620	.971	.540	.886
.260	.988			.620	.909
.360	.982				
.480	.988				
.560	.994				
.640	1.000				
.720	1.000				
.780	1.000				

C_1^2	λ	x	$b_{.9}$	$\frac{\sigma_o b_{.9}}{x}$	$(\frac{\sigma_o b_{.9}}{x})_{avg.}$	$\frac{\bar{\sigma}}{\sigma_o}$ exp.	$\frac{\bar{\sigma}}{\sigma_o}$ calc.	$\frac{\sigma(0)}{\sigma_o}$	$\Delta P/\Delta x$ $(\frac{psi}{inch})$
.691	.8574	17.75	.367	.228	.233	7.7	6.64	7.3	0
		29.75	.579	.214					
		41.75	.970	.256					
.691	.7077	5.75	.259	.496	.353	5.1	5.06	5.1	0
		17.75	.582	.361					
		29.75	.932	.345					
.694	.718	17.75	.363	.225	.299	5.3	5.15	5.4	0
		29.75	.790	.292					
		41.75	1.165	.306					
.528	.8182	5.75	.207	.396	.404	4.5	8.05	4.6	0
		17.75	.590	.366					
		29.75	1.220	.451					
.735*	.825	5.75	.345	.660		2.7		2.8	+.067
.693*	.836	17.75	.465	.288		6.2		5.8	+.067
.686*	.838	29.75	.655	.242		7.4		6.9	+.067
.516*	.773	5.75	.19	.364		4.9		5.6	+.03 + .0825x
.487*	.837	17.75	.54	.335		5.4		5.8	+.03 + .0825x

* Local data for pressure gradient cases